

Electronic Thesis and Dissertation Repository

12-1-2021 1:30 PM

Kindlin-1 is involved in spreading, migration, and protein regulation in epidermal SCC-13 cells

Naomi Mishan, *The University of Western Ontario*

Supervisor: Dagnino, Lina, *The University of Western Ontario*

Co-Supervisor: Damjanovski, Sashko, *The University of Western Ontario*

A thesis submitted in partial fulfillment of the requirements for the Master of Science degree in Biology

© Naomi Mishan 2021

Follow this and additional works at: <https://ir.lib.uwo.ca/etd>



Part of the [Cancer Biology Commons](#), [Cell Biology Commons](#), and the [Skin and Connective Tissue Diseases Commons](#)

Recommended Citation

Mishan, Naomi, "Kindlin-1 is involved in spreading, migration, and protein regulation in epidermal SCC-13 cells" (2021). *Electronic Thesis and Dissertation Repository*. 8301.
<https://ir.lib.uwo.ca/etd/8301>

This Dissertation/Thesis is brought to you for free and open access by Scholarship@Western. It has been accepted for inclusion in Electronic Thesis and Dissertation Repository by an authorized administrator of Scholarship@Western. For more information, please contact wlsadmin@uwo.ca.

Abstract

Kindlin-1 is a scaffold protein linking the cytoskeleton to the extracellular matrix. Loss of function mutations in the *FERMT1* gene (encoding Kindlin-1) cause gastrointestinal and skin defects associated with increased susceptibility to aggressive epidermal squamous cell carcinoma (SCC). This study investigated the consequences of targeted *FERMT1* inactivation in the SCC-13 cell line of epidermal SCC. My studies demonstrate Kindlin-1 is not essential for SCC-13 proliferation or clonogenic potential in culture. Kindlin-1 was required for cell spreading on collagen I, but not on laminin-332, and its absence enhanced SCC-13 directional migration. Finally, I identified several proteins involved in tumor formation and progression as novel potential targets of Kindlin-1 modulation in SCC-13 cells. To my knowledge, this is the first study evaluating Kindlin-1 function in human epidermal SCC cells, providing novel insights into the role of Kindlin-1 in epidermal carcinomas, which may aid in the development of therapies for cutaneous SCC.

Keywords

Kindlin-1

SCC-13

proliferation

migration

spreading

carcinoma

Summary for Lay Audience

Kindlin-1 is a necessary component of cells in the outermost layer of the skin, called the epidermis. Lack of Kindlin-1 in the body causes Kindler syndrome; a hereditary disease that gives rise to skin abnormalities. Humans with Kindler syndrome often develop cancer in the epidermis that is likely to spread throughout the body without medical intervention; known as squamous cell carcinoma (SCC). I studied the role of Kindlin-1 in cells called SCC-13, which are epidermal SCC cells. I compared SCC-13 cells that have Kindlin-1 with SCC-13 cells that were modified so that Kindlin-1 is no longer present. I found Kindlin-1 is not needed for the proliferation of SCC-13 cells. Cells without Kindlin-1 did not spread well, but they showed increased forward movement. Finally, I identified many proteins important for cancer formation and progression that are regulated by Kindlin-1. This study is the first of its kind to evaluate Kindlin-1 function in human epidermal SCC, and increases our understanding of Kindlin-1 function, important for the development of SCC treatments.

Co-Authorship Statement

Principal component analysis on reverse phase protein array data was conducted by Drs. S. Sayedyahosseini, M. Karimi and M. Bahmani. The images used for figure 3.9 were also generated by Drs. S. Sayedyahosseini, M. Karimi and M. Bahmani. All other data, figures (including creating fig. 3.9), and quantifications presented in this thesis were generated by Naomi Mishan.

Acknowledgments

First, I would like to thank my supervisor Dr. Lina Dagnino for always pushing me to be better. Your guidance and support have been invaluable and has taught me that there is always something to be learned. I would also like to thank my supervisor Dr. Sashko Damjanovski, for your constant support and guidance. You always had a positive attitude and made time to help with any issues I had. I never would have thought that enjoying your second-year cell biology course would have led me on this path.

To my advisory committee, Dr. Greg Kelly and Dr. John Di Guglielmo, thank you for all your advice and support throughout my project. A big thanks to all the present and previous members of the Dagnino lab for all their help and for making my time in the lab a positive experience. To Dr. Ivanova, thank you for the cell line which made my research possible. To Kevin Barr, thank you for all your assistance in my project, and providing comedic relief along the way. To Dr. Samar Sayedyahosseini, thank you for all our wonderful discussions, and all your help and advice in analyzing our RPPA data. Our tea times always brightened up my day. Thank you, Nancy and Melissa, for all of the experiments that you taught me, and guidance in navigating the equipment; you were always willing to help. To the Sash lab, thank you for giving me a foray into research when I was just wide-eyed undergrad, and for providing support in my research along the way. To Brad, thank you for helping me with zymography experiments, even though it didn't make it to my thesis, I learned a lot.

I would also like to thank Renee, for supporting me and always listening to my complaints. Our lunch dates provided fun memories, and much needed respite from the

demands of the last 2 years. A very big thank you to my amazing boyfriend Sam Bender, for his infinite support and help with my project and in life. Finally, I would like to thank my family for always being there for me and always supporting me in my endeavors.

Table of Contents

Abstract	ii
Summary for Lay Audience	iii
Co-Authorship Statement	iv
Acknowledgments	v
Table of Contents	vii
List of Tables	xii
List of Figures	xiv
List of Abbreviations	xv
1 Introduction	1
1.1 The Skin	1
1.1.1 Overview of the Epidermis	1
1.1.2 Architecture and Functions of the Epidermal Layers	7
1.2 Integrins	8
1.2.1 Integrins in the Epidermis	8
1.2.2 Integrins and Cancer	11
1.3 Skin Carcinogenesis	12

1.4	Keratinocyte Carcinomas.....	13
1.4.1	Basal Cell Carcinoma	13
1.4.2	Squamous Cell Carcinoma	14
1.5	Kindlin.....	15
1.5.1	The Kindlin Family of Proteins	15
1.5.2	Structure of Kindlin-1	19
1.5.3	Biological Functions of Kindlin-1	19
1.6	Kindlin-1 in Cancer.....	23
1.6.1	Lung Carcinoma	23
1.6.2	Breast Carcinoma	24
1.6.3	Colorectal Carcinoma	24
1.6.4	Pancreatic Carcinoma.....	25
1.6.5	Esophageal Carcinoma	25
1.6.6	Keratinocyte Carcinoma	25
1.7	Rationale, Hypothesis and Aims	26
2	Materials and Methods	28
2.1	Reagents.....	28
2.2	Materials and Equipment	30
2.3	Antibodies	32
2.4	Primers	32

2.5	Cell Lines and Culture	33
2.5.1	Parental and Kindlin-1-Deficient SCC-13 Cells	33
2.5.2	804G Rat Bladder Epithelial Cells	34
2.5.3	Generation of CRISPR/Cas9 Targeted SCC-13 Cells	34
2.6	Preparation of Lysates for Protein Analysis.....	37
2.7	Denaturing Polyacrylamide Gel Electrophoresis (SDS-PAGE) and Immunoblot Analysis.....	38
2.8	Proliferation Assays	39
2.8.1	Growth Curve Assays.....	39
2.8.2	BrdU Incorporation Assays	39
2.9	Spheroid Formation Assays	41
2.10	Cell Spreading Experiments.....	42
2.10.1	Analysis of Cell Spreading.....	42
2.10.2	CellProfiler Analysis of WGA Images	43
2.11	Migration Assays	44
2.12	Reverse Phase Protein Array (RPPA) Analysis	45
2.13	Statistical Analyses	46
3	Results	49
3.1	Abundance of Kindlin-1 Protein in SCC-13 Cell Lines	49
3.2	Proliferation of Kin-1 ^{KO1} and Kin-1 ^{KO2} Cells	49

3.3	Spheroid Forming Ability of Parental, Kin-1 ^{KO1} and Kin-1 ^{KO2} SCC-13 Cells	57
3.4	Cell Spreading on Laminin-332 Matrix and Collagen I	61
3.5	Directional Migration of Kin-1 ^{KO1} and Kin-1 ^{KO2} Cells.....	69
3.6	Proteomic Analysis using Reverse Phase Protein Arrays Reveals Differences in the Abundance of Proteins Associated with Carcinogenesis in Kindlin-1-Deficient SCC-13 Cells	75
3.6.1	Pathway Analysis of Proteins with Significantly Different Protein Abundances in Kin-1 ^{KO1} and Kin-1 ^{KO2} Cells	89
3.6.2	A Focused Examination of the 100 Differentially Expressed Proteins in Kin-1 ^{KO1} and Kin-1 ^{KO2} cells	93
3.6.3	Phosphoproteins with Significantly Altered Abundance in Kin-1 ^{KO1} and Kin-1 ^{KO2} cells	99
4	Discussion.....	103
4.1	Summary	103
4.2	Kindlin-1 is Dispensable for Proliferation and Clonogenic Potential in SCC-13 Cells.....	104
4.3	Defects in Cell Spreading on Collagen I, But Not on Laminin-332 Matrix	106
4.4	Loss of Kindlin-1 Enhances SCC-13 Migration in Culture.....	109

4.5	Reverse Phase Protein Array Analysis Reveal Differences in Protein Abundances Important for Carcinogenesis with the Loss of Kindlin-1 in SCC-13 Cells.....	111
4.5.1	Regulation of the Cell Cycle and Mitosis	111
4.5.2	Cell Responses to Stress	112
4.5.3	DNA Repair	114
4.5.4	Cytokine Signaling in the Immune System	115
4.5.5	Receptor Tyrosine Kinase Signaling.....	116
4.5.6	Proteins Involved in Negative Regulation of the PI3K/AKT Network	116
4.5.7	Signaling by RhoGTPases	117
4.6	Future Directions.....	118
4.7	Concluding Remarks	120
	References.....	122
	Curriculum Vitae	153

List of Tables

Table 1.1. Kindlin-1 binding partners	21
Table 2.1. Reagents	28
Table 2.2. Materials and equipment	30
Table 2.3. Antibodies.....	32
Table 2.4. Sequences of primers used to generate Kindlin-1 deficient SCC-13 cells.....	32
Table 3.1. Maximal mean area of cells spread on laminin-332 matrix.....	64
Table 3.2. Maximal mean area of cells spread on a low concentration of collagen I (1 $\mu\text{g}/\text{cm}^2$)	66
Table 3.3. Maximal mean area of cells spread on a medium concentration of collagen I (3 $\mu\text{g}/\text{cm}^2$)	70
Table 3.4. Proteins with increased abundance in Kindlin-1-deficient SCC-13 clonal lines	79
Table 3.5. Proteins with decreased abundance in Kindlin-1-deficient SCC-13 clonal lines	83
Table 3.6. Proteins with significantly increased or decreased abundance in Kin-1 ^{KO1} and Kin-1 ^{KO2} cells overrepresented in Reactome pathways.....	90
Table 3.7. Proteins with significantly increased or decreased abundance in Kin-1 ^{KO1} and Kin-1 ^{KO2} cells involved in regulating proliferation in SCC or keratinocytes	94
Table 3.8. Proteins with significantly increased or decreased abundance in Kin-1 ^{KO1} and Kin-1 ^{KO2} cells involved in regulating migration in SCC or keratinocytes.....	97

Table 3.9. Proteins with significantly increased or decreased abundance in Kin-1^{KO1} and Kin-1^{KO2} cells involved in the consensus integrin adhesome..... 100

Table 3.10. Phosphoproteins with significantly increased or decreased abundance in Kin-1^{KO1} and Kin-1^{KO2} cells 101

List of Figures

Figure 1.1. Schematic of the skin	3
Figure 1.2. Schematic of the epidermis.....	5
Figure 1.3. Model of integrin activation by adaptor proteins	10
Figure 1.4. Structural domains of Kindlin proteins.....	18
Figure 2.1. CRISPR/Cas9 targeting of FERMT1	36
Figure 3.1. Abundance of Kindlin-1 in Parental and CRISPR/Cas9 edited SCC-13 cells	51
Figure 3.2. Proliferation of Parental, Cas9 control, Kin-1 ^{KO1} , and Kin-1 ^{KO2} cells.....	54
Figure 3.3. Incorporation of BrdU into DNA in SCC-13 cell lines	56
Figure 3.4. Spheroid formation in Parental, Kin-1 ^{KO1} and Kin-1 ^{KO2}	60
Figure 3.5. Spreading of SCC-13 cells containing and lacking Kindlin-1 on laminin-332 matrix	63
Figure 3.6. Spreading of SCC-13 cell lines on a low concentration of collagen I	68
Figure 3.7. Spreading of SCC-13 cells on a medium concentration of collagen I	72
Figure 3.8. Directional migration of Parental, Kin-1 ^{KO1} and Kin-1 ^{KO2} SCC-13 cells.....	74
Figure 3.9. Principal component analysis and heat map of protein abundances in reverse phase protein arrays of SCC-13 cell lines	78

List of Abbreviations

Abbreviations	Full name
AK	Actinic keratosis
AKT	Protein kinase B
ALDH1	Aldehyde dehydrogenase 1
ANOVA	Analysis of variance
ATM	Serine-protein kinase ATM
AURKA	Aurora A
AXL	Tyrosine protein kinase receptor UFO
Bax	Apoptosis regulator BAX
BCC	Basal cell carcinoma
BrdU	Bromodeoxyuridine
BSA	Albumin Bovine Serum
CDC25C	Cell division cycle 25C
Cdc42	Cell division control protein 42 homolog
CDK1	Cyclin dependent kinase 1
CDK2	Cyclin dependent kinase 1
CDK5RAP2	Cyclin dependent kinase 5 regulatory subunit associated protein 2
CDKN1A	Cyclin dependent kinase inhibitor 1a
CDKN2A	Cyclin-dependent kinase inhibitor 2A
CHK1	Serine/threonine-protein kinase Chk1
CRISPR	Clustered regularly interspaced short palindromic repeats

cSCC	Cutaneous squamous cell carcinoma
DAB	3, 3'-diaminobenzidine
DMEM	Dulbecco's Modified Eagle Medium
DNA	Deoxyribonucleic acid
DTT	Dithiothreitol
ECM	Extracellular-matrix
EDTA	Ethylenediaminetetraacetic acid
EGFR	Epidermal growth factor receptor
EIF2AK3	Eukaryotic translation initiation factor 2 alpha kinase 3
EMT	Epithelial to mesenchymal transition
EPHA2	Ephrin type-A receptor 2
ERBB2	Receptor tyrosine-protein kinase erbb-2
ERBB3	Receptor tyrosine-protein kinase erbb-3
ERK	Extracellular signal regulated kinase
EZH2	Histone-lysine N-methyltransferase EZH2
FACS	Fluorescence activated cell sorting
FAK	Focal adhesion kinase
FBS	Fetal bovine serum
FERM	Four point one ezrin radixin moesin
FOXO3	Forkhead box O3
GAB2	Growth factor receptor bound protein 2-associated protein 2
GFP	Green fluorescent protein

GRB2	Growth factor receptor-bound protein 2
h	Hour(s)
HBSS	Hank's balanced salt solution
HDAC6	Histone deacetylase 6
HRP	Horseradish peroxidase
HSBP1	Heat Shock Factor Binding Protein 1
ICAP-1	Integrin cytoplasmic domain – associated protein 1
IgG	Immunoglobulin G
K1	Keratin 1
K10	Keratin 10
K14	Keratin 14
K5	Keratin 5
kDa	Kilodalton
LRG5	Leucine-rich repeat-containing G-protein coupled receptor 5
MAP1LC3A/B	Microtubule associated protein 1 light chain 3 alpha/beta
MAPK	Mitogen-activated protein kinase
MAPK14	Mitogen-activated protein kinase 14
MCF-7	Michigan Cancer Foundation 7
MDA-MB-231	MD Anderson Metastatic Breast 231
MDA-MB-468	MD Anderson Metastatic Breast 468
MEK	Mitogen-activated protein kinase
MIG-2	Mitogen-inducible gene 2

MLH1	DNA mismatch repair protein Mlh1
MMP	Matrix metalloproteinase
MMP7	Matrix metalloproteinase 7
MMP9	Matrix metalloproteinase 9
MUC1	Mucin 1
NaCl	Sodium chloride
NaF	Sodium Fluoride
OCT4	POU domain, class 5, transcription factor 1
PAK1	p21-activated kinase 1
PAK4	p21-activated kinase 4
PARG	Poly ADP-ribose glycohydrolase
PBS	Phosphate-buffered saline
PCA	Principle component analysis
PCNA	Proliferating cell nuclear antigen
PCR	Polymerase chain reaction
PFA	Paraformaldehyde
PH	Pleckstrin homology
PI3K	Phosphoinositide 3-kinase
PIK3CB	Phosphatidylinositol 4,5-bisphosphate 3-kinase catalytic subunit beta isoform
Plk-1	Polo-like kinase 1
PMSF	Phenylmethanesulphonyl fluoride
Poly-HEMA	Poly 2-hydroxyethyl methacrylate

PTPN11	Tyrosine-protein phosphatase non-receptor type 11
PTPN12	Protein tyrosine phosphatase non-receptor Type 12
PVDF	Polyvinylidene difluoride
RAB25	Ras-related protein rab-25
Rac1	Ras-related C3 botulinum toxin substrate 1
Ras	Rat sarcoma
RBBP8	DNA endonuclease RBBP8
RhoA	Ras homology gene family, member A
RICTOR	Rapamycin-insensitive companion of mTOR
ROS	Reactive oxygen species
RPA2	Replication Protein A2
RPPA	Reverse phase protein array
RRM1	Ribonucleoside-diphosphate reductase subunit M2
RTK	Receptor tyrosine kinase
SARA	Smad anchor for receptor activation
SCC	Squamous cell carcinoma
SD	Standard deviation
SDS	Sodium dodecyl sulphate
SDS-PAGE	Sodium dodecyl-sulfide polyacrylamide gel electrophoresis
SEM	Standard error of mean
siRNA	Small interfering ribonucleic acid
SOD2	Superoxide dismutase 2

SOX2	Transcription factor SOX-2
SRC	Proto-oncogene tyrosine-protein kinase
STAT1	Signal transducer and activator of transcription 1
SYK	Tyrosine-protein kinase SYK
TA	Transit amplifying
TBST	Tris-buffered saline with tween 20
TGF- β	Transforming growth factor beta
T β R1	Transforming growth factor beta receptor 1
ULK1	Serine/threonine-protein kinase ULK1
UV	Ultra-violet
VEGFR2	Vascular endothelial growth factor receptor 2
WEE1	Wee1-like protein kinase
WGA	Wheat germ agglutinin
WIPI1	Wd repeat domain, phosphoinositide interacting 1
Wnt	Wingless

1 Introduction

1.1 The Skin

The skin acts as a barrier between the organism and the external environment to protect against pathogens, UV light, water loss, and mechanical and chemical injury (reviewed in Baroni et al., 2012). The skin is composed of 2 main layers: the epidermis and the dermis, and it contains appendages such as hair follicles, sweat glands, and sebaceous glands (Fig. 1.1). The epidermis is the outermost layer of the skin and is mainly comprised of keratinocytes. The dermis is mainly composed of fibroblasts and connective tissue, which provide mechanical support to the skin (reviewed in Rittié, 2016). The epidermis is separated from the dermis by a basement membrane, a collection of extracellular matrix (ECM) proteins mainly comprised of collagen IV, laminin-332, perlecan, and nidogen (Behrens et al., 2012).

1.1.1 Overview of the Epidermis

The epidermis is a stratified squamous epithelium composed of undifferentiated cells in the stratum basale and several layers containing differentiated cells: stratum spinosum, stratum granulosum, and stratum corneum (reviewed in Baroni et al., 2012). The cell types found within the epidermis are Merkel cells, Langerhans cells, melanocytes and keratinocytes (Fig. 1.2). Keratinocytes are the most abundant cell type and provide the skin with its barrier functions. Melanocytes are responsible for producing and transferring melanin to keratinocytes determining skin colour, and for photoprotection. The Langerhans cells are the first immune defense of the skin, and the Merkel cells

Figure 1.1. Schematic of the skin. The skin is composed mainly of the epidermis and the dermis, separated by the basement membrane composed of extracellular matrix (ECM) proteins. The epidermis provides barrier functions to the skin and is composed mainly of keratinocytes. The dermis is composed mainly of fibroblasts and connective tissue, which provides the mechanical support to the skin. The skin contains appendages such as sweat glands, sebaceous glands, and hair follicles. Created with Biorender (<https://app.biorender.com/>).

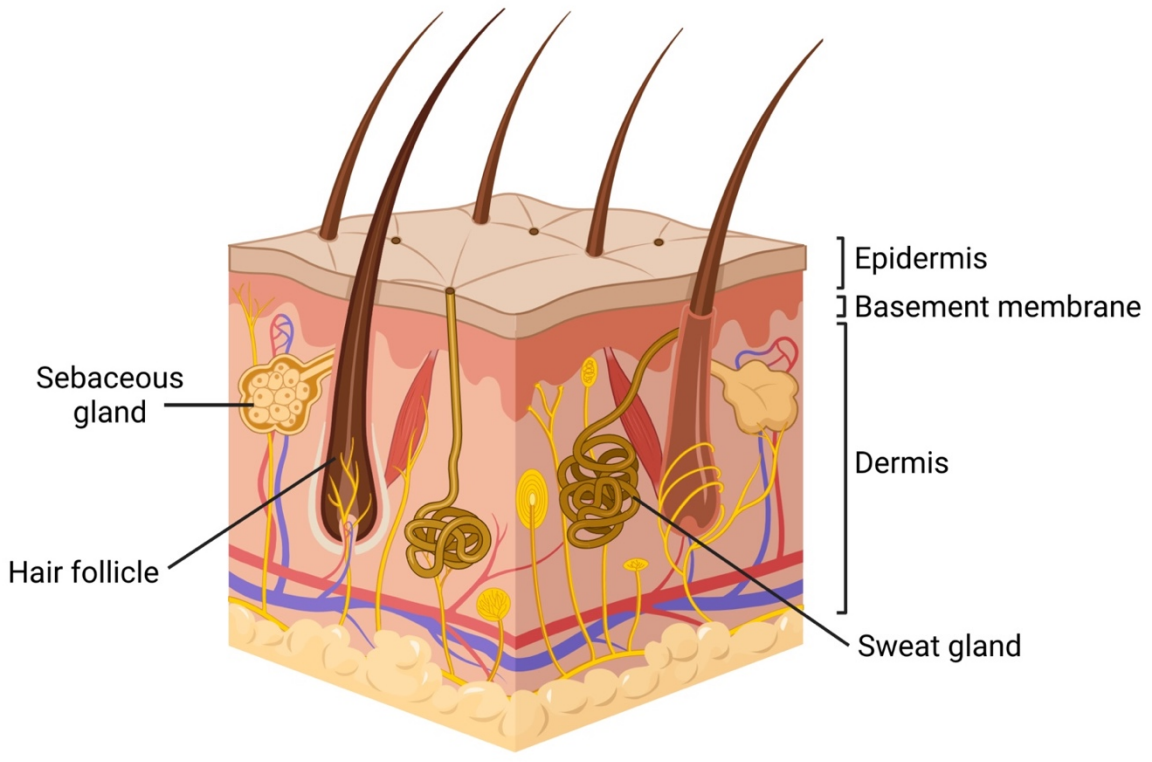
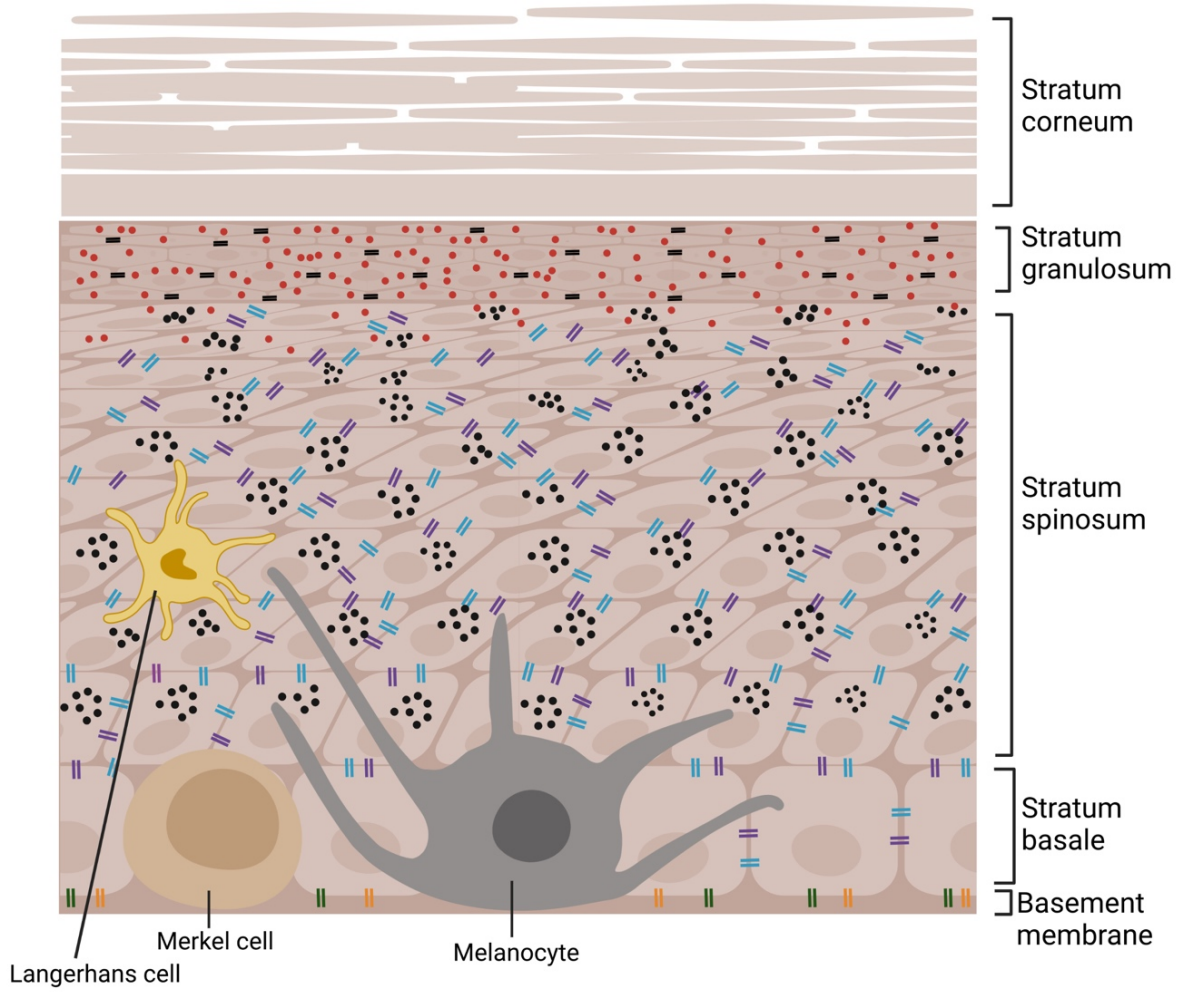


Figure 1.2. Schematic of the epidermis. The epidermis is made up of 4 cell layers termed stratum basale, stratum spinosum, stratum granulosum, and stratum corneum. The innermost layer is the stratum basale consisting of undifferentiated, basal keratinocytes. The stratum basale contains basal stem cells which proliferate to maintain the epidermis. Basal cells are attached to the basement membrane through hemidesmosomes (green) and focal adhesions (orange). As the basal stem cells divide, they produce transit amplifying (TA) cells that divide finitely in the inner layers of the stratum spinosum. Keratinocytes moving up the cell layers are exposed to a calcium gradient inducing differentiation. The cells in the stratum basale and spinosum are held together by cell-cell junctions termed desmosomes (purple) and adherens junctions (blue), while cells in the stratum granulosum adhere tightly to each other through tight junctions (black). Melanocytes in the basal layer produce and transfer melanosomes (black dots) to keratinocytes to protect their nuclei. Keratinocytes in the stratum spinosum and granulosum produce lamellar bodies (red dots) containing lipids important for forming the cornified envelope. Figure created with Biorender (<https://app.biorender.com/>).



Legend

- || = Hemidesmosomes
- || = Focal Adhesions
- || = Desmosomes
- || = Adherens Junctions
- = Tight Junctions
- = Melanosomes
- = Lamellar Bodies

act as mechanosensors for the sense of touch in the skin (reviewed in Baroni et al., 2012).

The epidermis is maintained by basal keratinocytes, which in turn consist of interfollicular stem cells and their undifferentiated progeny, transit amplifying (TA) cells.

The stem cells are slow cycling; capable of symmetrical division to produce either two stem or two TA cells, or asymmetric division to produce one stem cell and one transit amplifying cell. Transit amplifying cells can divide finitely, eventually losing their ability to divide in the stratum spinosum as they move toward the surface of the epidermis and slough off. This entire process takes up to four weeks in humans (Watt et al., 2016).

Basal cells can be characterized based on their expression of keratin 5 (K5), keratin 14 (K14) and high levels of β 1 integrins, whereas the cells of the suprabasal layers express keratin 1 (K1), keratin 10 (K10), increased levels of involucrin and, in intact epidermis, do not express integrins (Bott, 2014; Jones et al., 1993).

There is a balance between proliferation and differentiation that must be maintained to sustain a normal epidermis. For example, the proliferative capacity of stem cells is maintained by several proteins, including the transcription factor p63 (Koster et al., 2004). p63 expression is highest in stem cells and its repression results in decreased clonogenic potential (Senoo et al., 2007). Proliferation of keratinocytes is induced in response to various signals, such as those activated during wound healing, and to maintain epidermal homeostasis. The epidermal growth factor receptor (EGFR) becomes activated to maintain epidermal homeostasis, which signals through extracellular signal regulated kinase (Erk)- mitogen activated protein kinase (MAPK), resulting in the

activation of c-myc, inducing proliferation (Watt et al., 2008). Differentiation is induced through various processes, that include the downregulation of $\beta 1$ integrins, possibly due to a corresponding downregulation of Ras (reviewed in Watt, 2002).

1.1.2 Architecture and Functions of the Epidermal Layers

Basal keratinocytes strongly adhere to the underlying basement membrane through hemidesmosomes and focal adhesions (Arda et al., 2014). The stratum spinosum consists of several layers of keratinocytes, which exhibit moderate proliferation in the inner layers, as it contains transit amplifying cells which continue to proliferate finitely (Arda et al., 2014; Watt et al., 2016). The keratinocytes in this layer interdigitate and produce tonofilaments composed of keratins, which terminate at desmosomes, contributing to the strength of the skin (Arda et al., 2014). The stratum granulosum consists of flattened polygonal cells containing kerato-hyaline with pro-filaggrin (Arda et al., 2014). When pro-filaggrin is processed into filaggrin, it aids in packing keratin into tonofibrils (Fleckman et al., 1985). Granular keratinocytes form tight cell-cell junctions, important for the permeability barrier of the epidermis (Yoshida et al., 2013). The keratinocytes in the granular layer produce components of the cornified envelope that replaces the cell membrane in differentiated keratinocytes; first expressing proteins such as involucrin, which concentrate at the apical cell membrane and becomes cross-linked with other proteins through the action of transglutaminases (Kalinin et al., 2002). As cells move outward through the granular layer, they are exposed to higher levels of extracellular Ca^{2+} , causing lamellar granules containing lipids to be exocytosed from apical granular cells into the intercellular space (Kalinin et al., 2002). The lipids are in

turn cross-linked to scaffold proteins by transglutaminases, thus forming intercellular lamellae that replace the plasma membrane lipid bilayer (Kalinin et al., 2002).

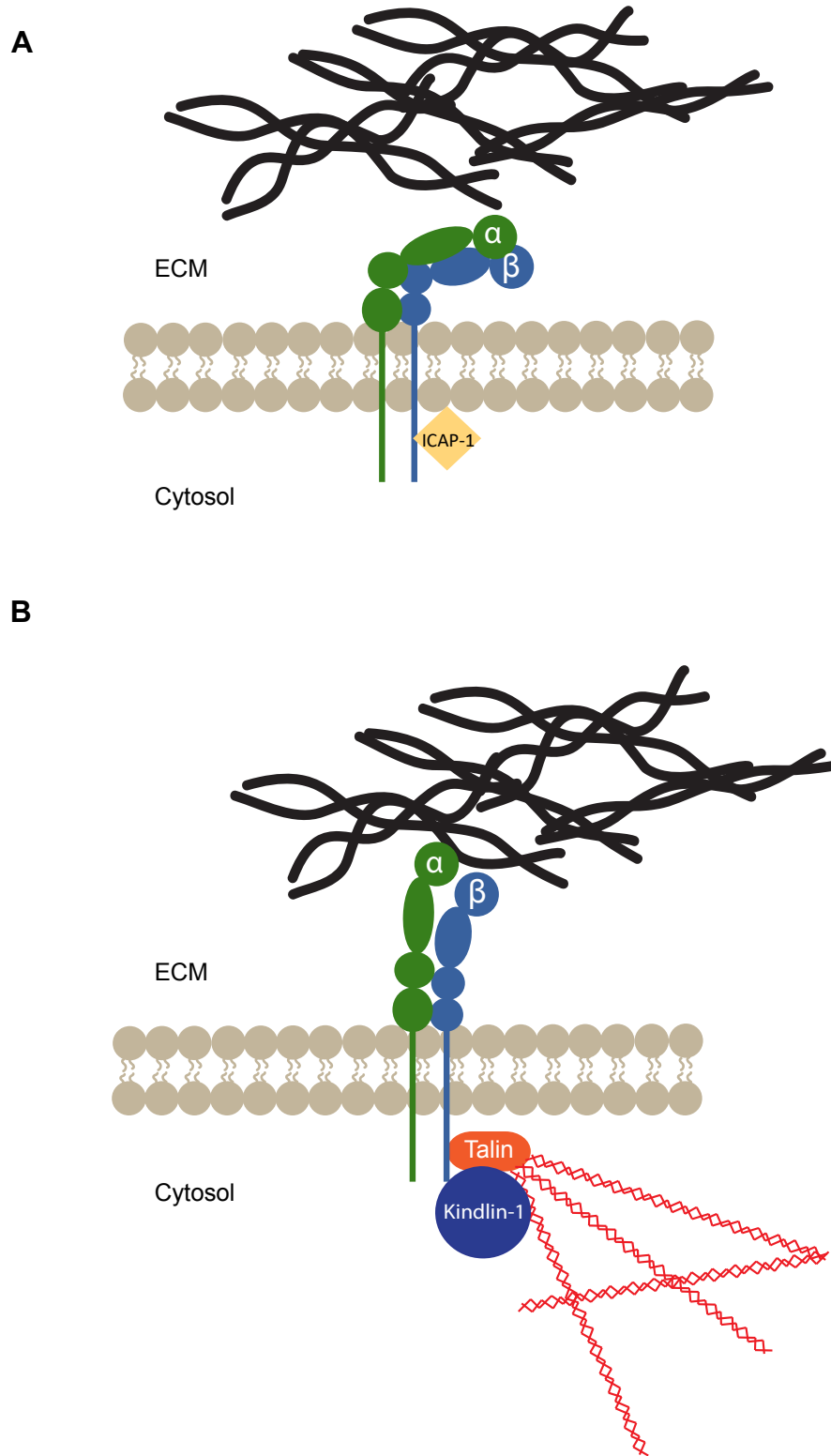
The stratum corneum is composed of flattened highly keratinized, enucleated cells termed corneocytes, that are continually sloughed off (Fuchs, 2008). The plasma membrane lipid bilayer in these cells is replaced with the proteins and lipids of the cornified envelope that connect to the dense network of keratin bundles, providing protection against water-loss, mechanical stress, and chemical and pathogen insults to the corneocytes (Madison, 2003).

1.2 Integrins

1.2.1 Integrins in the Epidermis

Integrins are heterodimeric transmembrane proteins composed of α and β subunits. There are 18 α and 8 β subunits, which give rise to 24 different heterodimers. The extracellular domains of distinct integrins bind to different ECM ligands, depending on the heterodimer formed (reviewed in Takada et al., 2007). In the intact epidermis, the most abundant heterodimers are $\alpha 2\beta 1$ (collagen receptor), $\alpha 3\beta 1$, and $\alpha 6\beta 4$ (laminin-332 receptors) (reviewed in Watt, 2002). $\alpha 3\beta 1$ integrins are key components of focal adhesions, which connect the actin cytoskeleton to laminin-332. The $\alpha 6\beta 4$ integrins are found in hemidesmosomes and connect keratin intermediate filaments to laminin-332 (Carter et al., 1990). The cytoplasmic tails of β integrins contain a proximal and distal NPxY motif, to which adaptor/signaling proteins, such as integrin cytoplasmic domain – associated protein 1 (ICAP-1), Talin and Kindlin, bind to modulate ligand binding (Fig. 1.3; Morse et al., 2014; Reszka et al., 1992).

Figure 1.3. Model of integrin activation by adaptor proteins. A) Integrins are in a low affinity state for their extracellular matrix (ECM) ligand (depicted in black) when they are in the bent conformation, induced by binding of inhibitor proteins, such as integrin cytoplasmic domain – associated protein 1 (ICAP-1) that block the binding of activating proteins. **B)** Integrins are brought into a high affinity state by binding of activating proteins such as Talin and Kindlins. These adaptor proteins bind to β integrin tails causing the integrin pair to straighten. Integrin binding to the ECM induces outside-in signaling such as signaling to induce actin polymerization (depicted in red).



Integrins are involved in bidirectional signalling. That is, the composition of intracellular adaptor/signalling proteins associated with integrins can affect the affinity of integrins for their ligands (inside-out signaling). Conversely, integrin binding to a ligand induces a variety of intracellular signaling cascades involved in cellular processes such as proliferation, adhesion, motility, differentiation, and survival (outside-in signaling) (Takada et al., 2007).

Whole organism deletion of $\alpha 6$ or $\beta 4$ integrins in mice results in blistering, loss of hemidesmosomes, and premature death, indicating the role of these proteins in adhesion to the basement membrane and proper epidermal function (Watt, 2002).

Global loss of $\beta 1$ integrins in mice is neonatally lethal, while targeted deletion of $\beta 1$ integrin in the epidermis results in blistering, reduced re-epithelialization upon wounding, and reduced spreading, proliferation and migration *in vitro* (Grose et al., 2002).

1.2.2 Integrins and Cancer

Integrins contribute to cancer development, maintenance and metastasis. $\alpha 6\beta 4$ integrins have been found to cooperate with mutant receptor tyrosine kinases (RTK) to induce proliferation, migration, and survival through activation of ERK and AKT/PI3K signaling (Janes et al., 2006). Furthermore, overexpression of $\alpha 6\beta 4$ integrins is associated with poor prognosis in epithelial cancers (Streulli et al., 2009). Integrins $\alpha 5\beta 1$ and $\alpha 2\beta 1$ have been shown to downregulate the activity and expression of p53, a tumor suppressor gene, contributing to tumor development and/or progression (Blandin et al., 2015).

Expression of $\alpha v\beta 6$ integrins in oral squamous cell carcinoma (SCC) cells in culture induces anchorage-independent expression of AKT, which prevents anchorage-dependent apoptosis (Janes et al., 2006). Integrins are known to regulate matrix metalloproteinase (MMP) expression, localization, and activation, which can enhance tumor invasion and progression (Blandin et al., 2015; Itoh et al., 2002). $\beta 1$ integrins are found to enable lymph node metastasis of head and neck SCC by anchoring of $\alpha 2\beta 1$, and $\alpha 6\beta 1$ integrins to laminin present in the lymphatic environment (Blandin et al., 2015).

1.3 Skin Carcinogenesis

Skin carcinogenesis is the process through which normal skin cells are transformed into cancer cells. Skin carcinogenesis has certain hallmarks to create a primary tumor, invade, and metastasize. For the primary tumor to form, gene mutations must arise to allow clonal expansion of cells harbouring the mutation, prevent cell death and senescence (Hanahan et al., 2011). To gain access to sufficient nutrients, the primary tumor must vascularize to establish a blood supply by inducing angiogenesis, or it must invade normal vascularized tissue. To begin local invasion and eventually metastasis, epithelial cells lose their adhesiveness to other cells, likely by downregulating E-cadherin, and undergo epithelial-mesenchymal transition (EMT). Metastasis to distant sites is induced when cancer cells intravasate into the lymph or blood stream, and then extravasate to a distant tissue to then form a microscopic tumor. That microscopic tumor must then establish itself in the new tissue environment and grow.

There are several types of skin cancers, named based on their cell type of origin. The most common skin cancer is basal cell carcinoma (BCC), followed by squamous cell

carcinoma (SCC) which together (termed keratinocyte carcinoma) account for an estimated 5.4 million cases of skin cancer in the U.S. according to the American Cancer Society (Didona et al., 2018). Also, keratinocyte carcinomas are the most common of all cancers in Canada, and constitute 40% of all cancers (*Canadian Cancer Statistics, 2014*). However, Canadian statistics regarding keratinocyte cancers are derived from only 4 provinces (Abbas et al., 2016). The most deadly skin cancer is melanoma, cancer of melanocytes that reside in the epidermis, which accounts for about 75% of all skin cancer deaths, despite comprising only 4% of skin cancer incidence (Davis et al., 2019). Other forms of skin cancer include Merkel cell carcinoma (Becker et al., 2018) and cutaneous lymphoma (Wilcox, 2018).

1.4 Keratinocyte Carcinomas

1.4.1 Basal Cell Carcinoma

Basal cell carcinoma is caused by malignant transformation of basal cells and adnexal appendages (Tanese, 2019). BCC is thought to arise *de novo* without precursor lesions (Didona et al., 2018). BCC is most prevalent in sun-exposed areas of light-skinned individuals, as the major risk factor for developing BCC is UV exposure (Didona et al., 2018). The most prevalent genetic mutations found in BCC result in activation of hedgehog signaling, through inactivation of repressors or stimulation of activators of the hedgehog pathway. A large fraction of BCC exhibit mutations in the gene that encodes Patched 1 (Hutchin et al., 2005; Marzuka et al., 2015). Despite the fact that BCC accounts for about 80% of keratinocyte cancer incidence, it has a mortality rate of 0.2%, and is most often treated by surgical removal (Didona et al., 2018).

1.4.2 Squamous Cell Carcinoma

Squamous cell carcinoma is cancer of the squamous epithelia. SCC can arise on the skin (cutaneous), on the epithelia that line the oral cavity, nasopharynx, oropharynx, hypopharynx, and larynx (these tumors are termed Head and Neck tumors) (Marur et al., 2008), lungs (Bonastre et al., 2016), and the esophagus (Chen et al., 2019). The most common type of SCC is cutaneous SCC (cSCC) representing 20-50% of all skin cancers (Que et al., 2018). A definitive diagnosis of SCC can only be achieved through biopsy of the lesion and histological examination of the specimen (Kallini et al., 2015). Ultraviolet radiation is the largest etiological agent that causes cSCC (Gordon, 2013). Cutaneous SCC has one of the highest mutational burdens of all cancers. Some of the most common mutations in cSCC are:

- *TP53*, which encodes p53, a tumor suppressor protein that induces apoptosis through the pro-apoptotic Bax pathway (Hanahan et al., 2000)
- *CDKN2A*, which encodes Cyclin-dependent kinase inhibitor 2A, a cell cycle checkpoint protein
- Ras, a signal transduction protein associated with pro-growth signals (Hanahan et al., 2000)
- Notch1, a receptor protein involved in differentiation, proliferation, and apoptosis in cSCC cells (South et al., 2014).

Unlike BCC, there are precancerous lesions in humans that precede SCC formation, termed actinic keratosis (AK). Actinic keratosis most frequently presents as scaling papules on sun-exposed areas (Moy, 2000). Histologically, AK is characterized by atypical keratinocytes with loss of polarity, nuclear pleomorphism, and an increase in mitotic figures in the basal layer of the epidermis (Siegel et al., 2017). It is unclear how many AKs undergo malignant transformation to become SCC, as the transition from the former to the latter is a continuum with no clear delineation between them. Estimates for

malignant conversion range from 0.025% to 20%, with higher rates seen in patients with multiple AKs (Siegel et al., 2017). There are two pathways identified for AK progression to SCC: classical and differentiated. In the classical pathway, AK cells of the lower third of the epidermis progress to the upper layers of the epidermis, which then turns invasive. In the differentiated pathway, atypical basal cells exhibiting AK characteristics undergo malignant transformation (Siegel et al., 2017). The most common risk factors for SCC metastasis is immunosuppression, tumor thickness, and local recurrence (Kallini et al., 2015).

The most common treatment for SCC is surgical excision with a wide surgical margin, however, if the lesion appear benign and not recurrent, it may be treated with cryosurgery (Kallini et al., 2015). When SCC is sufficiently advanced, such as with lymph node metastasis, treatment may involve removal of large areas of afflicted tissue, or amputation, followed by radiotherapy (Kallini et al., 2015). Certain genetic skin disorders can cause increased susceptibility to develop SCC. One such disorder is Kindler syndrome, caused by loss of functional Kindlin-1 (Saleva et al., 2018).

1.5 Kindlin

1.5.1 The Kindlin Family of Proteins

The Kindlin family of scaffold proteins includes three members in mammals. Kindlin-2 was first discovered in 1994, as an epidermal growth factor (EGF)-induced mRNA in a group of mitogen inducible genes and was named MIG-2 (Wick et al., 1994). The next protein identified in the Kindlin family was Kindlin-1. Kindlin-1 was identified by analyzing patient cohorts harbouring Kindler syndrome, where loss-of-function

mutations in Kindlin-1 lead to the syndrome (Siegel et al., 2003). To identify proteins similar to Kindlin-1, Siegel et al. (2003) evaluated genes with high sequence homology to Kindlin-1, which identified MIG-2, as well as the predicted gene MGC10966 (later termed Kindlin-2 and -3, respectively). The genes that encode Kindlin -1, -2, and -3 were subsequently named *FERMT1*, *FERMT2*, and *FERMT3*, respectively (Ussar et al., 2008). The Kindlin proteins contain a four-point-one ezrin, radixin, moesin (FERM) domain, which consists of three subdomains (F1, F2, and F3; Fig. 1.4A). Kindlins also contain a pleckstrin-homology (PH) domain within their F2 subdomain (Ussar et al., 2006). These subdomains contribute to the cloverleaf-like shape of Kindlin-1 (Fig. 1.4B; Rognoni et al., 2016). The FERM domain is involved in anchoring actin microfilaments to the plasma membrane, while the PH domain anchors the protein to the plasma membrane through interactions with phosphoinositides and contributes to integrin activation (Ussar et al., 2006; Yates et al., 2012). Uniquely, Kindlin-2 has a nuclear localization signal and has been found in the nucleus of certain tumor cells (Ussar et al., 2006). Kindlin-1 is exclusively expressed in epithelial cells, Kindlin-2 is ubiquitous, and Kindlin-3 is expressed in hematopoietic tissues (Ussar et al., 2006). In the skin, Kindlin-1 is expressed in the epidermis, whereas Kindlin-2 is present in keratinocytes and abundant in dermal fibroblasts (Ussar et al., 2006). Kindlin-1 and -2 are involved in integrin activation by binding directly to $\beta 1$ integrin tails at the NPxY distal motif via their FERM domain (Harburger et al., 2009).

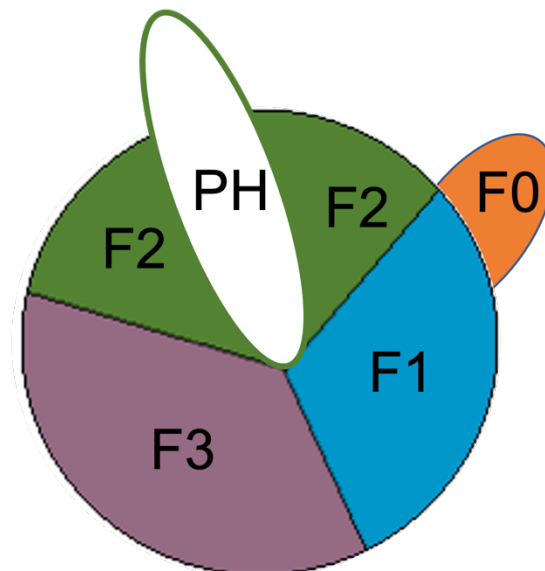
Figure 1.4. Schematic representation of the structural domains of Kindlin proteins.

Kindlins contain 5 structural domains. **A)** The F1, F2, and F3 domains contain a four-point-one ezrin, radixin, moesin (FERM) domain, important for anchoring actin to the plasma membrane, and binding to β integrin tails. Contained within the F2 domain is a pleckstrin homology (PH) domain, which anchors Kindlins to the plasma membrane and along with the F3 domain is involved in activating integrins. N terminal domain is on the left. **B)** The F domains of Kindlin-1 fold into a cloverleaf-like shape.

A



B



1.5.2 Structure of Kindlin-1

The Kindlin-1 gene, termed *FERMT1*, localizes to chromosome 20p12.3 (Lai-Cheong et al., 2009; Siegel et al., 2003). *FERMT1* is a 15-exon gene, 4931 bp long with a start codon in exon 2 and a stop codon in exon 15. It encodes a protein of 677 amino acids, with a calculated molecular mass of 77.3 kDa (Siegel et al., 2003). The N-terminus has sequence homology to talin (which binds and activates β integrin tails), and its C-terminus has homology to filopodin, involved in anchoring actin to focal adhesions.

Kindlin-1 is a phosphoprotein, and appears as a doublet on immunoblots with apparent molecular masses of 74 and 78 kDa (Herz et al., 2006). Herz et al. (2006) identified the phosphorylated form and the unphosphorylated form, respectively, as the 78-kDa and the 74-kDa species. It has been demonstrated that Kindlin-1 is phosphorylated by Polo-like kinase 1 (Plk-1) at centrosomes in mitotic cells, where it is involved in centrosome formation/maturation, and microtubule stability (Patel et al., 2016; Patel et al., 2013).

1.5.3 Biological Functions of Kindlin-1

Kindlin-1 is essential for normal development and skin homeostasis. In humans, loss of function mutations in the *FERMT1* gene cause Kindler syndrome, first identified in 1954 (Kindler, 1954). Individuals with Kindler syndrome suffer skin blistering and fragility, sun sensitivity at birth, which develops into poikiloderma, skin atrophy, palmoplantar hyperkeratosis, and webbed digits (Guerrero-aspizua et al., 2019; Kindler, 1954). Frequently, mucosal abnormalities are also present, causing hemorrhagic gingivitis and periodontal disease (Yildirim et al., 2017). Rarely, Kindler syndrome will present with ulcerative colitis, and esophageal and anal stenosis (Sadler et al., 2006).

In the epidermis, Kindlin-1 localizes to the basal aspect of basal keratinocytes at cell-matrix adhesion sites (Herz et al., 2006). Kindlin-1 is required for epidermal proliferation and polarization. Kindlin-1 deficient epidermis exhibits significantly reduced expression of the proliferative marker Ki67, and aberrant placement of transmembrane components at the basal aspect of the cell membrane (Herz et al., 2006). Basal keratinocytes lacking Kindlin-1 exhibit variable cell shape, whereas Kindlin-1 expressing basal cells retain a columnar shape, indicating Kindlin-1 is essential for maintaining normal cell morphology in the epidermis (Has et al., 2009). In culture, Kindlin-1-deficient basal keratinocytes exhibit abnormally elongated shape with multiple cell protrusions containing actin (Has et al., 2009). Kindlin-1 is required for normal activation of Rho-GTPases (Rac1, Cdc42, RhoA) and polarization to induce normal lamellipodia formation in keratinocytes (Has et al., 2009).

Kindlin-1 localizes to focal adhesions where it binds directly to the distal NPxY motif in $\beta 1$, $\beta 3$, and $\beta 6$ integrin cytoplasmic tails (Bandyopadhyay et al., 2012; Kloeker et al., 2004). Once bound to integrins, Kindlin-1 aids in talin-mediated activation of integrins, inducing a high affinity state for their ECM ligands and adhesion (Ussar et al., 2008).

Kindlin-1 binds to a variety of focal adhesion proteins, some of which are summarized in Table 1.1. Loss of Kindlin-1 does not affect the expression or localization of these proteins to focal adhesions; however, it can alter the distribution of focal adhesions in the cell (Has et al., 2009).

Table 1.1. Kindlin-1 binding partners

Protein	Reference
Migfilin	(Has et al., 2009)
β 1 integrin	(Has et al., 2009)
β 3 integrin	(Kloeker et al., 2004)
β 6 integrin	(Bandyopadhyay et al., 2012)
α -actinin	(Has et al., 2009)
Focal adhesion kinase (FAK)	(Has et al., 2009)
Kindlin-2	(Lai-Cheong et al., 2008)
Epidermal growth factor receptor (EGFR)	(Michael et al., 2019)
Src	(Qu et al., 2014)
T β R1	(Kong et al., 2016)
Smad3	(Kong et al., 2016)
Smad anchor for receptor activation (SARA)	(Kong et al., 2016)
Polo-like kinase 1 (Plk-1)	(Patel et al., 2013)
Aurora Kinase A	(Patel et al., 2013)
Cyclin dependent kinase 5 regulatory subunit associated protein 2 (CDK5RAP2)	(Patel et al., 2013)
Cyclin dependent kinase 1 (CDK1)	(Emmert et al., 2019)
Cyclin dependent kinase 2 (CDK2)	(Emmert et al., 2019)

Kindlin-1 is required for the recycling of internalized integrins to the plasma membrane, mediated by direct binding to β integrin tails. The recycling of integrins is important for integrin mediated processes such as cell spreading, migration and invasion (Margadant et al., 2013). Kindlin-1 regulates epidermal growth factor receptor (EGFR) surface protein levels in the skin through direct binding to EGFR, preventing its recycling by endocytosis (Michael et al., 2019). EGF signaling is important for regulating growth, differentiation, proliferation, and motility (Bakker et al., 2017). In terms of its regulation, Kindlin-1 is a transforming growth factor-beta (TGF- β) inducible gene, as exogenous expression of TGF- β leads to an increase in Kindlin-1 expression, inducing a mesenchymal phenotype (Kloeker et al., 2004). In MDA-MB-231 breast epithelial cells,

Kindlin-1 localizes to spindle poles in mitotic cells, driven by binding to and phosphorylation by Polo-like kinase 1 (Plk-1; Patel et al., 2013). At spindle poles, Kindlin-1 interacts with Plk-1, Aurora kinase A, and Cyclin dependent kinase 5 regulatory subunit associated protein 2 (CDK5RAP2) to induce normal centrosome formation (Patel et al., 2013). Additionally, Kindlin-1 is involved in regulating microtubule stability through interactions with histone deacetylase 6 (HDAC6) (Patel et al., 2016).

In mouse models, global loss of Kindlin-1 is neonatal lethal, owing to severe ulcerative colitis (Ussar et al., 2008). This differs from loss of Kindlin-1 in humans, where ulcerative colitis is rarely seen and is not lethal (Sadler et al., 2006). These differences may be due to high expression of Kindlin-1 in kidney, small intestines, and colon of mice, and differences in epidermal thickness between mice and humans (Ussar et al., 2006). To overcome the neonatal lethality of whole-organism loss of Kindlin-1 in mice, Rognoni et al. (2014) used a Cre-lox system to target deletion of Kindlin-1 to the skin. The study found Kindlin-1 is required for homeostasis of epidermal hair follicle stem cells, as loss of Kindlin-1 induces rapid expansion of the stem cell compartment and diminished stem cell composition later in life. This effect occurs independent of integrin binding, and is likely due to impaired $\alpha v \beta 6$ functionality preventing release of TGF- β from its inhibitor (Rognoni et al., 2014). Kindlin-1 is essential for normal Wnt/ β -catenin signaling, as loss of Kindlin-1 induces increased expression of canonical and non-canonical Wnts, as well as several Frizzled receptors, causing premature hair follicle anagen (Rognoni et al., 2014).

In mice and humans, loss of Kindlin-1 is associated with an increased risk of developing aggressive squamous cell carcinomas (Guerrero-aspizua et al., 2019; Rognoni et al., 2014). This increased incidence of SCC with the loss of Kindlin-1 may be due to Kindlin-1 role in protecting against UV-induced DNA damage, and cell stress (Emmert et al., 2017). Humans with Kindler syndrome have a 67% lifetime risk of developing SCC, and those that develop SCC have a 54% chance of developing metastatic disease (Guerrero-aspizua et al., 2019).

1.6 Kindlin-1 in Cancer

Kindlin-1 expression has been linked with different characteristics and outcomes on carcinoma development and progression, depending on the tissue of origin.

1.6.1 Lung Carcinoma

Kindlin-1 is overexpressed in 60% of lung carcinomas and its expression correlated with differentiated lung SCC (Weinstein et al., 2003; Zhan et al., 2012). Kindlin-1 was found in the nucleus of SCC cells on the invasive front indicating a cytoplasm to nuclear transition (Zhan et al., 2012). In lung adenocarcinoma cells, Kindlin-1 overexpression caused a decrease in EMT markers Vimentin and N-cadherin, and reduced hepatotactic migration on collagen I; matrix metalloproteinase 7 (MMP7) and MMP9 were also downregulated (Zhan et al., 2012). When Kindlin-1 overexpressing cells were xenografted onto mice, it impaired tumor growth, indicating Kindlin-1 negatively regulates lung carcinoma progression (Zhan et al., 2012).

1.6.2 Breast Carcinoma

High Kindlin-1 expression is associated with breast cancer aggressiveness, and high risk of lung metastasis (Sin et al., 2011). Kindlin-1 expression was higher in invasive metastatic breast cancer cell lines (MDA-MB-231 and MDA-MB-468), compared to poorly invasive cell lines (MCF-7 and SKBR3) (Sin et al., 2011). Stable expression of Kindlin-1 in MCF-7 cells causes more proliferation, clonogenicity, migration and cell spreading relative to controls, and an increase in mesenchymal markers Vimentin and N-cadherin, indicating Kindlin-1 increases breast cancer aggressiveness, likely due to an increase in TGF- β signaling (Sin et al., 2011). Loss of Kindlin-1 in MDA-MB-231 cells leads to a decrease in migration and invasion (Azorin et al., 2018).

In *in vivo* mouse models, knockout of Kindlin-1 delays mammary tumor onset (Sarvi et al., 2018) and diminishes tumor growth (Sin et al., 2011). Kindlin-1 knockout mice also exhibit reduced metastasis to lungs, likely due to a reduction in adhesion to the metastatic site due to diminished β 1 integrin activation (Sarvi et al., 2018).

1.6.3 Colorectal Carcinoma

High Kindlin-1 expression is correlated with progression of colorectal cancer and shorter overall survival (Kong et al., 2016). Stable overexpression of Kindlin-1 in colorectal cancer cells increased proliferation, clonogenicity, migration, invasion and expression of mesenchymal markers N-cadherin, Vimentin, leucine-rich repeat-containing G-protein coupled receptor 5 (LRG5), and MMP7; the opposite effect was found with depletion of Kindlin-1 (Kong et al., 2016). Injection of these cells overexpressing Kindlin-1 into mice causes an increase in tumor growth, indicating Kindlin-1 is required for colorectal cell

growth *in vivo* (Kong et al., 2016). As mentioned in Table 1.1, Kindlin-1 interacts directly with Smad3 and T β R1 at the N and C terminus respectively, and this interaction is important for activation of Smad3 and its translocation to the nucleus (Kong et al., 2016).

1.6.4 Pancreatic Carcinoma

Kindlin-1 expression is high in pancreatic cancer cells lines, but expressed at very low levels in normal pancreas (Mahawithitwong et al., 2013). *In vitro* loss of Kindlin-1 with siRNA in pancreas cancer cells causes a decrease in invasion and migration but has no effect on proliferation, indicating Kindlin-1 plays a role in pancreatic cancer metastasis (Mahawithitwong et al., 2013).

1.6.5 Esophageal Carcinoma

Kindlin-1 is upregulated in esophageal SCC compared to normal esophageal epithelium, and is positively correlated with tumor differentiation and progression (Wang et al., 2017). Interestingly, highly invasive esophageal SCC exhibit low expression of Kindlin-1, indicating Kindlin-1 may inhibit the invasive phenotype in these cancers (Wang et al., 2017). Esophageal epithelium is partially keratinized, similar to that seen in the epidermis, indicating there may be similarities in Kindlin-1 function in esophageal epithelium and the epidermis (Squier et al., 2001).

1.6.6 Keratinocyte Carcinoma

Knockout of Kindlin-1 in mouse cSCC cells causes increased levels of reactive oxygen species (ROS) following treatment with H₂O₂, leading to increased DNA damage and decreased ERK signaling which causes decreases in cell viability, and colony formation

(Emmert et al., 2017). This indicates Kindlin-1 protects against oxidative stress in cutaneous SCC. Additionally, individuals with Kindler syndrome, whom lack functional Kindlin-1, have a high incidence of metastatic SCC (Guerrero-aspizua et al., 2019). The general population carries a 0.001% risk for developing SCC, compared to Kindler syndrome patients, who have a 66% risk for developing SCC, as well as a 53% metastatic rate (Guerrero-aspizua et al., 2019). This indicates that the loss of Kindlin-1 causes a predisposition for metastatic SCC. The increased risk of metastatic SCC with the loss of Kindlin-1 in keratinocyte carcinoma differs from Kindlin-1 function in breast carcinoma (Sin et al., 2011), colorectal carcinoma (Kong et al., 2016), and pancreatic carcinoma (Mahawithitwong et al., 2013), where loss of Kindlin-1 causes a decrease in carcinoma progression, indicating Kindlin-1 may serve different functions based on the tissue of origin.

1.7 Rationale, Hypothesis and Aims

Previous work has shown that Kindlin-1 is important for the prevention of tumorigenesis, likely due to its protective effect against UV-induced DNA damage, and cell stress (Emmert et al., 2017). Furthermore, the loss of Kindlin-1 carries a large risk of developing aggressive epidermal SCC, suggesting its importance in preventing tumor progression. However, little work has been done to characterize how the loss of Kindlin-1 affects the behavior of human epidermal squamous cell carcinoma. Given that Kindlin-1 is thought to protect against carcinogenesis in normal keratinocytes, and that loss of Kindlin-1 in the epidermis contributes to tumorigenesis, ***I hypothesize that Kindlin-1 is essential for normal proliferation, adhesion, and motility in epidermal squamous***

carcinoma cells, such that loss of Kindlin-1 will alter these processes. To test this hypothesis, the specific aims of this study are:

1. *To determine the role of Kindlin-1 in epidermal squamous carcinoma cell proliferation and clonogenic potential.*
2. *To determine the contribution of Kindlin-1 to cell-ECM interactions.*
3. *To determine if Kindlin-1 is required for cell migration.*
4. *To identify novel signaling pathways regulated by Kindlin-1 in squamous carcinoma cells.*

2 Materials and Methods

2.1 Reagents

Reagents and their sources are listed in Table 2.1

Table 2.1. Reagents

Reagent	Source	Catalogue No.
5-Bromo-2'-Deoxy-Uridine	Roche, Indianapolis, IN	10280879001
Accutase® solution	Sigma-Aldrich, St. Louis, MO	A6956
Albumin Bovine Serum (BSA)	BioShop, Burlington, ON	ALB001
Ammonium persulfate	MP Biomedical, Santa Ana, CA	802811
Aprotinin	BioShop, Burlington, ON	APR200
B-27 supplement, serum free	Thermo Fischer Scientific, Waltham, MA	17504044
Bio-Rad Protein Assay Dye Reagent Concentrate	Bio-Rad Laboratories Inc., Hercules, CA	500-0006
BLUeye prestained protein ladder	FroggaBio, Concord, ON	PM007-0500F
Bromophenol blue	Fisher Scientific, Fairlawn, NJ	115-39-9
Clarity Western ECL Substrate	Bio-Rad Laboratories Inc., Hercules, CA	1705060
Dithiothreitol (DTT)	BioShop, Burlington, ON	3483-12-3
DNEasy Blood and Tissue kits	Qiagen, Toronto, ON	69506
Dulbecco's Modified Eagle Medium (DMEM) – high glucose	Sigma-Aldrich, St. Louis, MO	D6429
F-12 Nutrient mixture (Ham) with L-Glutamine	Life Technologies, Carlsbad, CA	11765-054

Table 2.1. Cont. Reagents

Reagent	Source	Catalogue No.
Fetal bovine serum (FBS)	Life Technologies, Carlsbad, CA	12483-020
Glycine	BioShop, Burlington, ON	56-40-6
Goat serum	Invitrogen, Carlsbad, CA	16210072
HCL	Caledon laboratories LTD	1789
Hoescht 33342, trihydrochloride, trihydrate	Invitrogen Molecular Probes	H1399
Igepal CA-630 (Nonidet P-40)	Fisher Scientific, Fairlawn, NJ	9002-93-1
Immu-mount™ mounting medium	Thermo Fischer Scientific, Waltham, MA	77-86-1
Leupeptin	BioShop, Burlington, ON	LEU001
Paraformaldehyde (PFA)	Sigma-Aldrich, St. Louis, MO	30525-89-4
Pepstatin	BioShop, Burlington, ON	PEP605
Phenylmethanesulphonyl fluoride (PMSF)	BioShop, Burlington, ON	PMS123
Poly 2-hydroxyethyl methacrylate (Poly-HEMA)	Sigma-Aldrich, St. Louis, MO	25249-16-5
Powdered skim milk	Carnation	Not available
Sodium Chloride (NaCl)	Caledon, Georgetown, ON	7647-14-5
Sodium deoxycholate	Sigma-Aldrich, St. Louis, MO	302-95-4
Sodium dodecyl sulphate (SDS)	BioShop, Burlington, ON	151-21-3
Sodium Fluoride (NaF)	Sigma-Aldrich, St. Louis, MO	S7920
Triton X-100	EMD, Darmstadt, Germany	CATX-1568
Trizma base	BioShop, Burlington, ON	77-86-1
Trypan Blue	ICN Biomedicals, Costa Mesa, CA	194600

Table 2.1. Cont. Reagents

Reagent	Source	Catalogue No.
Trypsin (0.25%) with 0.02% ethylenediaminetetraacetic acid (EDTA)	Thermo Fischer Scientific, Rockford, IL	25200072
Tween 20	Amresco, Solon, OH	0777
Rat Tail Collagen Type 1	Corning, Bedford, MA	35-4236

2.2 Materials and Equipment

Materials and equipment are listed in Table 2.2

Table 2.2. Materials and equipment

Material	Source	Catalogue No.
1.5-mL microcentrifuge tubes	Thermo Fischer Scientific, Waltham, MA	14-666-319
12-mm glass coverslips	VWR Scientific, Radnor, PA	48366-251
12-well cell culture plates	Fisher Scientific, Fairlawn, NJ	FB0129289
96-well cell culture plate	Corning, Bedford, MA	353872
Conical tubes, 15-mL	Sarstedt, Numbrecht, Germany	62.554.205
Conical tubes, 50-mL	Sarstedt, Numbrecht, Germany	62.547.205
Greiner Bio-One 10-mm cell culture dishes	VWR Scientific, Radnor, PA	664 160
Greiner Bio-One 24-well cell culture plates	VWR Scientific, Radnor, PA	662 160
25 mm syringe filter , 0.2 μ m pore size	Thermo Fischer Scientific, Waltham, MA	13-1001-06

Table 2.2. Cont. Materials and equipment

Material	Source	Catalogue No.
35-mm tissue culture dish with 2mm grid	Thermo Fischer Scientific, Waltham, MA	12-565-92
5-mL glass polystyrene tubes	BD Biosciences, Franklin Lakes, NJ	352235
Amersham TE-70 ECL semi-dry transfer unit	GE Healthcare Bio-Sciences, Mississauga, ON	80-6210-34
Disposable cell scraper	Fisher Scientific, Fairlawn, NJ	08-100-240
DU 640 Spectrophotometer	Beckman Coulter, Indianapolis, IN	410-066
Fisherbrand™ disposable cuvettes, 1.5 mL	Thermo Fischer Scientific, Waltham, MA	14-955-127
Immobilon polyvinylidene difluoride (PVDF) transfer membranes, 0.45 µm pore size	Millipore, Billerica, MA	IPVH00010
Leica DM IRBE inverted fluorescence microscope	Leica, Wetzlar, Germany	090-134.729-0000
T150 Cell Culture Flask	Thermo Fischer Scientific, Waltham, MA	130191
T25 Cell Culture Flask	Thermo Fischer Scientific, Waltham, MA	130189
T75 Cell Culture Flask	Thermo Fischer Scientific, Waltham, MA	130190
VesaDoc Imaging System	Bio-Rad Laboratories Inc.,	170-8280

2.3 Antibodies

Antibodies, their dilutions, and sources are listed in Table 2.3

Table 2.3. Antibodies

Antibodies	Dilution	Source	Catalogue No.	Lot No.
Goat anti-Mouse IgG (H+L), Alexa Fluor 555 conjugate	1:5 000	Life Technologies, Carlsbad, CA	A-21422	Not available
Mouse anti- γ -Tubulin	1:10 000	Sigma-Aldrich, St. Louis, MO	T6557	026M4832V
Mouse anti-BrdU	1:1 000	Developmental Studies Hybridoma Bank	G3G4	52242
Peroxidase-AffiniPure Goat anti-Mouse IgG (H+L)	1:5 000	Jackson ImmunoResearch, West Grove, PA	115-035-003	120344
Peroxidase-AffiniPure Goat anti-Rabbit IgG (H+L)	1:5 000	Jackson ImmunoResearch, West Grove, PA	111-035-003	120104
Peroxidase-AffiniPure Goat anti-Rabbit IgG (H+L)	1:5 000	Jackson ImmunoResearch, West Grove, PA	111-035-003	120104
Rabbit anti-Kindlin-1	1:250	Invitrogen, Carlsbad, CA	800-874-3723	710862
Wheat germ agglutinin (WGA) Alexa Fluor® 555 conjugate	1:400	Invitrogen, Carlsbad, CA	W32464	2110867

2.4 Primers

Primers and their sequences can be found in Table 2.4

Table 2.4. Sequences of primers used to generate Kindlin-1 deficient SCC-13 cells

Primer	Primer sequence (5'-3')
Exon 2 forward	ATATCTGGAGCACCTGGAACC
Exon 2 reverse	CACCAGCCATTAGTGGTGAGT
U6 promoter/gRNA cassette forward	GGTACCTCTAGAGCCATTTGTCTGC
U6 promoter/gRNA cassette reverse	TTTGCTAGCGAGGGCCTATTTCCCATGAT

2.5 Cell Lines and Culture

2.5.1 Parental and Kindlin-1-Deficient SCC-13 Cells

The SCC-13 cell line was a generous gift from Dr. Fiona Watt (King's College London, London, U.K.). SCC-13 cells were originally isolated from an epidermal facial tumor in a 56-year old woman (Rheinwald et al., 1981). Two monoclonal populations of SCC-13 cells in which the *FERMT1* gene was edited through CRISPR/Cas9 approaches (hereafter termed Kin-1^{KO1} and Kin-1^{KO2} cells) were generated in the Dagnino Laboratory by Dr. I. A. Ivanova, as described below (section 2.5.3).

All cells used were cultured in DMEM supplemented with 8% (v/v) fetal bovine serum (FBS) at 37°C in a humidified atmosphere containing 5% CO₂. Cells were passaged once they reached 80% confluency by gentle rinsing of the monolayer with phosphate buffered saline (PBS), followed by incubation with 0.25% trypsin with 0.02% (w/v) EDTA at 37°C. When approximately 100% of cells had detached, based on microscope examination (approx. 5 min), an equal volume of DMEM with 8% FBS was added to inhibit trypsin activity, and the resulting cell suspension was transferred to a 15-mL conical tube and centrifuged at 193 x *g* for 5 min at 22°C. The supernatant was removed, and the cell pellet was resuspended in DMEM with 8% FBS. Ten µL of the cell suspension were mixed with an equal volume of 0.4% trypan blue solution, and the number of viable, trypan-excluding cells in the cell suspension was determined with a hemocytometer. Cells were seeded as described for individual experiments.

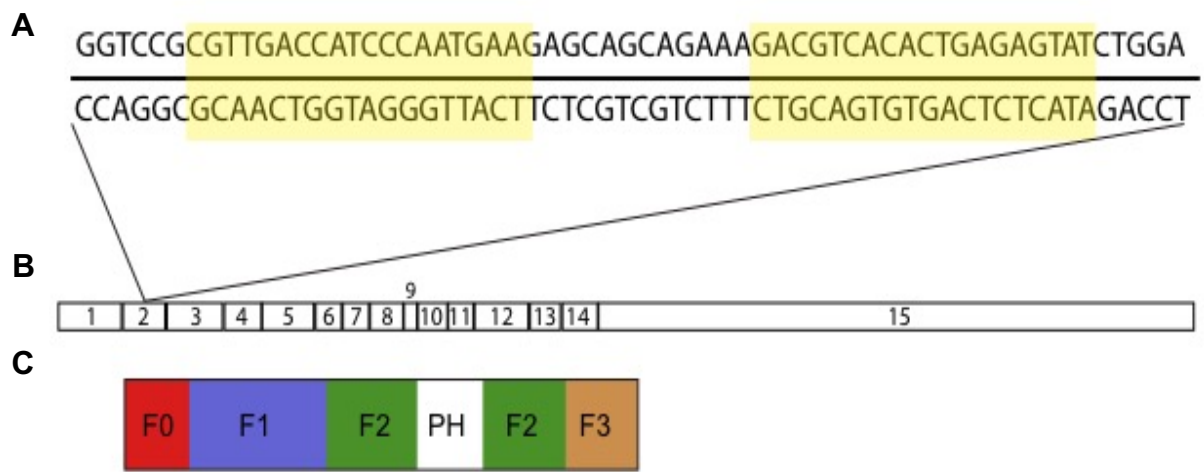
2.5.2 804G Rat Bladder Epithelial Cells

Dr. J.C. Jones (Northwestern University Medical School, Illinois, USA) generously provided our laboratory with 804G cells that secrete laminin-332 (Baker et al., 1996). 804G cells were maintained in DMEM supplemented with 8% FBS. To collect conditioned medium containing laminin-332 matrix, 804G cells were cultured in T150 cell culture flasks until confluent, as described (Dagnino et al., 2010). The culture medium was aspirated, cells were rinsed twice with 5 mL of PBS. The PBS was aspirated, replaced with 25 mL of serum-free DMEM and the cells were cultured at 37°C for 2 days. The conditioned medium was collected in a sterile 50-mL conical tube, centrifuged at $193 \times g$ for 5 min at 22°C, and filter sterilized through a 0.2- μm syringe filter. The conditioned medium was stored at 4°C and used within 2 weeks after harvesting.

2.5.3 Generation of CRISPR/Cas9 Targeted SCC-13 Cells

SCC-13 clonal cell lines with inactivation of the *FERMT1* gene were generated by Dr. I. Ivanova, using CRISPR-Cas9 gene editing. To this end, SCC-13 cells were transiently transfected with a pSpCas(BB)2A-GFP-based vector (Addgene plasmid # 48140; <http://n2t.net/addgene:48140>; RRID:Addgene_48140) (Ran et al., 2013), which was modified to encode two gRNAs (Table 2.4) that targeted exon 2 of the *FERMT1* gene (Fig. 2.1; Ivanova et al., unpublished). Cell transfections were conducted with polyethyleneimine, following procedures described in (Dagnino et al., 2010). Seventy-two hours after transfection, the cells were trypsinized, and green fluorescent protein (GFP)-expressing cells were purified and sorted using fluorescence activated cell sorting (FACS).

Figure 2.1. CRISPR/Cas9 targeting of *FERMT1*. Schematic of CRISPR targeting of *FERMT1*. **A)** Yellow highlighted regions indicate sgRNA sequences used to induce 2 double stranded breaks in *FERMT1*. **B)** Position of sgRNA within the genomic exons of *FERMT1*. **C)** sgRNA position corresponds to the very beginning of Kindlin-1 protein (F0 domain).



Single cells were seeded into each well of a 96-well plate to generate monoclonal populations. FACS experiments were conducted at the London Regional Flow Cytometry Facility of the Robarts Research Institute using a Becton Dickinson FACSAria III cell sorter (BD Biosciences, Mississauga, ON, Canada) with FACSDiVa software (v8.0.1).

To screen the monoclonal populations obtained for evidence of successful *FERMT1* gene editing, DNEasy Blood and Tissue kits (69506, Qiagen) were used to isolate genomic DNA (following the manufacturer's instructions), following 35-45 days of culture. The genomic DNA was analyzed by polymerase chain reaction (PCR), using primers to amplify the targeted *FERMT1* regions (Table 2.4). Amplicon sizes from the clonal cell populations were compared to amplicon size in Parental SCC-13 cells, and those with detectably smaller sizes were further cultured for protein analysis to confirm lack of detectable Kindlin-1 protein (Ivanova et al., unpublished).

2.6 Preparation of Lysates for Protein Analysis

Cells were plated onto 10-cm cell culture dishes and allowed to grow until 70-80% confluent. Cells were rinsed with ice-cold PBS and lysed by addition of ice-cold radioimmunoprecipitation assay (RIPA) buffer containing freshly added protease inhibitors (50 mM Tris-HCl pH 7.4, 150 mM NaCl, 1% Igepal CA-630, 0.5% sodium deoxycholate, 1mM PMSF, 1 µg/ml NaF, 1 µg/ml aprotinin, 1µg/ml pepstatin, 1 µg/ml leupeptin). Cell culture plates were placed on ice. The cells were gently scraped from the culture dishes using a sterile disposable cell scraper and transferred to 1.5-mL microfuge tubes. The lysates were incubated on ice for 20 min followed by centrifugation at 13,000 $\times g$ for 10 min at 4°C. The supernatant was then transferred to a clean microfuge tube.

The protein concentrations of the cell lysates were determined using a Bradford protein quantification Bio-Rad Protein Assay Dye Reagent Concentrate (Bio-Rad Laboratories, Hercules, CA). Absorbance of the samples was determined with a DU 650 Spectrophotometer (Beckman Coulter, Mississauga ON). For immunoblot experiments, 70 µg of lysate was added to a 1.5-mL microfuge tube and mixed with 1/6 volume of 6x Laemmli buffer (1 M Tris-HCl pH 6.8, 20% SDS, 4 mg/ml bromophenol blue, 40% glycerol, 0.06 g/ml DTT). The samples were heated for 10 min at 99°C prior to loading on denaturing polyacrylamide gels.

2.7 Denaturing Polyacrylamide Gel Electrophoresis (SDS-PAGE) and Immunoblot Analysis

Lysates were resolved by SDS-PAGE using 5% (w/v) stacking and 10% (w/v) separating polyacrylamide gels. Proteins in the gel were transferred to 0.45-µm polyvinylidene fluoride (PVDF) membranes using a TE-70 ECL semi-dry transfer apparatus (Amersham Bioscience). Membranes were blocked with 5% (w/v) non-fat milk diluted in Tris-buffered saline containing 0.05% (v/v) Tween-20 (TBST, 100 mM Tris-HCl pH 7.5, 1.5 M NaCl) for 1 h at 22°C or 16 h at 4°C (conditions which I found to be equivalent). For antibody probing, the membranes were placed in a tray containing 5 mL of primary antibody diluted in TBST (as per Table 2.3) and incubated with gentle rocking for 1 h at 22°C. Membranes were washed thrice with TBST, 5 min per wash, followed by incubation with 5 mL of HRP-conjugated secondary antibody solution (1:5 000 (v/v) in TBST containing 5% (w/v) non-fat milk) for 1 h at 22°C or 16 h at 4°C. The membranes were washed thrice with TBST (10 min per wash). Clarity Western ECL substrates were

mixed (1:1, v/v), and added to the membranes. Protein signals were visualized using a VersaDoc 4000 MP Imaging System (Bio-Rad Laboratories Inc.) with Quantity One software (V4.6.3).

2.8 Proliferation Assays

2.8.1 Growth Curve Assays

To generate cell growth curves and determine doubling times, 5×10^5 cells/mL of Parental SCC-13, Cas9 control, Kin-1^{KO1} and Kin-1^{KO2} cells were seeded onto 24-well cell culture dishes and cultured at 37°C. Every 24 h, up to 96 h after plating, cells were rinsed with 500 μ L of PBS, and detached from the culture dish with 250 μ L of 0.25% (v/v) trypsin with 0.02% (w/v) EDTA. Once all of the cells detached (~5 min), as determined through visual inspection with a microscope, 25 μ L of FBS were added to neutralize the trypsin. Ten μ L of cell suspension were mixed with an equal volume of 0.4% trypan blue solution, and the number of trypan blue-excluding cells in the solution was determined with a hemocytometer. Doubling times for each line were determined from the cell numbers obtained between 24 and 72 h for each replicate, using the following equation:

$$\frac{\ln(2)}{\ln\left(\frac{\text{final cell count}}{\text{initial cell count}}\right)} \times t$$

2.8.2 BrdU Incorporation Assays

Parental, Kin-1^{KO1} and Kin-1^{KO2} SCC-13 cells were plated in 1 mL DMEM with 8% (v/v) FBS in triplicate on a 24-well cell culture plate at a seeding density of 1×10^5 cells/mL and cultured overnight. Medium was replaced with 1 mL of pre-warmed (37°C) medium containing 10 μ M BrdU and incubated for 2 h at 37°C. The cells were rinsed twice with 1

mL of PBS and fixed with ice-cold freshly diluted 4% (w/v) paraformaldehyde (PFA) in PBS for 20 min at 22°C with rocking. The PFA was quenched with 1 mL of 100 mM glycine in PBS, and cells permeabilized with 250 μ L of 0.1% (v/v) Triton X-100 and 0.1% (w/v) bovine serum albumin (BSA) in PBS for 20 min at 22°C with rocking. DNA was denatured by incubation with 250 μ L of 2M HCl for 20 min at 22°C. The HCl was removed, and the samples were subjected to five 10-min washes with 1 mL PBS each. Cells were incubated with 250 μ L blocking solution (3% (w/v) skim milk containing 5% (v/v) goat serum in PBS) for 1 h at 22°C with rocking, and then incubated with 250 μ L of mouse anti-BrdU antibody (G3G4) diluted with PBS 1:1000 (v/v) for 1 h at 22°C with rocking. Cells were rinsed thrice, 10 min per wash, in PBS with rocking at 22°C. Cells were then incubated with 250 μ L of goat anti-mouse Alexa 555 diluted 1:500 (v/v) in blocking solution for 1 h at 22°C with rocking and protected from the light. DNA was stained with 250 μ L of Hoechst 33342 in PBS diluted 1:10 000 (v/v, 1 ng/ μ L, final) for 5 min with rocking at 22°C, protected from the light. Wells were covered with 12-mm glass coverslips, mounted with 5 μ L of Immu-mount medium, and allowed to dry overnight at 4°C, protected from the light. Fluorescence micrographs were obtained with a Leica DM IRBE fluorescence microscope equipped with an ORCA-ER digital camera (Hamamatsu Photonics), using Volocity 6.1.1 software (Improvision). The number of BrdU-positive cells were determined and compared to the total number of nuclei to assess the fraction of BrdU-positive cells.

2.9 Spheroid Formation Assays

Spheroid formation assays were conducted using 6-well plates or 35-mm grid cell culture dishes. To this end, the culture surfaces were coated with 2.5 mL of 1.2 % (w/v) Poly-HEMA dissolved in 95% ethanol and allowed to evaporate in a laminar flow hood for 16 h at 22°C. The plates were sterilized in a laminar flow hood by exposing them to UV light for 1 h prior to use. To generate spheroids, Parental, Kin-1^{KO1} and Kin-1^{KO2} SCC-13 cells were cultured in T25 flasks until 80% confluent, then rinsed twice with 3 mL PBS, and detached with 2 mL 0.25% (v/v) trypsin with 0.02% (w/v) EDTA. Once the cells had detached, as determined through visual inspection with a microscope (~5 min), an equal volume of DMEM with 8% (v/v) FBS was added. The cell suspension was transferred to a 15-mL conical tube and centrifuged at 193 $\times g$ for 5 min at 22°C. The supernatant was removed, and the cell pellet was resuspended in spheroid medium (DMEM/F12, 1:1 (v/v)) supplemented with 2% (v/v) B27 supplement, 20 ng/mL EGF, 4 μ g/mL insulin and 0.4% (w/v) BSA). The number of cells in this suspension was determined with a hemocytometer, and cell density was adjusted to 6 500 cell/mL. Aliquots containing 2.5 mL of the cell suspension were plated in triplicate wells and cultured at 37°C. Fresh spheroid medium (250 μ L) was added to each well every 5 days. Phase contrast images of all spheroids in each well were obtained using a Leica DM IRBE microscope equipped with an ORCA-ER digital camera (Hamamatsu Photonics), using Volocity 6.1.1 software (Improvision), 5, 10, and 15 days after plating. Spheroids were analyzed using the manual tool in ImageJ (V1.51) to trace all spheroids to determine spheroid perimeter

and area. This approach also allowed the determination of the number of spheroids in each well.

2.10 Cell Spreading Experiments

2.10.1 Analysis of Cell Spreading

For cell spreading assays on laminin-332 matrix, 24-well plates were coated with 1 mL of laminin-332 matrix-containing conditioned medium from 804G cells as described above, for 1 h at 37°C. The conditioned medium was aspirated and Parental, Kin-1^{KO1} or Kin-1^{KO2} SCC-13 cells, suspended in 1 mL of DMEM with 8% (v/v) FBS, were plated in triplicate at a seeding density of 3x10⁴ cells/well and incubated at 37°C. For cell spreading assays on collagen I, 24-well plates were coated with collagen 1 (1 µg/cm² or 3 µg/cm², as indicated in individual experiments) for 1 h at 22°C. The collagen solution was aspirated, the wells were rinsed with 1 mL of PBS thrice, and Parental, Kin-1^{KO1} and Kin-1^{KO2} SCC-13 cells, suspended in 1 mL of DMEM with 8% (v/v) FBS, were plated in triplicate at a seeding density of 3x10⁴ cells/well, and cultured at 37°C. At timed intervals indicated in individual experiments, the cell culture plates were rinsed with 1 mL of Hanks balanced salt solution (HBSS) and fixed with 200 µL of freshly diluted, ice cold 4% (w/v) PFA in PBS. The cells were then incubated for 20 min at 22°C with rocking. Cells were rinsed twice with HBSS and labelled with 200 µL of Alexa Fluor® 555-conjugated wheat germ agglutinin (WGA, 5.0 µg/mL) for 10 min at 22°C with rocking and protected from the light. Cells were rinsed twice with HBSS, and nuclei were labelled with Hoechst 33342 diluted in PBS (1 ng/µL) for 5 min at 22°C, with rocking. Cells were rinsed thrice in HBSS, mounted with Immu-mount mounting medium, covered with 12-mm glass coverslips,

and allowed to dry overnight at 4°C, protected from the light. Photomicrographs were obtained using a Leica DM IRBE microscope equipped with an ORCA-ER digital camera (Hamamatsu Photonics, Hamamatsu City, Shizuoka, Japan), using Volocity 6.1.1 software (Improvision, Coventry, United Kingdom). Photomicrographs were analyzed using CellProfiler to render cell outlines, as described below. The area of 100 cells was determined for each experiment.

2.10.2 CellProfiler Analysis of WGA Images

To automate cell surface area measurements, a CellProfiler software (V3.1.9) pipeline was created to render the cell contour and measure the cell area. Images of nuclei stained with Hoechst 33342, and plasma membranes stained with the Alexa Fluor® 555-conjugated WGA were converted into greyscale. A threshold was applied to each image separately, using a global threshold. This allowed the calculation of a single threshold value for each image which classified pixels above this threshold value as foreground, and below this threshold as background. The global threshold was calculated using the robust background method, which assumed the pixel intensities were normally distributed, and removed 2% of the lower fraction of pixel intensities and 0.5% of the upper fraction of pixel intensities as outlier pixel intensity values. These percentages were experimentally determined by visually determining the effect of fractions of outliers removed on the thresholding of the cells to achieve the most accurate thresholding of each cell and manually set in the software. The median and standard deviation of the remaining pixels were then determined by the software, and the global threshold for each image was calculated as the median + 5 times the standard deviation

of pixel intensities (the number of standard deviations added to the median was established by visually determining the effect of taking into account different numbers of standard deviations on the thresholding of the cells and manually setting in the software).

This thresholding produced a black and white image for nuclei and cell membranes, where background was converted to black, and foreground to white. The outline of each nucleus from the threshold nuclei image was identified by the software using the Otsu thresholding method, which separated the two classes of pixels (foreground and background) by minimizing the variance within each class. The nuclei outlines were then mapped onto the corresponding cell in the thresholded cell image to ensure only cells with identifiable nuclei were rendered. Once the nuclei outlines were mapped onto their corresponding cell, the outline of each cell was identified using the same Otsu thresholding method as for the nuclei images. Cell outlines were plotted onto the original input cell image by the software, and visually verified to ensure only correctly rendered cell outlines were considered for further analysis. The cell outlines that were approved as correctly rendered were then used to calculate the area of each cell. The area of one hundred cells were measured for each cell line in each biological replicate.

2.11 Migration Assays

For scrape-wound migration assays, Parental, Kin-1^{KO1} and Kin-1^{KO2} SCC-13 cells were suspended in DMEM with 8% (v/v) FBS and plated in triplicate onto 12-well cell culture plates, at a seeding density of 2×10^6 cells/mL, and cultured to confluence. The cell monolayer was scraped using a p10 pipette tip to create a scrape in the monolayer. The

culture medium was aspirated to remove cell debris and replaced with 1 mL fresh DMEM with 2% (v/v) FBS. Phase-contrast images of the denuded area were obtained using a Leica DM IRBE microscope equipped with an ORCA-ER digital camera (Hamamatsu Photonics), using Volocity 6.1.1 software (Improvision) immediately following scraping, and every 4 h subsequently, up to 12 h. The cell-free area in the scrape-wound was determined using the MRI Wound Healing plugin from ImageJ.

2.12 Reverse Phase Protein Array (RPPA) Analysis

To obtain total cellular protein in the form of cell pellets Parental, Kin-1^{KO1} and Kin-1^{KO2} SCC-13 cells were cultured in 10-cm dishes to 80% confluency with DMEM supplemented with 8% (v/v) FBS. Cells were detached from the culture surface with a disposable cell scraper and centrifuged at 140 x *g* for 5 min at 22°C. The supernatant was removed by aspiration and cell pellets were immediately frozen to -80°C. The cell pellets were processed and analyzed at the RPPA core facility of the MD Anderson Cancer Center (Houston, TX, USA). To this end, relative protein levels were determined from curves generated using serial lysate dilutions spotted onto nitrocellulose membranes, which were subsequently probed with a given antibody, and visualized with a 3, 3'-diaminobenzidine (DAB) colorimetric reaction, followed by densitometry analysis. Protein levels were then normalized for sample loading, determined using SYPRO Ruby protein fluorescence dye staining.

Using the log₂-median centered values of protein intensity, principal component analysis (PCA) was conducted by Drs. S. Sayedyahosseini, M. Karimi and M. Bahmani using free, publicly available RStudio Cloud software (<https://rstudio.cloud/plans/free>). PCA is a

dimensionality-reduction method, which is used to reduce the number of dimensions of a large data set, by grouping a large set of variables into a single variable, termed principal components, that contains most of the information from the larger set of variables. The principal components can then be represented as the axes in a coordinate system, with the samples placed within the system based on how much each principal component explains the variation for each sample. RStudio Cloud was also utilized to identify those proteins whose abundance was significantly different between Parental, and Kin-1^{KO1} and Kin-1^{KO2} cells, thus allowing the generation of heatmaps.

Those proteins identified to have significantly different abundance between Parental and Kin-1^{KO1} and Kin-1^{KO2} cells were then separated based on mean-fold difference in levels from the mean calculated protein levels in Kin-1^{KO1} together with Kin-1^{KO2} clones, relative to Parental SCC-13 cells.

2.13 Statistical Analyses

For immunoblot analysis of Kindlin-1 abundance, three biological replicates were analyzed and normalized to γ -tubulin abundance. Statistical significance of the normalized protein abundances was determined using an ordinary unpaired one-way analysis of variance (ANOVA) with Tukey's post hoc test. Significance was set at $P < 0.05$.

For proliferation studies using growth curves, each biological replicate contained triplicate samples (i.e. three technical replicates, obtained from triplicate culture wells).

The significance of differences in doubling times was determined using an ordinary unpaired one-way ANOVA with Tukey's post hoc test. Significance was set at $P < 0.05$.

For proliferation studies using BrdU labelling, each biological replicate contained triplicate technical replicates, with at least 300 nuclei/sample (100/well) counted. To determine the significance of the number of BrdU positive cells in cell lines containing or lacking Kindlin-1, I used an unpaired one-way ANOVA with Tukey's post hoc test. Significance was set at $P < 0.05$.

For spheroid formation assays, each biological replicate contained triplicate technical replicates. A two-way mixed model ANOVA with Tukey's post hoc test was used to determine the significance of spheroid number, and perimeter between Parental and Kin-1^{KO1} and Kin-1^{KO2} cells. One-way repeated measures ANOVA with Tukey's post hoc test was used to determine the significance of spheroid number across each time point for each cell line. To determine the significance of spheroid perimeter bins at each time point for each cell line, a two-way mixed model ANOVA with Tukey's post hoc test was conducted. Significance was set at $P < 0.05$.

For cell spreading studies, each biological replicate contained duplicate technical replicates, with 100 cells/sample (50/well). In these experiments, maximum cell spread was calculated for each replicate in each cell line by setting the area values at the time point with the greatest mean area to 100%, and the mean area of the other time points was expressed as the percentage of the greatest mean area. Differences in the percent of maximum spread between Parental and Kin-1^{KO1} and Kin-1^{KO2} cells was determined using a two-way mixed model ANOVA with Tukey's post hoc test. Significance was set at $P < 0.05$.

For scrape-wound experiments, each biological replicate included triplicate technical replicates. Wound area values were converted to a percent of the wound area at time zero (with wound area at time zero set to 100%). The significance of differences in the percentage of wound area between Parental and Kin-1^{KO1} and Kin-1^{KO2} cells was determined using a two-way mixed model ANOVA with Tukey's post hoc test.

Significance was set at $P < 0.05$.

For RPPA studies, there were three biological replicates per sample, containing three technical replicates. The significance in differences of relative protein abundance was determined using an unpaired t-test, comparing the mean protein levels from three biological replicates (comprised of the mean of three technical replicates) in Parental cells to the mean protein levels of both Kin-1^{KO1} and Kin-1^{KO2} lines. Significance was set at $P < 0.05$

All statistical analysis was done with GraphPad Prism version 6.

3 Results

3.1 Abundance of Kindlin-1 Protein in SCC-13 Cell Lines

To investigate the role of Kindlin-1 in epidermal squamous carcinoma cells, two monoclonal populations of CRISPR/Cas9 gene-edited SCC-13 cells (hereafter termed Kin-1^{KO1} and Kin-1^{KO2} cells) were generated in our laboratory (Ivanova et al., unpublished). To confirm that editing of the *FERMT1* gene had generated Kindlin-1-deficient cell populations, I first investigated the abundance of Kindlin-1 protein in Parental, Cas9 control, Kin-1^{KO1} and Kin-1^{KO2} SCC-13 cell lines. Cas9 control cells are a polyclonal population of SCC-13 cells, transiently transfected with a Cas9 plasmid lacking guide RNA, generated as a negative control to determine if Cas9 expression alone results in off-target effects. To this end, I prepared protein lysates and analyzed them by immunoblot with antibodies against Kindlin-1 or γ -tubulin (used as a loading control). Kindlin-1 was present in both Parental and Cas9 control cells at similar levels, whereas Kindlin-1 protein was undetectable in both Kin-1^{KO1} and Kin-1^{KO2} cells (Fig. 3.1). This confirms CRISPR/Cas9 editing of the *FERMT1* gene, with a resulting loss of detectable Kindlin-1 protein in Kin-1^{KO1} and Kin-1^{KO2} cells.

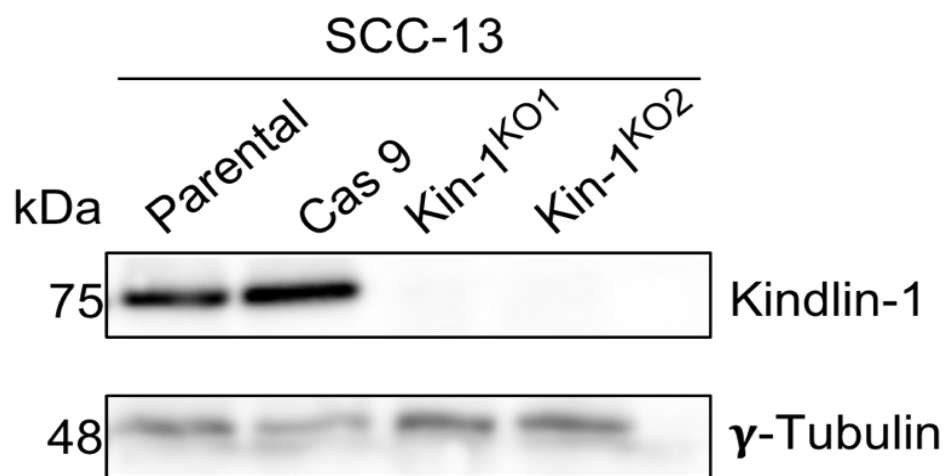
3.2 Proliferation of Kin-1^{KO1} and Kin-1^{KO2} Cells

To determine the consequences of loss of Kindlin-1 protein on SCC-13 cell proliferation, I assessed changes in cell numbers as a function of time in exponentially proliferating Parental, Cas9 control, Kin-1^{KO1} and Kin-1^{KO2} SCC-13 cells. I determined cell numbers at 24-hour intervals following seeding. Parental SCC-13 cell numbers modestly increased 24 h after plating, likely reflecting the combined effects of plating efficiency, as cells attach

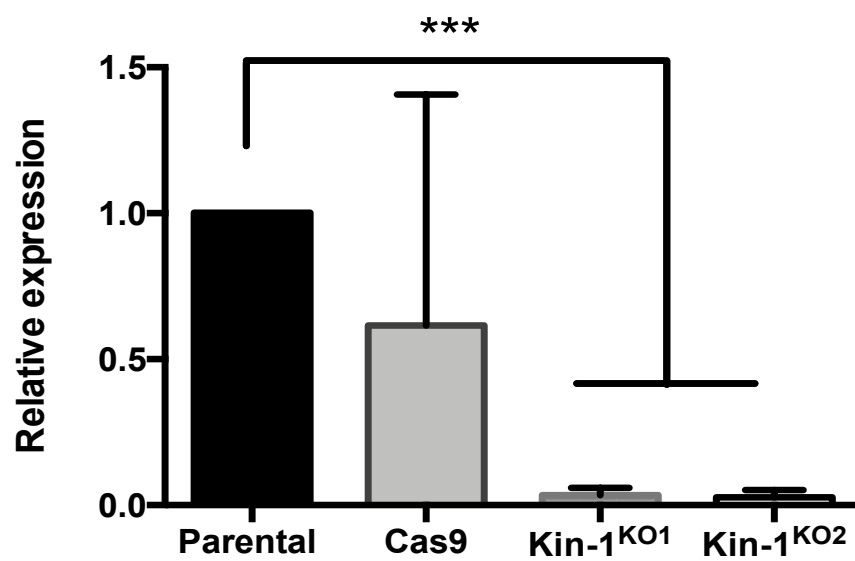
Figure 3.1. Abundance of Kindlin-1 in Parental and CRISPR/Cas9 edited SCC-13 cells. A)

Immunoblot of Kindlin-1 expression using cell lysates from Parental, Cas 9 control, Kin-1^{KO1} and Kin-1^{KO2} SCC-13 cell lines, embedded in PVDF membrane, probed with antibodies against Kindlin-1 and γ -Tubulin (used as loading control). **B)** Densitometric quantification of Kindlin-1 levels in the indicated SCC-13 cell lines. The results are expressed relative to Kindlin-1 abundance, normalized to γ -Tubulin, in Parental SCC-13 cells, which is set to 1.0. The data are shown as the mean + SD (one-way ANOVA with Tukey's post hoc test, n=3). ***p<0.001

A



B



to the culture dish and begin to proliferate (Fig. 3.2A). Between 24 and 72 h of growth, Parental cells exhibited linear growth, indicative of an exponentially proliferating cell population, which continued to 96 h. Cas9 control cells also exhibited a modest increase in cell number at 24 h compared to the initial plating density. By 72 h, the Cas9 control cells were in the exponential phase, which, similar to the Parental cells, continued to 96 h (Fig. 3.2A). Both Kin-1^{KO1} and Kin-1^{KO2} cells had a slight reduction in cell number 24 h after plating, likely reflecting plating efficiency. However, similar to Parental cells, they showed exponential cell growth between 24 and 72 h. The growth of Kin-1^{KO1} and Kin-1^{KO2} cells between 72 and 96 h, contrasted with that of the Parental and Cas9 control cells, as the former showed slower growth, (shallower slope) which likely reflected the beginning of the plateau phase (Fig. 3.2A).

Doubling times were calculated using the cell numbers measured 24 and 72 h after plating, because during this period all of the cell lines were in the exponential phase of growth, a requirement for accurate determination of doubling times (Hall et al., 2014).

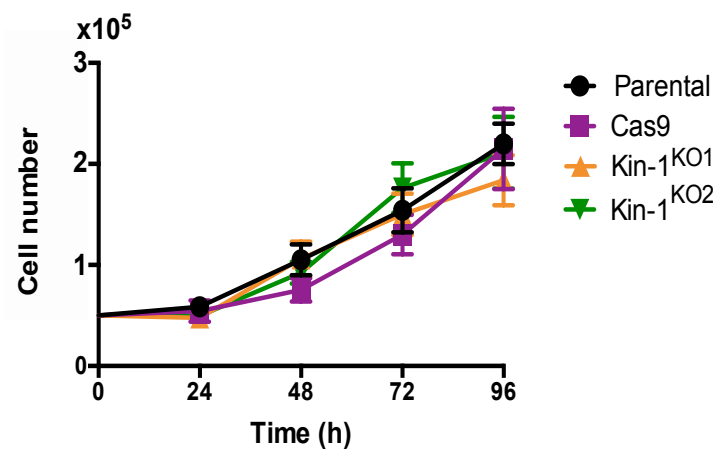
The mean doubling time of the Parental cells was 36.5 ± 2.9 h. There were no significant differences in the doubling times of Cas9 control, Kin-1^{KO1} and Kin-1^{KO2} cells compared to Parental cells (Figure 3.2B).

To complement these proliferation assays, I also analyzed the fraction of cells in the S-phase of the cell cycle, using a 2-h bromodeoxyuridine (BrdU) pulse. I then analyzed the fraction of cells that showed BrdU incorporation into newly synthesized DNA, using immunofluorescence microscopy (Fig. 3.3A). The mean percentage of cells in S-phase for Parental, Kin-1^{KO1} and Kin-1^{KO2} cell lines was 25.4 ± 3.8 , 32.8 ± 3.8 , and 25.6 ± 1.8 ,

Figure 3.2. Proliferation of Parental, Cas9 control, Kin-1^{KO1}, and Kin-1^{KO2} cells. A)

Parental, Cas9 control, Kin-1^{KO1}, and Kin-1^{KO2} SCC-13 cells were plated at a density of 5×10^4 cells/mL. At the indicated times after plating, the cells were trypsinized and the number of trypan blue-excluding cells was determined. **B)** Doubling times for each cell type were calculated from cell number values obtained between 24 and 72 h after plating. The data are expressed as the mean + SEM (one-way ANOVA with Tukey's post-hoc test, n=4).

A



B

Cell Line	Doubling time (h) (mean ± SEM)
Parental	36.5 ± 2.9
Cas9	42.1 ± 11.2
Kin-1 ^{KO1}	35.1 ± 7.2
Kin-1 ^{KO2}	31.5 ± 6.1

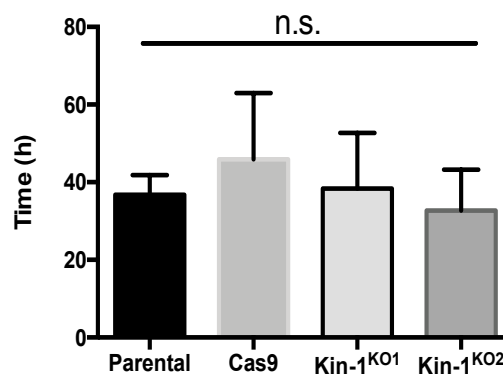
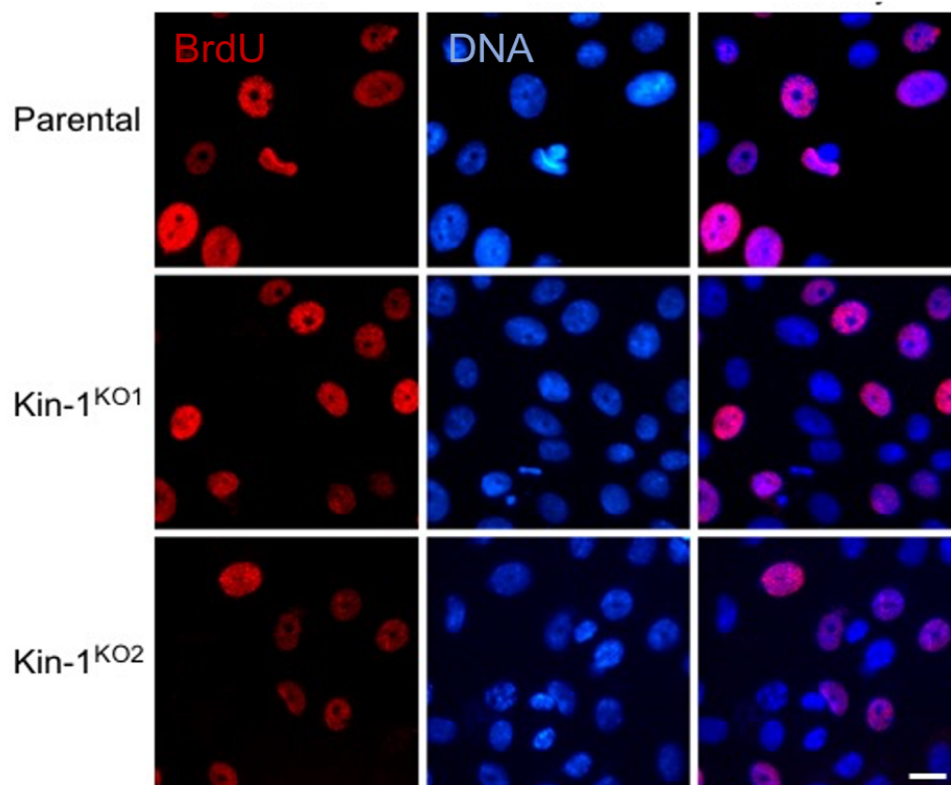
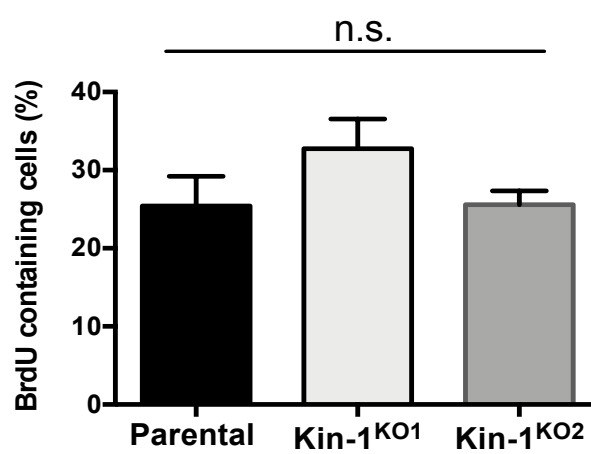


Figure 3.3. Incorporation of BrdU into DNA in SCC-13 cell lines. Parental, Kin-1^{KO1} and Kin-1^{KO2} SCC-13 cells were grown overnight and incubated with 10 μ M bromodeoxyuridine (BrdU) for 2 h prior to processing for immunofluorescence microscopy, using anti-BrdU antibodies. **A)** Representative micrographs of BrdU-positive nuclei for each cell line. DNA was visualized with Hoechst 33342 (BrdU – red, Hoechst – blue, merged – violet). Scale bar is 6 microns. **B)** The fraction of cells containing BrdU is represented as mean + SEM. An one-way ANOVA was conducted with a Tukey's post-hoc test, n=4.

A



B



respectively, with no significant differences among Parental, Kin-1^{KO1} and Kin-1^{KO2} SCC-13 cell lines (Fig. 3.3B). These results indicate Kindlin-1 is not essential for proliferation of SCC-13 cells in culture.

The temporary expression of Cas9 only, in the absence of any guide RNA, did not result in off-target effects in Cas9 control cells in both immunoblot experiments and growth curve assays, when compared to Parental cells. Similar levels of Kindlin-1 were observed in Parental and in Cas9 cells (Fig. 3.1B). Furthermore, doubling times in Parental and Cas9 control cells were comparable (Fig. 3.2B), indicating that transient Cas9 expression in SCC-13 cells was unlikely to be associated with detectable off-target effects.

Consequently, all subsequent experiments evaluating the effect of inactivating the *FERMT1* gene using Kin-1^{KO1} and Kin-1^{KO2} SCC-13 cells were conducted using the Parental cells as controls.

3.3 Spheroid Forming Ability of Parental, Kin-1^{KO1} and Kin-1^{KO2} SCC-13 Cells

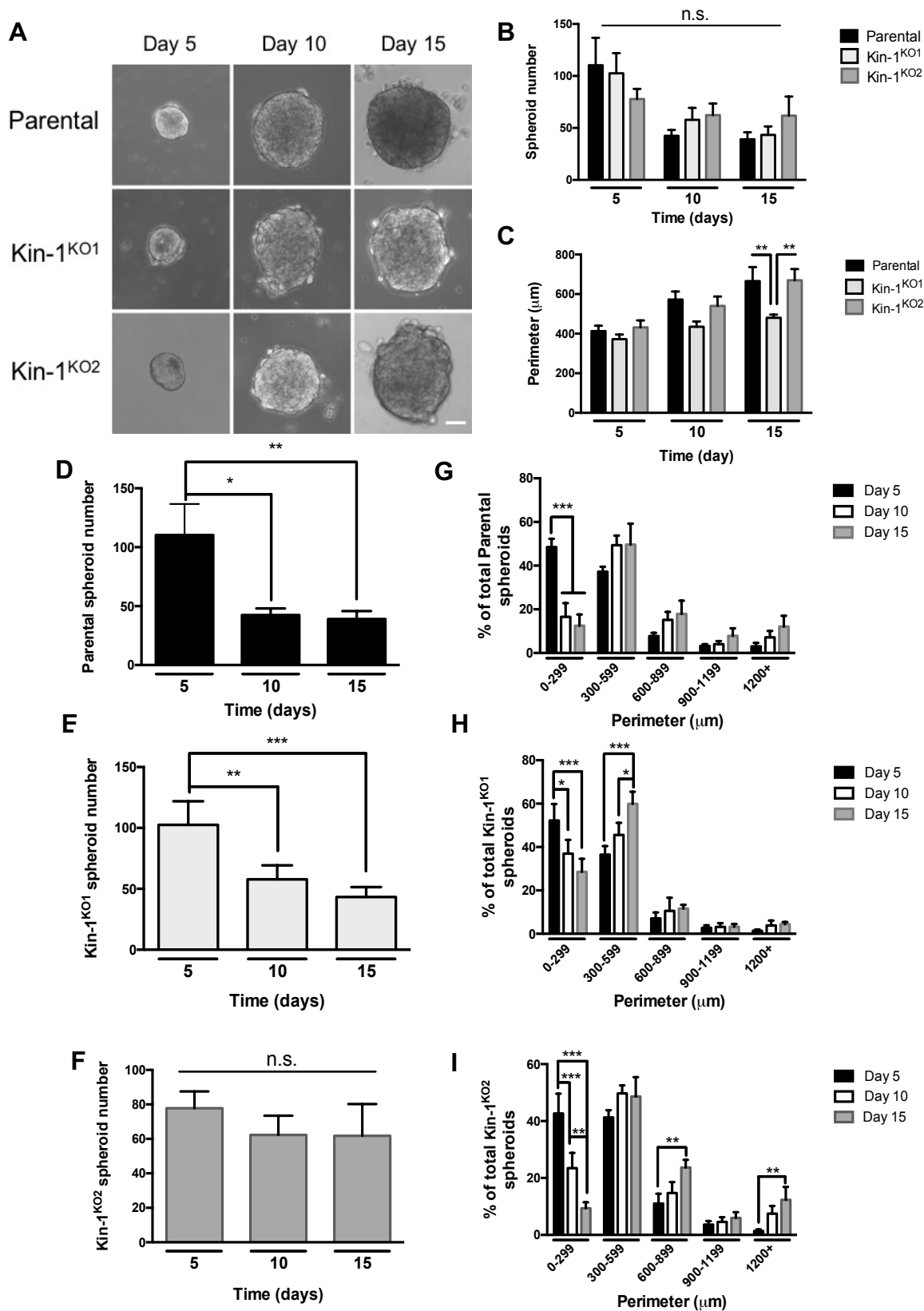
There is a growing body of evidence consistent with the notion that tumor formation is mediated by a small population of slow cycling cells, capable of cell renewal, termed cancer stem cells (Yu et al., 2012). Tumor cell renewal capacity (clonogenicity) can be modeled through evaluation of spheroid formation in 3-D cultures (Adhikary et al., 2013; Shaheen et al., 2016). To evaluate the spheroid-forming capacity of SCC-13 cells containing or lacking Kindlin-1, single cells were cultured in low-attachment surfaces coated with poly-HEMA, to allow formation of spheroids in suspension. Changes in spheroid abundance and size were measured at 5-day intervals, concluding on the 15th day after seeding. On the 2nd day, Parental cells began to form multi-cellular clusters,

with each cell in the cluster being clearly delineated. By days 3 and 4, the clusters had increased in size, and individual cells were no longer distinct; more closely resembling *bona fide* spheroids. At day 5, spheroids had a clear border, generally round in shape, with a somewhat irregular appearance on the surface, possibly reflecting the individual cells that make up a spheroid (Fig. 3.4A). The mean number of spheroids in Parental SCC-13 cultures at day 5 was 110.3 ± 26.4 spheroids, whereas on day 10 there were 42.4 ± 5.6 spheroids (Fig. 3.4D). Parental spheroid numbers remained stable between days 10 and 15. The decrease in spheroid number at days 10 and 15, relative to day 5 was significant. This decrease in spheroid number at days 10 and 15, relative to day 5 was also observed in Kin-1^{KO1} cells (Fig. 3.4E). However, there were no observable differences in spheroid numbers for Kin-1^{KO2} cells (Figure 3.4F). No significant differences in spheroid numbers were observed between Parental, Kin-1^{KO1} and Kin-1^{KO2} at all time points measured (Fig. 3.4B).

At day 5, most Parental spheroids had a small perimeter (0-299 μm), with very few spheroids of 900 μm or greater (Fig. 3.4G). Days 10 and 15 had significantly less Parental spheroids with a small perimeter (0-299 μm) relative to day 5. At days 10 and 15 there were more spheroids with a perimeter of 300 μm or greater, compared to day 5, however this difference was not significant.

At day 5, Kin-1^{KO1} and Kin-1^{KO2} spheroids, also had a majority of spheroids with a small perimeter (0-299 μm) (Fig. 3.4H, I respectively), with a significant decrease in the number of spheroids of that size at days 10 and 15 (Fig. 3.4H, I). By day 15, Kin-1^{KO1} had significantly more spheroids with a perimeter between 300-599 μm , relative to days 5

Figure 3.4. Spheroid formation in Parental, Kin-1^{KO1} and Kin-1^{KO2}. **A)** Representative micrographs of spheroids at the indicated time points. Single cells were cultured in spheroid media on culture plates coated with poly-HEMA and imaged at the indicated time points. Scale bar is 48 microns. **B)** Spheroid number at each time point is represented as mean + SEM. Two-way ANOVA was conducted with Tukey's post hoc test, n=4. **C)** Spheroid perimeter at each time point, represented as mean + SEM. Two-way ANOVA was conducted with Tukey's post hoc test, n=4. ****p<0.01.** **D, E, F)** Spheroid number at days 5, 10 and 15 for Parental, Kin-1^{KO1} and Kin-1^{KO2} cells, respectively, represented as mean + SEM. One-way ANOVA was conducted with Tukey's post hoc test, n=4. **G, H, I)** Spheroid perimeter distribution at days 5, 10 and 15 for Parental, Kin-1^{KO1} and Kin-1^{KO2} cells, respectively, represented as mean + SEM. Two-way ANOVA was conducted with Tukey's post hoc test, n=4. *p<0.05, **p<0.01, ***p<0.001.



and 10 (Fig. 3.4H). Conversely, Kin-1^{KO2} at day 15 had significantly more spheroids with a perimeter between 600-899 μm and 1200 μm or greater, compared to day 5 (Fig. 3.4I). There were significant differences in spheroid perimeter between Parental, Kin-1^{KO1} and Kin-1^{KO2} cell lines, however it was only observable on day 15, in which Kin-1^{KO1} spheroids had significantly smaller mean perimeter compared to Parental and Kin-1^{KO2} spheroids (Fig. 3.4C).

3.4 Cell Spreading on Laminin-332 Matrix and Collagen I

Cell spreading is dependent upon a variety of factors, including adhesion to the underlying ECM and formation of mature focal adhesions, which in keratinocytes involve Kindlin-1 (McGrath, 2007; Ussar et al., 2008). I assessed spreading of SCC-13 cells expressing and lacking Kindlin-1 on laminin-332 matrix at timed intervals following plating. Epidermal cells interact with laminin-332 through $\alpha3\beta1$ and $\alpha6\beta4$ integrins (Watt, 2002), and Kindlin-1 is a known modulator of $\beta1$ integrin function.

Cell spreading was assessed at 2-h intervals following plating, by processing the cells for fluorescence microscopy using Alexa Fluor® 555-conjugated wheat germ agglutinin (WGA). This approach allowed me to visualize the plasma membrane, as WGA is a lectin that binds to glycoproteins present at the cell membrane. Upon plating, cells began to attach to the culture surface and spread. In Parental cells, mean cell area at 2 h was similar to that observed at 6 h, which was also the case in Kin-1^{KO1} and Kin-1^{KO2} cells (Fig. 3.5). To calculate mean relative areas, I determined the time point when the greatest mean cell area was observed for each cell line and each biological replicate (set to 100%; Table 3.1). The mean cell area values at the other time points were then expressed as a

Figure 3.5. Spreading of SCC-13 cells containing and lacking Kindlin-1 on laminin-332

matrix. SCC-13 Parental, Kin-1^{KO1} and Kin-1^{KO2} cells were plated and allowed to adhere on laminin-332 matrix coated 24-well plates. At the indicated time points, cells were processed for fluorescence microscopy using wheat germ agglutinin (WGA) Alexa Fluor[®] 555 to visualize the cell surface, and Hoechst 33342 to visual the nuclear DNA. **A)**

Representative micrographs depicting cell surface with WGA (red) at the indicated time points. Scale bar is 12 microns. **B)** Representative micrographs depicting cell surface with

WGA (red) at 2 h, with the coloured outline added by CellProfiler software which is used to measure the area within. Bar is 12 microns. **C)** Bar graph representing mean cell area

measured for each cell line at the indicated time points, relative to the largest mean

area measured for the corresponding individual cell line, set to 100%. The mean cell area

for each experiment was derived from the area of 100 cells. A two-way ANOVA was

conducted with a Tukey's post-hoc test, with $p < 0.05$. Results are mean + SEM, $n = 6$.

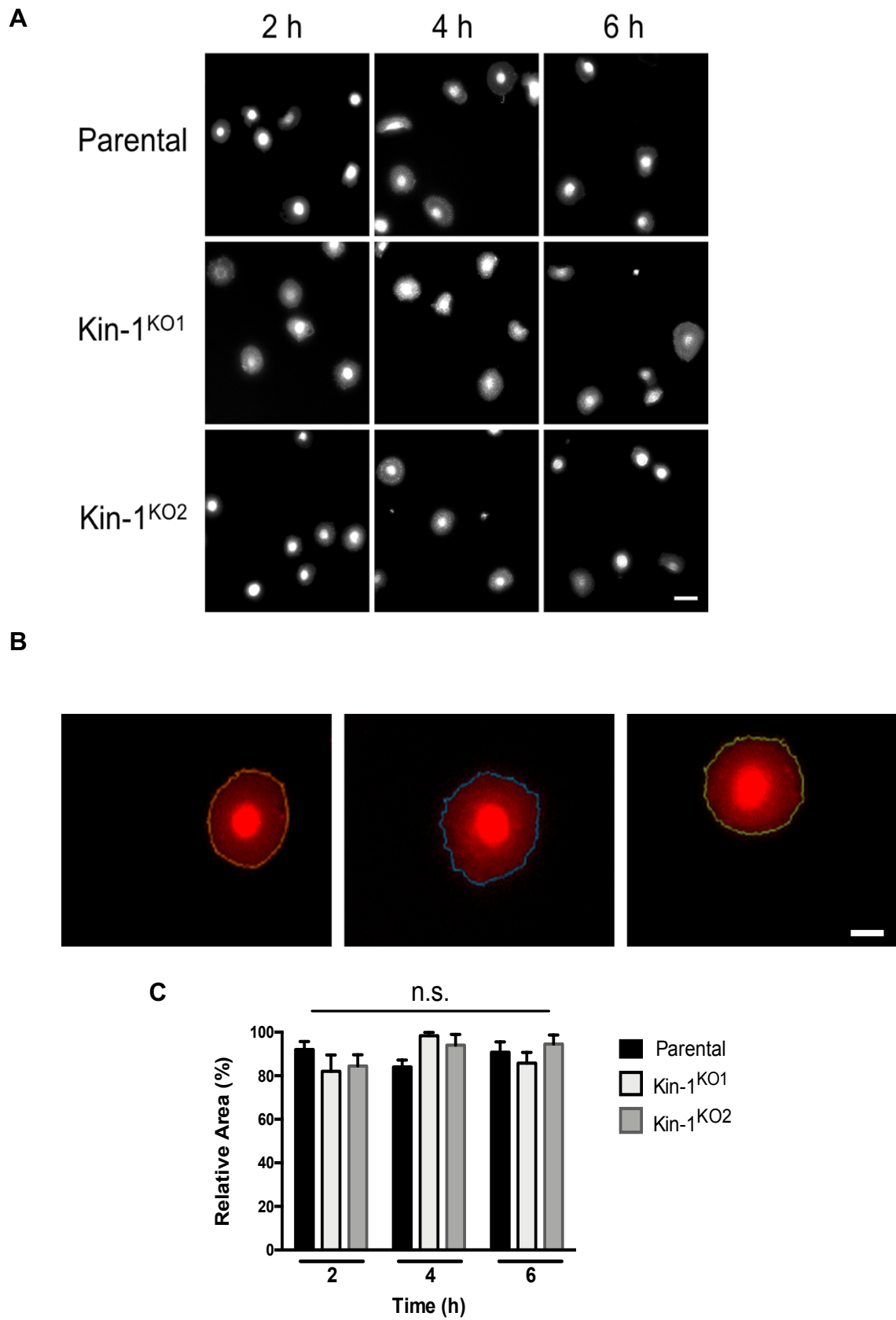


Table 3.1. Maximal mean area of cells spread on laminin-332 matrix

Biological replicate	Parental			Kin-1 ^{KO1}			Kin-1 ^{KO2}		
	Mean area ^a (μm ²)	SD	Time (h)	Mean area ^a (μm ²)	SD	Time (h)	Mean area ^a (μm ²)	SD	Time (h)
1	4244.3	1994.9	2	4818.6	4092.0	4	3815.6	1602.9	6
2	4683.5	2502.5	2	2747.8	1014.6	6	2773.2	1164.5	6
3	4084.6	2519.4	6	4067.7	1453.1	4	3148.9	1117.3	4
4	4492.7	2585.6	6	4807.7	2229.1	2	3858.9	1799.9	6
5	4247.3	1940.8	6	5432.3	5183.9	4	3493.9	1681.2	6
6	3222.5	1237.8	2	2793.7	1295.2	4	3055.8	1714.7	4

^a Mean area of 100 cells.

percentage. The mean relative area for Parental, Kin-1^{KO1} and Kin-1^{KO2} cells 2 h after plating was $92.0 \pm 3.6\%$, $82.1 \pm 7.5\%$, and $84.5 \pm 5.1\%$, respectively. There were no significant differences in the mean relative areas of cells containing or lacking Kindlin-1 at any time points measured (Fig. 3.5C).

I next determined the role of Kindlin-1 in the ability $\alpha2\beta1$ integrins to bind to and spread on collagen I. Whereas collagen IV is the main collagen isoform present in the intact epidermis, collagen I is found in healing epidermis (Xue et al., 2015). Notably, both collagen IV and collagen I are ligands for $\alpha2\beta1$ integrins in epidermal cells (Boraschi-Diaz et al., 2017; Nguyen et al., 2012). I plated Parental, Kin-1^{KO1} and Kin-1^{KO2} cells onto a low or a medium concentration of collagen I ($1 \mu\text{g}/\text{cm}^2$ and $3 \mu\text{g}/\text{cm}^2$, respectively), as the density of ECM ligands can impact the ability of cells to spread, based on availability of unbound ligands (Millon-Frémillon et al., 2008). At 1, 2, 4, 6, and 24 h after plating, cells were fixed and processed for fluorescence microscopy using fluorescently-labelled WGA, to visualize the cell membrane. The relative mean cell area on collagen I was calculated as described above for the laminin-332 matrix experiments (Table 3.2). The area of Parental cells seeded on $1 \mu\text{g}/\text{cm}^2$ increased over time, with the most pronounced change in mean area observed from 1 to 2 h (Fig. 3.6C). During this period, the area increased from $63.8 \pm 1.1\%$ to $77.9 \pm 7.9\%$ of maximum spread, which was measured at 24 h. Kin-1^{KO1} and Kin-1^{KO2} cells saw a similar change in mean cell area, increasing, respectively, from $58.7 \pm 6.1\%$ to $74.9 \pm 7.1\%$, and $53.9 \pm 1.7\%$ to $67.2 \pm 7.5\%$, from 1 to 2 h. There were no significant differences in the mean relative area of Parental, Kin-1^{KO1} and Kin-1^{KO2} cells spread on $1 \mu\text{g}/\text{cm}^2$ collagen I at any time point measured (Fig. 3.6C).

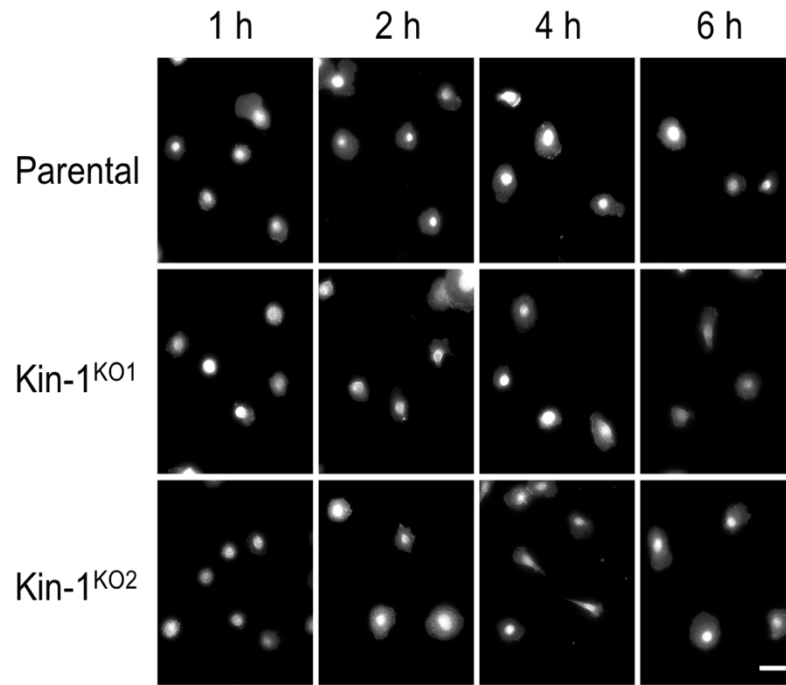
Table 3.2. Maximal mean area of cells spread on a low concentration of collagen I (1 $\mu\text{g}/\text{cm}^2$)

	Parental			Kin-1 ^{KO1}			Kin-1 ^{KO2}		
Biological replicate	Mean area ^a (μm^2)	SD	Time (h)	Mean area ^a (μm^2)	SD	Time (h)	Mean area ^a (μm^2)	SD	Time (h)
1	4607.7	2459.6	24	4933.8	2770.9	24	5679.7	2809.5	24
2	5365.1	2253.7	24	6611.7	3159.3	24	3478.9	1703.7	24
3	4696.1	3342.9	24	5176.0	2526.8	24	4297.5	1651.0	24

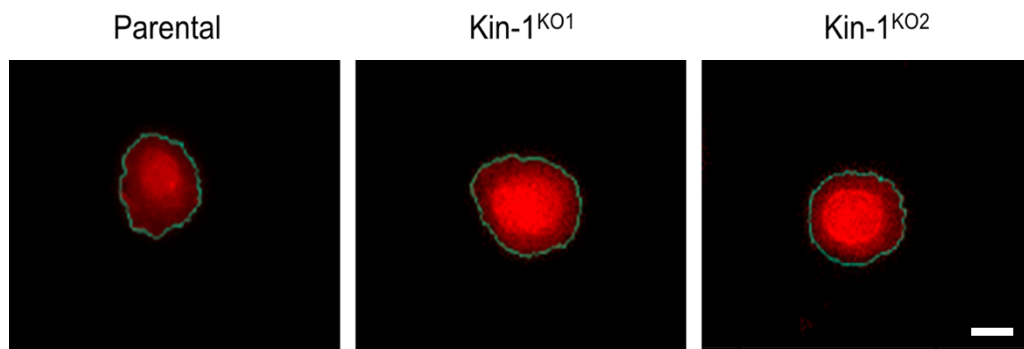
^a Mean area of 100 cells

Figure 3.6. Spreading of SCC-13 cell lines on a low concentration of collagen I. SCC-13 Parental, Kin-1^{KO1} and Kin-1^{KO2} cells were grown on 24-well plates coated with Collagen I (1 $\mu\text{g}/\text{cm}^2$). At the indicated time points, cells were fixed and processed for fluorescence microscopy using wheat germ agglutinin (WGA) Alexa Fluor[®] 555 to visualize the cell surface, and Hoechst 33342 to visualize the nuclear DNA. **A)** Representative micrographs depicting cell surface with WGA (red) at the indicated time points. Scale bar is 12 microns. **B)** Representative micrographs depicting cell surface with WGA (red) at 1 h, with the coloured outline added by CellProfiler software which is used to measure the area within. Bar is 12 microns. **C)** Bar graph representing mean cell area measured for each cell line at the indicated time points, relative to the greatest mean cell area measured for the corresponding individual cell line, set to 100%. The mean cell area for each experiment was derived from the area of 100 cells. A two-way ANOVA and Tukey's post-hoc test was conducted with $p < 0.05$, Results are mean + SEM, $n=3$.

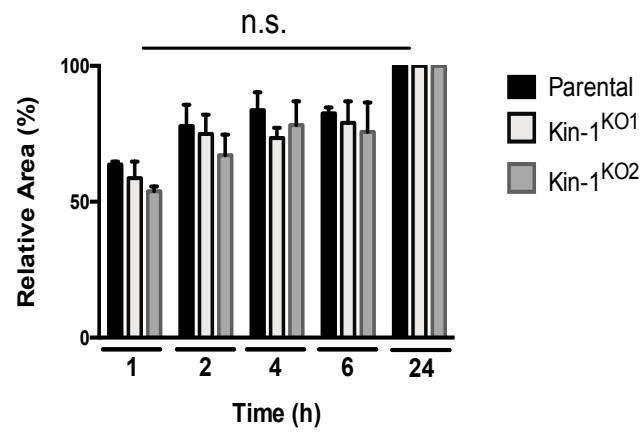
A



B



C



In contrast, the data for cells lacking Kindlin-1 plated on $3 \mu\text{g}/\text{cm}^2$ collagen I (Table 3.3) demonstrated significant differences in the mean relative area of the cells compared to Parental cells (Fig. 3.7). Parental cells had a significantly larger mean relative area compared to cells lacking Kindlin-1 1, 2 and 6 h after plating (Fig. 3.7C). The most pronounced difference was observed at 6 h, at which Parental cells had a mean relative area of $91.4 \pm 3.9\%$, compared to Kin-1^{KO1} and Kin-1^{KO2} cells which had a mean relative area of $72.8 \pm 7.1\%$, and $72.6 \pm 2.7\%$, respectively. However, by 24 h there were no differences in mean relative area between Parental ($98.4 \pm 1.6\%$), Kin-1^{KO1} ($94.1 \pm 5.9\%$) and Kin-1^{KO2} ($100.0 \pm 0.0\%$) cells (mean \pm SEM), indicating that cells lacking Kindlin-1 exhibit delays in spreading when seeded onto surfaces coated with a medium concentration of collagen I.

3.5 Directional Migration of Kin-1^{KO1} and Kin-1^{KO2} Cells

Kindlin-1 is found at focal adhesions in keratinocytes where it participates in modulating cell migration (Herz et al., 2006). To establish Kindlin-1 role in cell migration in SCC-13 cells, monolayers of Parental, Kin-1^{KO1} and Kin-1^{KO2} cells were cultured to confluence, at which time a wound scrape was created to induce directional migration into the cell-free area. I then measured the reduction in cell-free area over time (Fig. 3.8). Four hours after scraping, Parental cells had reduced the cell-free area by about 22% and by 8 h they had migrated to cover approximately 50% of the cell-free area. Following 24 h of Parental cell migration, there remained 37% of cell-free area. By 4 h significant differences in migration between the Parental, and Kin-1^{KO1} and Kin-1^{KO2} cells were

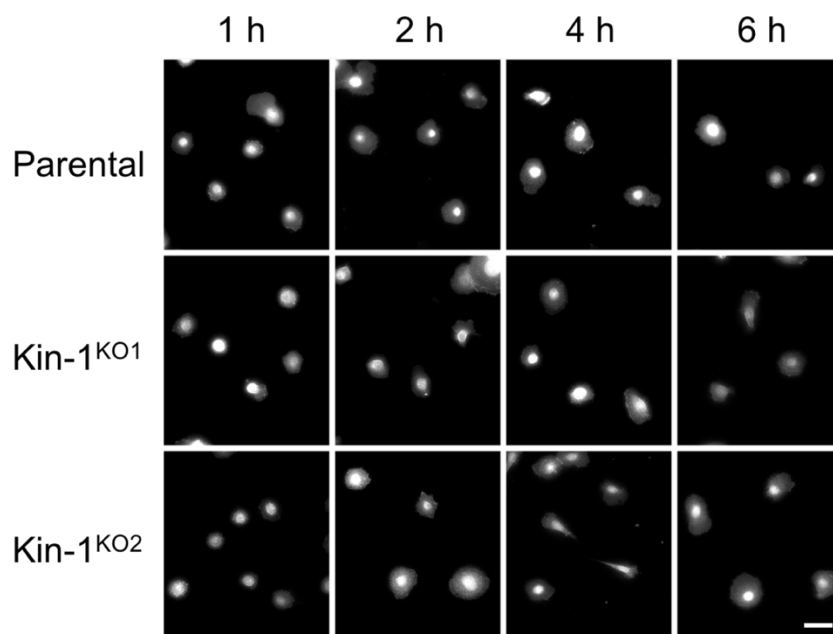
Table 3.3. Maximal mean area of cells spread on a medium concentration of collagen I (3 $\mu\text{g}/\text{cm}^2$)

Biological replicate	Parental			Kin-1 ^{KO1}			Kin-1 ^{KO2}		
	Mean area ^a (μm^2)	SD	Time (h)	Mean area ^a (μm^2)	SD	Time (h)	Mean area ^a (μm^2)	SD	Time (h)
1	4569.8	1929.7	24	6137.8	3063.8	24	5339.1	2834.7	24
2	5313.5	3597.8	24	6227.9	3394.5	24	5717.1	3998.0	24
3	4448.4	1932.5	6	7572.3	8868.3	4	4175.1	2293.3	24
4	4819.7	3261.9	24	6638.5	4540.2	24	5078.3	3234.8	24
5	4457.3	2927.4	24	4658.8	4827.2	24	4187.7	2064.4	24

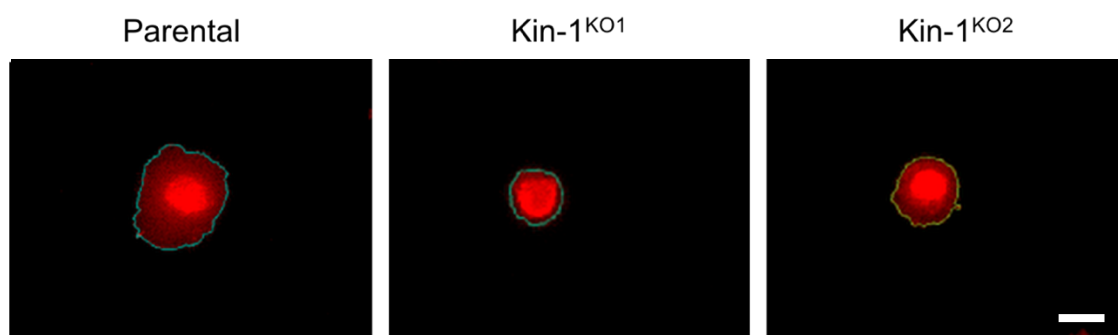
^a Mean area of 100 cells.

Figure 3.7. Spreading of SCC-13 cells on a medium concentration of collagen I. SCC-13 Parental, Kin-1^{KO1} and Kin-1^{KO2} cells were grown on 24-well plates coated with collagen I (3 $\mu\text{g}/\text{cm}^2$). At the indicated time points, cells were fixed and processed for fluorescence microscopy using wheat germ agglutinin (WGA) Alexa Fluor[®] 555 to visualize the cell surface, and Hoechst 33342 to visualize the nuclear DNA. **A)** Representative micrographs depicting cell surface with WGA (red) at the indicated time points. Scale bar is 12 microns. **B)** Representative micrographs depicting cell surface with WGA (red) at 1 h, with the coloured outline added by CellProfiler software which is used to measure the area within. Bar is 12 microns. **C)** Bar graph representing cell area measured for each cell line at the indicated time points, relative to the largest mean area measured for the corresponding individual cell line, set to 100%. The mean cell area for each experiment was derived from the area of 100 cells. A two-way ANOVA with Tukey's post hoc test was conducted with * $p < 0.05$, ** $p < 0.01$. Results are mean + SEM, $n = 5$.

A



B



C

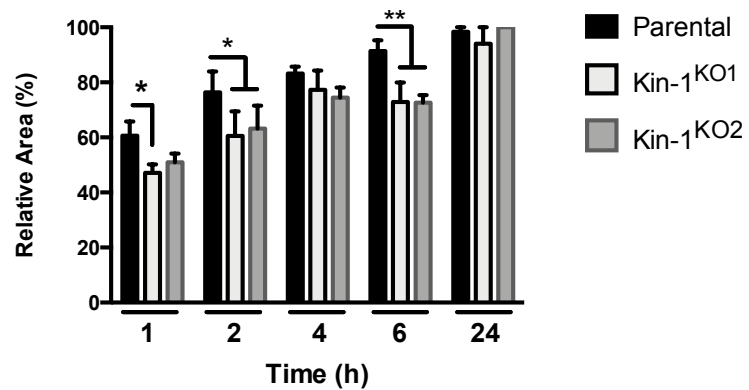
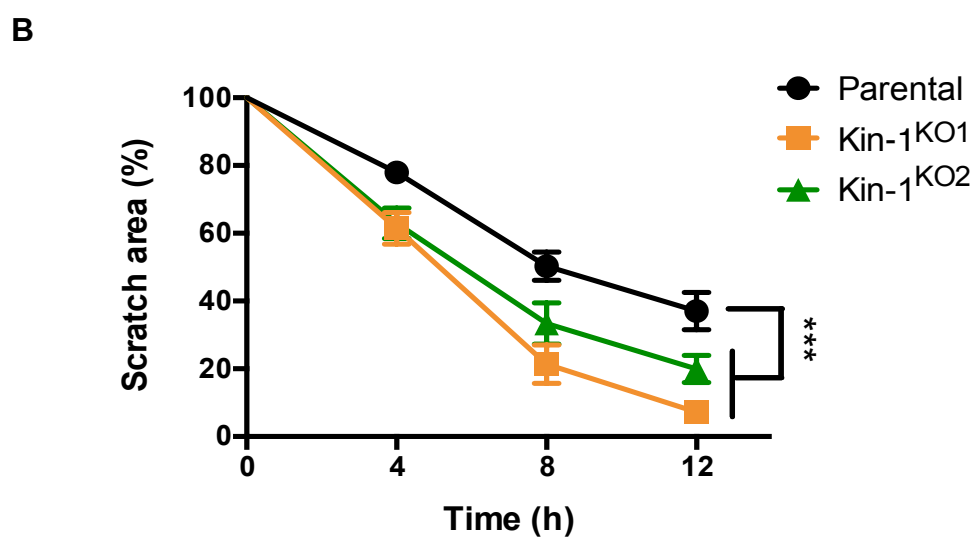
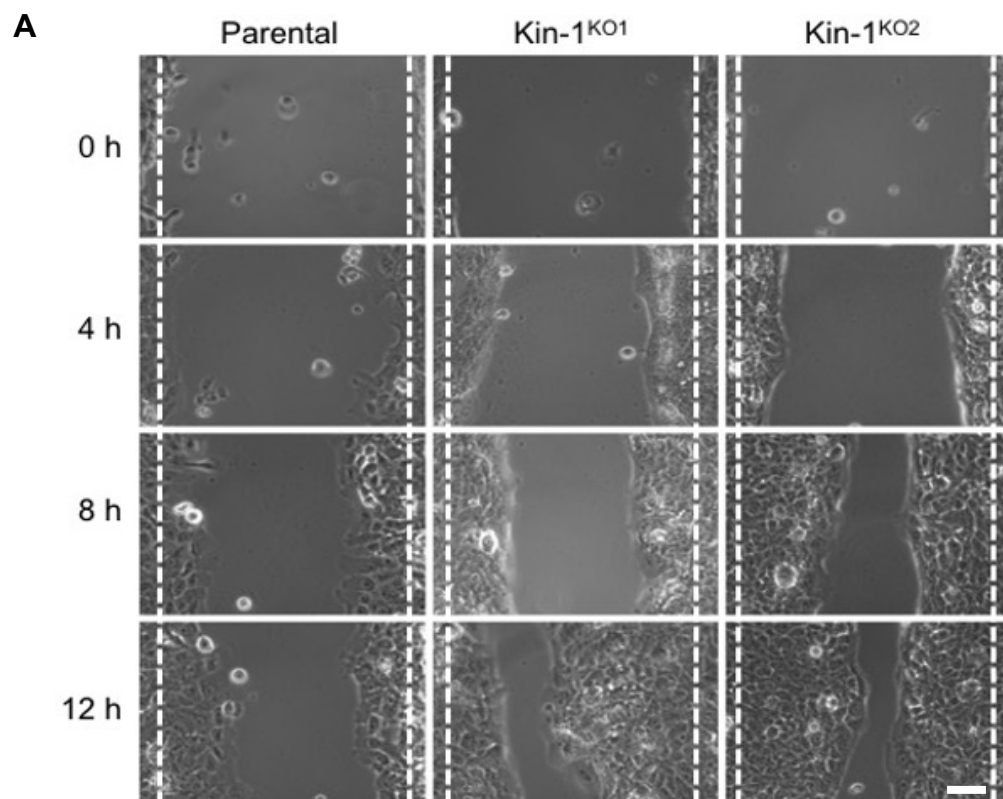


Figure 3.8. Directional migration of Parental, Kin-1^{KO1} and Kin-1^{KO2} SCC-13 cells. Cells were plated at a density 2×10^6 cells/mL and cultured for 16 h. Confluent monolayers were scraped with a p10 pipette tip and imaged every 4 h. **A)** Representative phase-contrast images of the denuded area at the indicated time points. Scale bar is 24 microns. **B)** Denuded area remaining at the indicated time points. The results are shown as the mean denuded area + SEM, relative to the mean original denuded area for each cell line (t=0), set to 100%. A two-way ANOVA with Tukey's post-hoc test was conducted with *** $p < 0.001$. Results are mean + SEM, n=3.



evident, as reflected by the distance cells travelled into the denuded area (Fig. 3.8A). The cell-free area at 4 h in Parental cell cultures was $77.9 \pm 2.8\%$, whereas that of Kin-1^{KO1} and Kin-1^{KO2} was, respectively, 61.5 ± 4.7 , and $63.0 \pm 4.5\%$, relative to the initial wound area (mean \pm SEM). This demonstrates greater migration in the cells lacking Kindlin-1, which persisted at all subsequent time points measured. At the final 12-h time point, the cell-free areas in Kin-1^{KO1} and Kin-1^{KO2} cell cultures were $7.2 \pm 2.7\%$ and $20.0 \pm 4.0\%$, respectively. By contrast, the wound area in Parental cell cultures was $37.0 \pm 5.6\%$ of the initial wound area (mean \pm SEM; Fig. 3.8B). These results indicate that loss of Kindlin-1 in SCC-13 cells enhances directional cell migration.

3.6 Proteomic Analysis using Reverse Phase Protein Arrays Reveals Differences in the Abundance of Proteins Associated with Carcinogenesis in Kindlin-1-Deficient SCC-13 Cells

To identify potential novel pathways modulated by Kindlin-1 in squamous carcinoma cells, I conducted functional proteomic studies, screening reverse phase protein arrays (RPPA) of protein lysates isolated from Parental, Kin-1^{KO1} and Kin-1^{KO2} cells. The arrays were probed with antibodies against 466 different proteins known to be important contributors to carcinogenic pathways, a subset of which identified post-translational modifications.

Using the median centered \log_2 values of protein levels, principal component analysis (PCA) of the abundance of proteins in the arrays was conducted by Drs. S.

Sayedyahosseini, M. Karimi and M. Bahmani. PCA is a dimensionality-reduction method, which is used to reduce the number of dimensions of a large data set, by grouping a

large set of variables into a single variable, termed principal components, that contains most of the information from the larger set of variables. The principal components can then be represented as the axes in a coordinate system, with the samples placed within the system based on how much each principal component explains the variation for each sample.

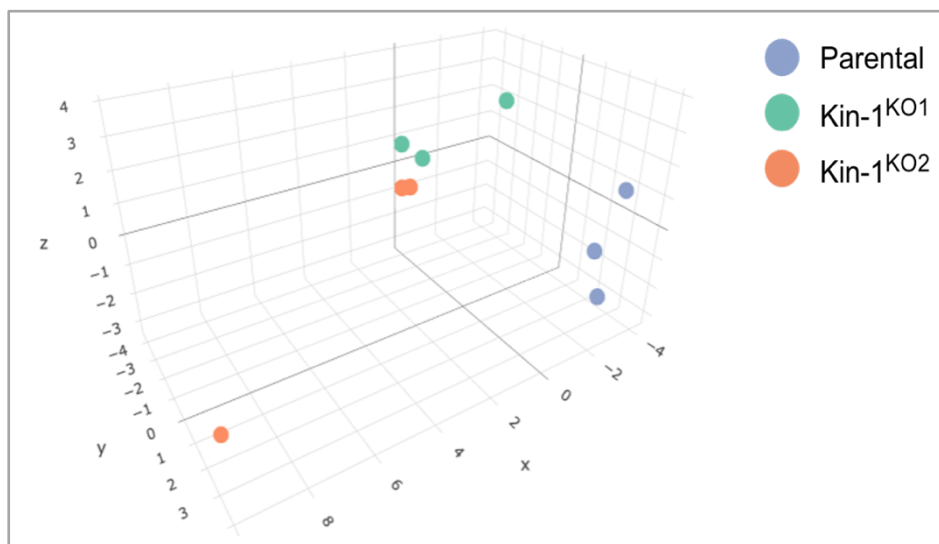
The coordinate system produced by PCA revealed that overall protein levels of Parental cells differed from those in both Kin-1^{KO1} and Kin-1^{KO2} cells (Fig. 3.9A). The data from Parental samples (blue) clustered tightly toward the x-axis, whereas both Kin-1^{KO1} (green) and Kin-1^{KO2} (orange) sample data clustered toward the z-axis, indicating that the levels of proteins are dictated by different principal components as a result of the loss of Kindlin-1.

Further analysis using unpaired t-tests identified 100 protein whose abundance was significantly different in both Kin-1^{KO1} and Kin-1^{KO2} cells, compared to Parental cells (Tables 3.4 and 3.5). A heatmap of the 30 proteins with the most pronounced differences in abundance is shown in Figure 3.9B. Many of the proteins that cluster together in the heatmap with increased abundance in Kindlin-1-deficient cells are involved in DNA damage responses, such as:

- Poly ADP-ribose glycohydrolase (PARG; Steffen et al., 2012)
- DNA endonuclease RBBP8 (RBBP8; Mozaffari et al., 2021)
- Aurora A/B/C phosphorylated at Thr288, Thr232 and Thr198 (AURKA; Wang et al., 2014)
- Serine/threonine-protein kinase Chk1 (CHK1; Tho et al., 2012)
- DNA mismatch repair protein Mlh1 (MLH1; Gray et al., 2006)
- Serine-protein kinase ATM (ATM; Ismail et al., 2011)
- Ribonucleoside-diphosphate reductase subunit M2 (RRM1; Shu et al., 2020)

Figure 3.9. Principal component analysis and heat map of protein abundances in reverse phase protein arrays of SCC-13 cell lines. Cell pellets were sent to the M.D. Anderson Cancer center for reverse phase protein array (RPPA) analysis using 466 antibodies against various proteins. **A)** Principal component analysis of RPPA data in R studio groups variables that have similar values along vectors to place samples in a coordinate system so as to have the most separation between variable groups. Unpaired t-tests of protein levels with $p < 0.05$, revealed 30 proteins with the most pronounced differences in abundances in both Kin-1^{KO1} and Kin-1^{KO2} cells compared to Parental cells, which was used to generate **B)** a clustered heatmap. Magenta represents proteins with high abundance and blue represents low abundance. N=3.

A



B

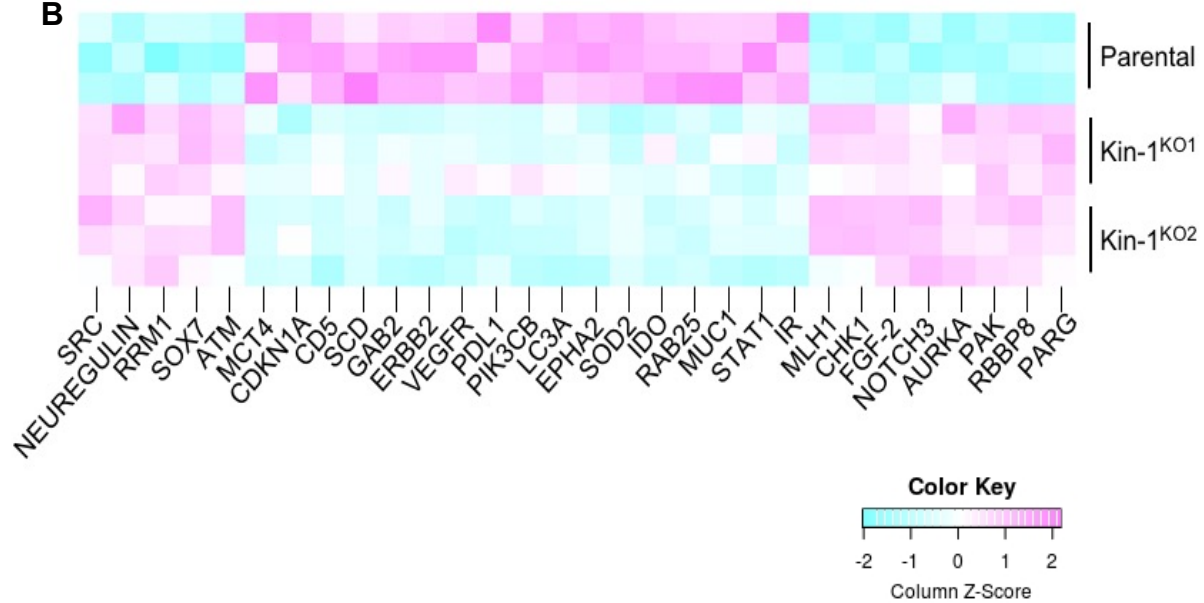


Table 3.4. Proteins with increased abundance in Kindlin-1-deficient SCC-13 clonal lines

Protein name	Protein symbol	Relative protein abundance in RPPA ^a				Mean fold difference ^c
		Parental ^b	Kin-1 ^{KO1} ^b	Kin-1 ^{KO2} ^b	Kin-1 ^{KO1} + Kin-1 ^{KO2} ^b	
Neuregulin-1	NRG1	0.39	0.94	0.82	0.88	2.27
Tyrosine protein kinase receptor UFO	AXL	0.52	1.27	0.95	1.11	2.12
DNA mismatch repair protein Mlh1	MLH1	1.10	2.16	2.27	2.21	2.02
Basic fibroblast growth factor	FGF2	0.78	1.40	1.59	1.50	1.91
Serine/threonine-protein kinase Chk1	CHEK1	1.26	2.34	2.47	2.41	1.91
DNA endonuclease RBBP8	RBBP8	1.07	1.81	1.85	1.83	1.71
Mixed lineage kinase domain like pseudokinase	MLKL	1.14	1.99	1.89	1.94	1.70
Neurogenic locus notch homolog protein 3	NOTCH3	0.94	1.32	1.64	1.48	1.57
Cell division cycle 25C	CDC25C	1.07	1.74	1.57	1.65	1.55
Mismatch repair endonuclease PMS2	PMS2	1.26	1.99	1.90	1.94	1.55
Serine-protein kinase ATM	ATM	0.84	1.25	1.30	1.28	1.52
Caveolin 1	CAV1	0.45	0.58	0.78	0.68	1.52
Transcriptional regulator ATRX	ATRX	1.09	1.42	1.69	1.55	1.42
Wee1-like protein kinase	WEE1	0.99	1.23	1.54	1.38	1.40
Aurora A/B/C phosphorylated at Thr288, Thr232 and Thr198	AURKA	0.90	1.27	1.26	1.26	1.40

Table 3.4. Cont. Proteins with increased abundance in Kindlin-1-deficient SCC-13 clonal lines

Protein name	Protein symbol	Relative protein abundance in RPPA ^a				Mean fold difference ^c
		Parental ^b	Kin-1 ^{KO1} _b	Kin-1 ^{KO2} _b	Kin-1 ^{KO1} + Kin-1 ^{KO2} _b	
DNA methyltransferase 1	DNMT1	1.53	1.99	2.28	2.14	1.39
Poly ADP-ribose glycohydrolase	PARG	1.19	1.74	1.56	1.65	1.39
CD276 antigen	CD276	0.70	0.87	1.05	0.96	1.37
Protein tyrosine phosphatase non-receptor Type 12	PTPN12	1.04	1.45	1.40	1.43	1.37
Transcription factor SOX-7	SOX7	0.80	1.17	1.04	1.10	1.37
Epidermal growth factor receptor	EGFR	0.72	0.91	1.06	0.98	1.37
DNA mismatch repair protein Msh2	MSH2	1.15	1.47	1.66	1.56	1.36
Mothers against decapentaplegic homolog 4	SMAD4	1.28	1.62	1.84	1.73	1.35
Breast cancer type 1	BRCA1	1.24	1.72	1.62	1.67	1.34
5'-AMP-activated protein kinase catalytic subunit alpha-1/2 phosphorylated at Tyr172	PRKAA1-2	0.67	0.84	0.93	0.89	1.32
p21-activated kinase 4/5/6 phosphorylated at Ser474, Ser602 and Ser560	PAK4-6	1.09	1.45	1.41	1.43	1.31
Ribonucleoside-diphosphate reductase subunit M2	RRM2	1.09	1.38	1.40	1.39	1.28

Table 3.4. Cont. Proteins with increased abundance in Kindlin-1-deficient SCC-13 clonal lines

Protein name	Protein symbol	Relative protein abundance in RPPA ^a				Mean fold difference ^c
		Parental ^b	Kin-1 ^{KO1} _b	Kin-1 ^{KO2} _b	Kin-1 ^{KO1} + Kin-1 ^{KO2} _b	
Serine/threonine-protein kinase Chk2	CHEK2	0.98	1.23	1.28	1.25	1.27
Proto-oncogene tyrosine-protein kinase	SRC	0.57	0.71	0.72	0.71	1.26
p21-activated kinase 1	PAK1	0.95	1.22	1.16	1.19	1.25
DNA damage-binding protein 1	DDB1	0.61	0.79	0.74	0.77	1.25
Cell division cycle protein 2	CDT2	1.07	1.22	1.44	1.33	1.25
DNA repair protein complementing XP-A cells	XPA	0.91	1.17	1.06	1.11	1.23
Caspase 8	CASP8	0.95	1.10	1.22	1.16	1.22
Serine/threonine-protein kinase Chk2phosphorylated at Tyr68	CHEK2	0.95	1.11	1.19	1.15	1.21
Replication Protein A2 phosphorylated at Ser4 and Ser8	RPA2	1.04	1.25	1.26	1.26	1.21
Proliferating Cell Nuclear Antigen	PCNA	0.96	1.09	1.18	1.13	1.19
Ribonucleoside-diphosphate reductase large subunit	RRM1	0.91	1.08	1.07	1.08	1.18
Von Hippel-Lindau tumor suppressor	VHL	0.96	1.11	1.15	1.13	1.18
ATR Serine/Threonine Kinase	ATR	0.96	1.12	1.13	1.13	1.17
Protein C-ets-1	ETS1	0.91	1.03	1.09	1.06	1.17

Table 3.4. Cont. Proteins with increased abundance in Kindlin-1-deficient SCC-13 clonal lines

Protein name	Protein symbol	Relative protein abundance in RPPA ^a				Mean fold difference ^c
		Parental ^b	Kin-1 ^{KO1} _b	Kin-1 ^{KO2} _b	Kin-1 ^{KO1} + Kin-1 ^{KO2} _b	
Ribosomal protein S6 kinase beta-1 phosphorylated at Tyr389	RPS6KB1	1.25	1.46	1.44	1.45	1.16
Forkhead box O3	FOXO3	0.97	1.13	1.09	1.11	1.15
DNA repair endonuclease XPF	ERCC4	0.79	0.90	0.89	0.89	1.13
p21-activated kinase 4	PAK4	0.83	0.95	0.91	0.93	1.12
Forkhead box O3 phosphorylated at Ser318 and Ser321	FOXO3	0.93	1.04	1.04	1.04	1.11
Serine-protein kinase ATM phosphorylated at Ser1981	ATM	1.01	1.07	1.12	1.09	1.08
Glycogen synthase kinase 3 beta	GSK3B	1.02	1.08	1.10	1.09	1.07

^a Relative protein levels were determined from curves generated using serial lysate dilutions spotted on nitrocellulose membranes, subsequently probed with a given antibody. The values shown are also normalized for protein loading.

^b Mean values of 3 biological replicates.

^c Fold relative difference in abundance found from the mean calculated levels in Kin-1^{KO1} together with Kin-1^{KO2} clones, relative to Parental SCC-13 cells. Abundance in Parental SCC-13 cells have been set to 1.

Table 3.5. Proteins with decreased abundance in Kindlin-1-deficient SCC-13 clonal lines

Protein name	Protein symbol	Relative protein abundance in RPPA ^a				Mean fold difference ^c
		Parental ^b	Kin-1 ^{KO1} _b	Kin-1 ^{KO2} _b	Kin-1 ^{KO1} + Kin-1 ^{KO2} _b	
Mucin 1	MUC1	2.88	1.07	1.04	1.05	-2.73
Stimulator of interferon genes protein	STING1	0.81	0.45	0.18	0.32	-2.56
Claudin 7	CLDN7	2.36	1.26	0.81	1.03	-2.29
Microtubule associated protein 1 light chain 3 alpha/beta	MAP1LC3A/B	1.73	0.94	0.68	0.81	-2.13
Epiplakin 1	EPPK1	1.91	0.93	0.91	0.92	-2.09
Cyclin dependent kinase inhibitor 1a	CDKN1A	1.18	0.54	0.63	0.59	-2.02
Acetyl-coenzyme A synthetase	ACSS2	1.10	0.55	0.63	0.59	-1.86
Ephrin type-A receptor 2 phosphorylated at Tyr588	EPHA2	1.71	0.98	0.87	0.92	-1.85
Signal transducer and activator of transcription 1 phosphorylated at Tyr701	STAT1	2.14	1.29	1.13	1.21	-1.77
Transferrin Receptor protein 1	TFRC	1.53	1.03	0.79	0.91	-1.69
Vascular endothelial growth factor receptor 2	VEGFR	1.15	0.68	0.77	0.72	-1.59

Table 3.5. Cont. Proteins with decreased abundance in Kindlin-1-deficient SCC-13 clonal lines

Protein name	Protein symbol	Relative protein abundance in RPPA ^a				Mean fold difference ^c
		Parental _b	Kin-1 ^{KO1} _b	Kin-1 ^{KO2} _b	Kin-1 ^{KO1} + Kin-1 ^{KO2} _b	
Ras-related protein rab-25	RAB25	1.65	1.08	1.02	1.05	-1.58
Indoleamine 2,3-dioxygenase 1	IDO1	1.54	1.03	0.93	0.98	-1.58
Wd repeat domain, phosphoinositide interacting 1	WIPI1	1.29	0.79	0.91	0.85	-1.52
Tumor necrosis factor receptor superfamily member 12	TNFRSF12	1.60	1.22	0.92	1.07	-1.49
Insulin receptor	INSR	2.14	1.44	1.45	1.44	-1.48
Stearoyl-coa Desaturase	SCD	1.26	0.85	0.86	0.86	-1.47
DNA repair protein RAD51 homolog 1	RAD51	1.53	1.07	1.03	1.05	-1.45
Notch 1	NOTCH1	0.88	0.70	0.55	0.62	-1.41
Monocarboxylate transporter 4	MCT4	0.78	0.57	0.55	0.56	-1.39
Heat Shock Factor Binding Protein 1 phosphorylated at Ser82	HSBP1	1.07	0.86	0.68	0.77	-1.38
Insulin like growth factor binding protein 3	IGFBP3	1.28	0.99	0.90	0.94	-1.35
Bcl-2 like 11	BCL2L11	1.36	0.96	1.09	1.03	-1.33

Table 3.5. Cont. Proteins with decreased abundance in Kindlin-1-deficient SCC-13 clonal lines

Protein name	Protein symbol	Relative protein abundance in RPPA ^a				Mean fold difference ^c
		Parental _b	Kin-1 ^{KO1} _b	Kin-1 ^{KO2} _b	Kin-1 ^{KO1} + Kin-1 ^{KO2} _b	
Eukaryotic translation initiation factor 2 alpha kinase 3	EIF2AK3	0.98	0.80	0.68	0.74	-1.31
Serine/threonine-protein kinase ULK1 phosphorylated at Ser757	ULK1	1.53	1.20	1.15	1.18	-1.30
Growth factor receptor bound protein 2-associated protein 2	GAB2	1.12	0.90	0.82	0.86	-1.30
Vascular endothelial growth factor receptor 2 phosphorylated at Tyr1175	VEGFR	1.26	1.03	0.92	0.98	-1.29
Receptor tyrosine-protein kinase erb-3	ERBB3	1.65	1.33	1.23	1.28	-1.29
Succinate dehydrogenase complex iron sulfur subunit b	SDHB	0.96	0.77	0.72	0.75	-1.28
Serine/threonine-protein kinase receptor R3	ACVRL1	1.05	0.81	0.86	0.83	-1.26
Receptor tyrosine-protein kinase erb-2 phosphorylated at Tyr1248	ERBB2	1.14	0.92	0.91	0.91	-1.25

Table 3.5. Cont. Proteins with decreased abundance in Kindlin-1-deficient SCC-13 clonal lines

Protein name	Protein symbol	Relative protein abundance in RPPA ^a				Mean fold difference ^c
		Parental _b	Kin-1 ^{KO1} _b	Kin-1 ^{KO2} _b	Kin-1 ^{KO1} + Kin-1 ^{KO2} _b	
Superoxide dismutase 2	SOD2	1.37	1.07	1.13	1.10	-1.25
Epithelial discoidin domain-containing receptor 1	DDR1	1.16	0.90	0.96	0.93	-1.24
Glutamate dehydrogenase 1	GLUD1	0.83	0.70	0.70	0.70	-1.19
Rapamycin-insensitive companion of mTOR	RICTOR	1.43	1.12	1.28	1.20	-1.19
Tyrosine-protein phosphatase non-receptor type 11 phosphorylated at Tyr548	PTPN11	1.17	0.99	0.99	0.99	-1.19
DNA polymerase subunit gamma-1	POLG	1.05	0.90	0.88	0.89	-1.19
Tyrosine-protein kinase SYK	SYK	0.97	0.83	0.81	0.82	-1.18
Programmed cell death 1 ligand 1	PDL1	1.13	0.97	0.94	0.96	-1.18
RAC-alpha serine/threonine-protein kinase phosphorylated at Thr308	AKT1/2/3	1.01	0.87	0.86	0.86	-1.17

Table 3.5. Cont. Proteins with decreased abundance in Kindlin-1-deficient SCC-13 clonal lines

Protein name	Protein symbol	Relative protein abundance in RPPA ^a				Mean fold difference ^c
		Parental _b	Kin-1 ^{KO1} _b	Kin-1 ^{KO2} _b	Kin-1 ^{KO1} + Kin-1 ^{KO2} _b	
Bcl-2 binding component 3	BBC3	0.91	0.75	0.80	0.78	-1.17
Tyrosine-protein phosphatase non-receptor type 11	PTPN11	1.16	0.97	1.02	1.00	-1.16
Dipeptidyl peptidase 4	DPP4	0.90	0.75	0.80	0.78	-1.16
Tyrosine-protein kinase ABL1 phosphorylated at Tyr412	ABL1	1.12	0.99	0.95	0.97	-1.16
Phosphatidylinositol 4,5-bisphosphate 3-kinase catalytic subunit beta isoform	PIK3CB	1.11	0.99	0.95	0.97	-1.15
T-cell surface glycoprotein CD5	CD5	0.95	0.86	0.82	0.84	-1.14
Low-density lipoprotein receptor-related protein 6 phosphorylated at Ser1490	LRP6	1.13	1.01	0.99	1.00	-1.13
Growth factor receptor-bound protein 2	GRB2	1.12	0.99	1.01	1.00	-1.12
Eukaryotic translation initiation factor 4E	EIF4E	1.17	1.03	1.06	1.05	-1.12
Wee1-like protein kinase phosphorylated at Ser642	WEE1	1.01	0.90	0.95	0.92	-1.10

Table 3.5. Cont. Proteins with decreased abundance in Kindlin-1-deficient SCC-13 clonal lines

Protein name	Protein symbol	Relative protein abundance in RPPA ^a				Mean fold difference ^c
		Parental ^b	Kin-1 ^{KO1} _b	Kin-1 ^{KO2} _b	Kin-1 ^{KO1} + Kin-1 ^{KO2} _b	
Mitogen-activated protein kinase 14 phosphorylated at Thr180 and Tyr182	MAPK14	0.98	0.91	0.89	0.90	-1.09
Programmed cell death protein 1	PDCD1	0.99	0.93	0.89	0.91	-1.09

^a Relative protein levels were determined from curves generated using serial lysate dilutions spotted on nitrocellulose membranes, subsequently probed with a given antibody. The values shown are also normalized for protein loading.

^b Mean values of 3 biological replicates.

^c Fold relative difference in abundance found from the mean calculated levels in Kin-1^{KO1} together with Kin-1^{KO2} clones, relative to Parental SCC-13 cells. Abundance in Parental SCC-13 cells have been set to 1.

Contrastingly, many of the proteins with decreased abundance in Kin-1^{KO1} and Kin-1^{KO2} cells, relative to Parental SCC-13 cells, are associated with proliferation, including:

- Cyclin dependent kinase inhibitor 1a (CDKN1A; Missero et al., 2014)
- Receptor tyrosine-protein kinase erbb-2 (ERBB2; Rao et al., 2015)
- Vascular endothelial growth factor receptor 2 phosphorylated at Tyr1175 (VEGFR; Johnson et al., 2012)
- Phosphatidylinositol 4,5-bisphosphate 3-kinase catalytic subunit beta isoform (PIK3CB; Yang et al., 2019)
- Ephrin type-A receptor 2 phosphorylated at Tyr588 (EPHA2; Wang et al., 2021),
- Ras-related protein rab-25 (RAB25; Jeong et al., 2019)
- Signal transducer and activator of transcription 1 phosphorylated at Tyr701 (STAT1; Clifford et al., 2000).

3.6.1 Pathway Analysis of Proteins with Significantly Different Protein Abundances in

Kin-1^{KO1} and Kin-1^{KO2} Cells

Mean fold differences were determined from the proteins identified by unpaired t-tests to be significantly different (calculated as the mean abundance of Kin-1^{KO1} combined with Kin-1^{KO2} cells, and then compared to Parental cells). Of the 100 significantly different proteins, 48 showed increased abundance (Table 3.4), and 52 showed decreased abundance (Table 3.5) in Kin-1^{KO1} and Kin-1^{KO2} cells relative to Parental cells. The 100 proteins that significantly differed in their levels were then analyzed for overrepresented pathways using Reactome software and were filtered to only include results with a significant p value ($p < 0.05$). The software identified pathways overrepresented in the list of 100 proteins (Table 3.6), including those pathways related to: cell cycle mitotic, cellular responses to stress, DNA repair, cytokine signaling in the immune system, signaling by receptor tyrosine kinases, negative regulation of the PI3K/AKT network, and signaling by RhoGTPases.

Table 3.6. Proteins with significantly increased or decreased abundance in Kin-1^{KO1} and Kin-1^{KO2} cells overrepresented in Reactome pathways

Cell Function	Protein symbol	Increase (+) or decrease (-) ^a
Cell cycle, mitotic (10 proteins)	RPA2	+
	AURKA	+
	GSK3B	+
	SRC	+
	PCNA	+
	RRM2	+
	CDC25C	+
	WEE1	+
	CDKN1A	-
	ABL1	-
Cellular response to stress (12 proteins)	VHL	+
	ETS1	+
	RPA2	+
	ATM	+
	GSK3B	+
	ATR	+
	HSBP1	-
	WIPI1	-
	CDKN1A	-
	EIF2AK3	-
	MAPK14	-
	SOD2	-
DNA repair (19 proteins)	RBBP8	+
	BRCA1	+
	PMS2	+
	ATM	+
	ERCC4	+
	CHEK1	+
	CHEK2	+
	ATR	+
	CDT2	+
	RPA2	+
	MLH1	+
	XPA	+
	NRG1	+
	MSH2	+
	PCNA	+
	PARG	+
DDB1	+	

Table 3.6. Cont. Proteins with significantly increased or decreased abundance in Kin-1^{KO1} and Kin-1^{KO2} cells overrepresented in Reactome pathways

Cell Function	Protein symbol	Increase (+) or decrease (-) ^a
DNA repair (19 proteins)	ABL1	-
	RAD51	-
Cytokine signaling in Immune system (18 proteins)	PTPN12	+
	FOXO3	+
	PAK4	+
	FGF2	+
	GAB2	-
	SYK	-
	CDKN1A	-
	SOD2	-
	TNFRSF12A	-
	PTPN11	-
	GRB2	-
	PIK3CB	-
	MUC1	-
	BCL2L11	-
	EIF4E	-
	AKT	-
STAT1	-	
MAPK14	-	
Signaling by receptor tyrosine kinases (22 proteins)	SRC	+
	FGF2	+
	CAV1	+
	EGFR	+
	PTPN12	+
	PAK4	+
	CHEK1	+
	PAK1	+
	NRG1	+
	AXL	+
	PTPN11	-
	ERBB3	-
	PIK3CB	-
	AKT	-
	GAB2	-
	CD274	-
STAT1	-	

Table 3.6. Cont. Proteins with significantly increased or decreased abundance in Kin-1^{KO1} and Kin-1^{KO2} cells overrepresented in Reactome pathways

Cell Function	Protein symbol	Increase (+) or decrease (-) ^a
Signaling by receptor tyrosine kinases (22 proteins)	VEGFR	-
	INSR	-
	RICTOR	-
	MAPK14	-
	GRB2	-
Negative regulation of PI3K/AKT network (11 proteins)	EGFR	+
	FGF2	+
	SRC	+
	NRG1	+
	GAB2	-
	PIK3CB	-
	ERBB3	-
	AKT	-
	INSR	-
	PTPN11	-
GRB2	-	
Signaling by RhoGTPases (11 proteins)	AURKA	+
	CAV1	+
	CDC25C	+
	PAK4	+
	PAK1	+
	SRC	+
	TFRC	-
	ABL1	-
	GRB2	-
	EPHA2	-
	MAPK14	-

^a Proteins with increased abundance in Kin-1^{KO1} and Kin-1^{KO2} cell relative to Parental cells are denoted with "+". Proteins with decreased abundance in Kin-1^{KO1} and Kin-1^{KO2} cell relative to Parental cells are denoted with "-".

3.6.2 A Focused Examination of the 100 Differentially Expressed Proteins in Kin-1^{KO1} and Kin-1^{KO2} cells

From the RPPA data, I next examined for proteins associated with proliferation, migration, and adhesion, as these may help give insight into the molecular underpinnings of these experiments – the role of Kindlin-1 in these cellular processes. I conducted a literature review of all 100 proteins identified to be significantly different with the loss of Kindlin-1, searching for each proteins' function in SCC or keratinocytes. This identified many proteins involved in proliferation, such as proliferating cell nuclear antigen (PCNA) and epidermal growth factor receptor (EGFR) (Table 3.7). It also revealed many proteins involved in migration such as proto-oncogene tyrosine-protein kinase (SRC) and p21-activated kinase 1 (PAK1) (Table 3.8). However, this process yielded very few proteins that are involved in adhesion: tyrosine protein kinase receptor UFO (AXL; Cichoń et al., 2014), growth factor receptor-bound protein 2 (GRB2; Giubellino et al., 2008), and SRC (Ainger et al., 2015).

Therefore, to objectively identify proteins involved in adhesion, I cross-referenced the 100 proteins identified by RPPA with proteins that are known to be involved in the consensus integrin adhesome. The consensus integrin adhesome was determined through meta-analysis of proteomic data of components of integrin adhesion complexes in a variety of cell types, under a variety of conditions to identify ubiquitous adhesion proteins (Horton et al., 2016; Winograd-Katz et al., 2014; Zaidel-Bar et al., 2007). Using

Table 3.7. Proteins with significantly increased or decreased abundance in Kin-1^{KO1} and Kin-1^{KO2} cells involved in regulating proliferation in SCC or keratinocytes

Protein name	Protein Symbol	Mean fold difference ^a	Reference ^b
RAC-alpha serine/threonine-protein kinase phosphorylated at Thr308	AKT1/2/3 (pY308)	-1.17	(Lu et al., 2021)
Serine-protein kinase ATM	ATM	1.52	(Ismail et al., 2011)
ATR Serine/Threonine Kinase	ATR	1.17	(Parikh et al., 2014)
Aurora A/B/C phosphorylated at Thr288, Thr232 and Thr198	AURKA (pY288, pY232, pY198)	1.40	(Davis et al., 2020)
Cell division cycle 25C	CDC25C	1.55	(Liu et al., 2020)
Cell division cycle protein 2	CDT2	1.25	(Vanderdys et al., 2018)
Serine/threonine-protein kinase Chk1	CHEK1	1.91	(Tho et al., 2012)
Serine/threonine-protein kinase Chk2	CHEK2	1.27	(Tian et al., 2020)
DNA endonuclease RBBP8	CTIP	1.71	(Mozaffari et al., 2021)
DNA damage-binding protein 1	DDB1	1.25	(Cang et al., 2007)
DNA methyltransferase 1	DNMT1	1.39	(Li et al., 2020)
Dipeptidyl peptidase 4	DPP4	-1.16	(Shih et al., 2018)
Epidermal growth factor receptor	EGFR	1.37	(Cañueto et al., 2017)
Ephrin type-A receptor 2 phosphorylated at Tyr588	EPHA2 (pY588)	-1.85	(Wang et al., 2021)
Receptor tyrosine-protein kinase erbB-2 phosphorylated at Tyr1248	ERBB2	-1.25	(Pollock et al., 2015)
Receptor tyrosine-protein kinase erbB-3	ERBB3	-1.29	(Dahlhoff et al., 2015)
Protein C-ets-1	ETS1	1.17	(Nagarajan et al., 2009)
Growth factor receptor-bound protein 2	GRB2	-1.12	(Giubellino et al., 2008)
Insulin like growth factor binding protein 3	IGFBP3	-1.35	(Liu et al., 2018)

Table 3.7. Cont. Proteins with significantly increased or decreased abundance in Kin-1^{KO1} and Kin-1^{KO2} cells involved in regulating proliferation in SCC or keratinocytes

Protein name	Protein Symbol	Mean fold difference ^a	Reference ^b
Mitogen-activated protein kinase 14 phosphorylated at Thr180 and Tyr182	MAPK14 (pT180, pY182)	-1.09	(Liu et al., 2014)
Notch 1	NOTCH1	-1.41	(Zhang et al., 2016)
Neuregulin-1	NRG1	2.27	(Hegde et al., 2019)
Proliferating Cell Nuclear Antigen	PCNA	1.19	(Kawahira, 1999)
Proliferating Cell Nuclear Antigen	PCNA	1.19	(Kawahira, 1999)
Phosphatidylinositol 4,5-bisphosphate 3-kinase catalytic subunit beta isoform	PIK3CB	-1.15	(Lu et al., 2021)
DNA polymerase subunit gamma-1	POLG	-1.19	(Singh et al., 2018)
Protein tyrosine phosphatase non-receptor Type 12	PTPN12	1.37	(Su et al., 2013)
Ras-related protein rab-25	RAB25	-1.58	(Jeong et al., 2019)
Rapamycin-insensitive companion of mTOR	RICTOR	-1.19	(Back et al., 2012)
Replication Protein A2 phosphorylated at Ser4 and Ser8	RPA2 (pS4, pS8)	1.21	(Chen et al., 2017)
Ribonucleoside-diphosphate reductase subunit M2	RRM2	1.28	(Wang et al., 2021)
Mothers against decapentaplegic homolog 4	SMAD4	1.35	(Hernandez et al., 2019)
Proto-oncogene tyrosine-protein kinase	SRC	1.26	(Ainger et al., 2015)
Signal transducer and activator of transcription 1 phosphorylated at Tyr701	STAT1 (pY701)	-1.77	(Clifford et al., 2000)
Tumor necrosis factor receptor superfamily member 12A	TNFRSF12A	-1.49	(Hu et al., 2019)
Vascular endothelial growth factor receptor 2	VEGFR	-1.59	(Johnson et al., 2012)
Wee1-like protein kinase	WEE1	1.40	(Ghelli Luserna Di Rorà et al., 2020)

Table 3.7. Cont. Proteins with significantly increased or decreased abundance in Kin-1^{KO1} and Kin-1^{KO2} cells involved in regulating proliferation in SCC or keratinocytes

Protein name	Protein Symbol	Mean fold difference ^a	Reference ^b
Wee1-like protein kinase phosphorylated at Ser642	WEE1 (pS642)	-1.10	(Katayama et al., 2005)

^a Fold relative difference in abundance found from the mean calculated levels in Kin-1^{KO1} together with Kin-1^{KO2} clones, relative to Parental SCC-13 cells. Abundance in Parental SCC-13 cells have been set to 1.

^b Protein function in SCC of a variety of tissue origin.

Table 3.8. Proteins with significantly increased or decreased abundance in Kin-1^{KO1} and Kin-1^{KO2} cells involved in regulating migration in SCC or keratinocytes

Protein name	Protein Symbol	Mean fold difference ^a	Reference ^b
RAC-alpha serine/threonine-protein kinase phosphorylated at Thr308	AKT1/2/3 (pY308)	-1.17	(Lu et al., 2021)
Tyrosine protein kinase receptor UFO	AXL	2.12	(Cichoń et al., 2014)
Caveolin-1	CAV1	1.52	(Trimmer et al., 2013)
Epithelial discoidin domain-containing receptor 1	DDR1	-1.24	(Hidalgo-Carcedo et al., 2011)
Dipeptidyl peptidase 4	DPP4	-1.16	(Long et al., 2018)
Ephrin type-A receptor 2 phosphorylated at Tyr588	EPHA2 (pY588)	-1.85	(Wang et al., 2021)
Receptor tyrosine protein kinase erb-2 phosphorylated at Tyr1248	ERBB2	-1.25	(Rao et al., 2015)
Receptor tyrosine-protein kinase erb-3	ERBB3	-1.29	(Dahlhoff et al., 2017)
Growth factor receptor-bound protein 2	GRB2	-1.12	(Giubellino et al., 2008)
Mitogen-activated protein kinase 14 phosphorylated at Thr180 and Tyr182	MAPK14 (pT180, pY182)	-1.09	(Liu et al., 2014)
Notch 1	NOTCH1	-1.41	(Zhang et al., 2016)
p21-activated kinase 1	PAK 1	1.25	(Chow et al., 2012)
p21-activated kinase 4	PAK 4	1.12	(Won et al., 2019)
Phosphatidylinositol 4,5-bisphosphate 3-kinase catalytic subunit beta isoform	PIK3CB	-1.15	(Lu et al., 2021)
Ras-related protein rab-25	RAB25	-1.58	(Jeong et al., 2019)
Transcription factor SOX-7	SOX7	1.37	(Hong et al., 2021)
Proto-oncogene tyrosine-protein kinase	SRC	1.26	(Ainger et al., 2015)
Tumor necrosis factor receptor superfamily member 12A	TNFRSF12A	-1.49	(Hu et al., 2019)

^a Fold relative difference in abundance found from the mean calculated levels in Kin-1^{KO1} together with Kin-1^{KO2} clones, relative to Parental SCC-13 cells. Abundance in Parental SCC-13 cells have been set to 1.

^b Protein function in SCC of a variety of tissue origin.

this approach, 5 proteins were identified that had increased abundance in Kindlin-1-deficient SCC-13 cells, and 8 proteins with decreased abundance (Table 3.9).

3.6.3 Phosphoproteins with Significantly Altered Abundance in Kin-1^{KO1} and Kin-1^{KO2} cells

Some of the antibodies used in the RPPA analysis recognized post-translational modifications (specifically, phosphorylation). Of the 100 hits identified to have significantly different abundances in both Kin-1^{KO1} and Kin-1^{KO2} cells relative to Parental cells, 20 were assessed with antibodies against proteins with post translational modifications (Table 3.10). The phosphorylation of most of these proteins increases the activation of the protein, whereas the phosphorylation of Serine/threonine-protein kinase ULK1 (ULK1), Wee1-like protein kinase (WEE1), and Forkhead box O3 (FOXO3), are deactivating (references provided in Table 3.10).

These RPPA results indicate that Kindlin-1 impacts the abundance of many proteins associated with tumor formation and/or progression. Furthermore, pathway analysis and literature review identified pathways that are likely impacted as result of Kindlin-1-deficiency in SCC-13 cells, such as those associated with proliferation, migration, adhesion, and DNA repair.

Table 3.9. Proteins with significantly increased or decreased abundance in Kin-1^{KO1} and Kin-1^{KO2} cells involved in the consensus integrin adhesome

Protein name	Protein Symbol	Mean fold difference ^a
Tyrosine-protein kinase ABL1 phosphorylated at Tyr412	ABL1	-1.16
RAC-alpha serine/threonine-protein kinase phosphorylated at Thr308	AKT1/2/3 (pY308)	-1.17
Caspase 8	CASP8	1.22
Caveolin-1	CAV1	1.52
Growth factor receptor-bound protein 2	GRB2	-1.12
Heat Shock Factor Binding Protein 1 phosphorylated at Ser82	HSBP1	-1.38
Insulin receptor phosphorylated at Tyr1248	INSR	-1.25
p21-activated kinase 1	PAK 1	1.25
Phosphatidylinositol 4,5-bisphosphate 3-kinase catalytic subunit beta isoform	PIK3CB	-1.15
Tyrosine-protein phosphatase non-receptor type 11 phosphorylated at Tyr548	PTPN11	-1.19
Protein tyrosine phosphatase non-receptor Type 12	PTPN12	1.37
Proto-oncogene tyrosine-protein kinase	SRC	1.26
Tyrosine-protein kinase SYK	SYK	-1.18

^a Fold relative difference in abundance found from the mean calculated levels in Kin-1^{KO1} together with Kin-1^{KO2} clones, relative to Parental SCC-13 cells. Abundance in Parental SCC-13 cells have been set to 1.

Table 3.10. Phosphoproteins with significantly increased or decreased abundance in Kin-1^{KO1} and Kin-1^{KO2} cells

Protein Symbol	Phosphorylation Site	Phosphorylation is: Activating (A) or Deactivating (D)	Mean fold difference ^a	Reference ^b
EPHA2	Y588	A	-1.85	(Brückner et al., 1997)
STAT1	Y701	A	-1.77	(Sadzak et al., 2008)
HSBP1	S82	A	-1.38	(Geum et al., 2002)
ULK1	S757	D	-1.30	(Fan et al., 2015)
VEGFR	Y1175	A	-1.29	(Takahashi et al., 2001)
ERBB2	Y1248	A	-1.25	(Ishizawa et al., 2007)
PTPN11	Y542	A	-1.19	(Lu et al., 2001)
AKT1/2/3	T308	A	-1.17	(Gao et al., 2014)
ABL1	Y412	A	-1.16	(Kim et al., 2020)
LRP6	S1490	A	-1.13	(Vijayakumar et al., 2017)
WEE1	S642	D	-1.10	(Katayama et al., 2005)
MAPK14	T180, Y182	A	-1.09	(Chen et al., 2012)
AURKA	T288, T232, T198	A	1.40	(Ertych et al., 2014)
PRKAA1-2	T172	A	1.32	(Fogarty et al., 2016)
PAK4-6	S474, S602, S560	A	1.31	(Chong et al., 2001)
CHEK2	T68	A	1.21	(Zoppoli et al., 2012)
RPA2	S4, S8	A	1.21	(Rector et al., 2017)
RPS6KB1	T389	A	1.16	(Pullen et al., 1997)

Table 3.10. Cont. Phosphoproteins with significantly increased or decreased abundance in Kin-1^{KO1} and Kin-1^{KO2} cells

Protein Symbol	Phosphorylation Site	Phosphorylation is: Activating (A) or Deactivating (D)	Mean fold difference ^a	Reference ^b
FOXO3	S318, S321	D	1.11	(Arden, 2004)
ATM	S1981	A	1.08	(So et al., 2009)

^a Fold relative difference in abundance found from the mean calculated levels in Kin-1^{KO1} together with Kin-1^{KO2} clones, relative to Parental SCC-13 cells. Abundance in Parental SCC-13 cells have been set to 1.

^b Protein function in SCC of a variety of tissue origin.

4 Discussion

4.1 Summary

Loss-of-function mutations of *FERMT1*, which encodes Kindlin-1, cause several abnormalities in humans, collectively termed Kindler syndrome, characterized by skin defects and increased susceptibility to developing aggressive epidermal squamous cell carcinoma (Que et al., 2018). This has led efforts to investigate the role of Kindlin-1 in keratinocytes, to better understand why the loss of Kindlin-1 expression increases susceptibility to the development of aggressive SCC. Previous work has shown that Kindlin-1 has protective effects against UV-induced DNA damage and cell stress in mouse SCC (Emmert et al., 2017). Given the increased incidence of aggressive SCC as a result of loss-of-function mutations in *FERMT1*, the goal of this study was to characterize the consequences of inactivating Kindlin-1 expression in SCC-13 epidermal carcinoma cells, to better understand Kindlin-1 function within human SCC. My studies (expanded on below) demonstrate that Kindlin-1 is dispensable for SCC-13 proliferation, or maintenance of clonogenic potential in culture. Changes in cell spreading on collagen I were identified in SCC-13 cells with the loss of Kindlin-1, which were not observed in cells spreading on laminin-332 matrix. I also determined that Kindlin-1 is involved in directional migration, as loss of Kindlin-1 enhanced SCC-13 migration in culture. Finally, I have identified a large number of proteins that differ in abundances in Kindlin-1-deficient cells.

4.2 Kindlin-1 is Dispensable for Proliferation and Clonogenic Potential in SCC-13 Cells

From proliferation studies, I discovered the loss of Kindlin-1 did not impact proliferation in the SCC-13 cells in culture (Fig. 3.2 and 3.3). Whereas there are no studies looking at the effect of loss of Kindlin-1 on proliferation in epidermal SCC cells, knockout of Kindlin-1 with siRNA in pancreatic carcinoma cells did not impact proliferation (Mahawithitwong et al., 2013). However, other epithelial carcinomas, such as breast and colorectal carcinomas, as well as keratinocytes show decreased proliferation with the loss of Kindlin-1 (Herz et al., 2006; Kong et al., 2016; Sin et al., 2011). This discrepancy between the different cell types in the effect of Kindlin-1 on proliferation may reflect differences in the regulation of pathways that control proliferation in epidermal carcinoma cells compared to keratinocytes, and breast and colorectal carcinomas. To address this possibility, future work can focus on identifying the main effectors of proliferative control in SCC-13 cells by adding inhibitors and activators of key proteins in proliferative pathways such as the RAS-MEK-ERK pathway (Neu et al., 2017). This would give insight into the pathway and proteins that control proliferation in epidermal SCC cells, that may aid in understanding and treatment of epidermal SCC.

The spheroid formation assay models for the presence of stem-like cells which can self-renew, proliferate in culture over the long term, and display an enhanced ability to form tumors *in vivo* (Adhikary et al., 2013). Loss of Kindlin-1 did not impact the number of spheroids formed (Figure 3.4B), suggesting Kindlin-1 is not essential for spheroid formation. Previous work in the SCC-13 cell line showed that of the 4×10^4 cells plated,

only 60 spheroids formed, meaning 0.15% of cells cultured were able to form spheroids (Adhikary et al., 2013). However, in my studies, 0.68% of Parental SCC-13 cells plated formed spheroids (110 spheroids formed out of a total of 1.6×10^4 cells plated, Figure 3.4B), indicating that in my hands, Parental SCC-13 cells formed 4.5 times more spheroids than previously reported. Despite the discrepancy in the number of spheroids formed, both results reflect less than 1% of all cells exhibiting stem-like capacity, which is within the normal range for stem-like cells in a cancer cell population (Al-Hajj et al., 2004; Dontu et al., 2005).

Differences in perimeter size at day 15 between Parental and Kin-1^{KO1} spheroids (Fig. 3.4C) may reflect differences in the fraction of stem-like cells within the population. Research in keratinocytes suggests that the fate of colony growth in monolayers is dictated by the proliferative properties of the cells, where small colonies are derived from transit amplifying cells, that proliferate finitely before becoming terminally differentiated. By contrast, large colonies are formed from stem cells that are capable of self-renewal, allowing for continuous growth (Watt, 1988). It is possible that the larger mean perimeter of Parental spheroids reflects that there are more stem-like cells present in the cell population to form larger spheroids, than in Kin-1^{KO1} cell population, which may have more transit amplifying cells. Alternatively, it is possible that the differences in perimeter reflect faster proliferation of stem-like cells in the Parental spheroids, compared to the Kin-1^{KO1} cell population. Studies looking at markers of stem-like cells in spheroids such as ALDH1, EZH2, SOX2, and OCT4 (Adhikary et al., 2013), as

well as their proliferative status through the use of BrdU would need to be performed on Parental, Kin-1^{KO1} and Kin-1^{KO2} spheroids to differentiate between these options.

4.3 Defects in Cell Spreading on Collagen I, But Not on Laminin-332 Matrix

There were no detectable spreading defects observed on laminin-332 matrix obtained from conditioned medium with the loss of Kindlin-1 (Fig. 3.5). There are 2 main integrin pairs responsible for adhesion on laminin-332: $\alpha3\beta1$, found at focal adhesions, and $\alpha6\beta4$ found at hemidesmosomes (Watt, 2002). The presence of $\alpha6\beta4$ integrins may aid in adhesion to the laminin-332 matrix, a necessary step for cell spreading (McGrath, 2007). Furthermore, Kindlin-2 has been shown to replace Kindlin-1 to activate integrins and induce cell adhesion to laminin-332 in keratinocytes (He et al., 2011).

The lack of differences seen in Parental cell spreading on laminin-332 matrix from 2 to 6 h (Fig. 3.5) is possibly due to laminin-332 inducing rapid spreading (Kariya et al., 2012). It was previously reported that keratinocytes were largely spread on laminin-332 within 40 min of plating (Kariya et al., 2012). However, since my studies concluded at 6 h, it is also possible that I did not capture cells at their maximum spreading, and the lack of difference from 2 to 6 h may reflect a delay in spreading caused by extension and retraction cycles of the membrane as the cells spread (Herz et al., 2006). To test this in SCC-13 cells, spreading of SCC-13 cells containing and lacking Kindlin-1 should be evaluated at earlier and later time points. Additionally, spreading was assessed on laminin-332 matrix obtained from conditioned medium of 804G cell cultures, which was not quantified for laminin content and therefore the laminin content could not be altered. Evaluating SCC-13 cell spreading on different concentrations of laminin-332 may

reveal differences in cell spreading between SCC-13 cells containing and lacking Kindlin-1, as the concentration of ligands can impact spreading (Millon-Frémillon et al., 2008). Gaudet et al. (2003) utilized the spreading of 3T3 fibroblasts on collagen I to propose a hypothesis of cell spreading on different densities of collagen I. That study suggested that, at low densities of the ligand, the limiting factor for spreading is the availability of collagen I, whereas at higher densities of the ligand, the limiting factor for spreading is integrin affinity for the collagen I ligand. This is because at lower densities of collagen, there are many integrin receptors for each collagen molecule, and therefore the affinity of the receptor is less important for spreading. However, when there are more collagen molecules, the ratio of receptor to ligand is lower, and the affinity of each integrin receptor is more important.

This hypothesis has bearing on my evaluation of SCC-13 spreading on low and medium concentrations of collagen I. Spreading on a low concentration of collagen I revealed no differences in spreading between SCC-13 cells containing or lacking Kindlin-1 (Fig. 3.6), however, there was a delay in spreading on a medium concentration of collagen I in Kin-1^{KO1} and Kin-1^{KO2} cells, compared to Parental cells (Fig. 3.7) This may be due to the fact that loss of Kindlin-1 may result in lower affinity of $\alpha2\beta1$ integrin to collagen I, caused by reduced integrin activation. While talin expression alone is reportedly sufficient for integrin activation, a reduction in $\beta1$ integrin activation has been established with the loss of Kindlin-1 in keratinocytes and carcinoma cells, indicating that there is a synergistic effect with the co-expression of talin and Kindlin-1, which is lost when Kindlin-1 is not present (Ussar et al., 2008). Differences in spreading at low

concentrations of collagen I were not seen in my study, likely because even though there may be less integrin activation in Kindlin-1 knockout cells, there are still many more integrins relative to ligands in all cells. Thus, this high abundance of integrins relative to ligand in Parental, Kin-1^{KO1} and Kin-1^{KO2} results in similar spreading, as all the available collagen I was bound to integrins, even though Parental cells may have more activated integrins.

Whereas, at medium concentrations of collagen I, there is a lower integrin to ligand ratio, and the affinity of each integrin to its ligand plays a more prominent role in spreading. Therefore, cells with integrins which display lower affinity for their ligand (such as may occur in the Kindlin-1 knockout cells) may cause suboptimal ligand binding, resulting in less efficient, and altered spreading. This concept could be tested by measuring the affinity of $\alpha2\beta1$ integrin for collagen I in the presence and absence of Kindlin-1 in SCC-13 cells. This could be accomplished using an integrin soluble ligand binding assay, where live SCC-13 cells expressing and lacking Kindlin-1 are held in suspension culture and exposed to specific concentrations of collagen I ligand. The binding of $\alpha2\beta1$ integrin to the ligand can be detected using antibodies and measured using flow cytometry (Wang et al., 2021).

Another important regulator of cell spreading is integrin clustering (avidity), which occurs when integrins bind to their ligand, inducing more integrins to localize to that adhesion site, increasing adhesion strength (Margadant et al., 2011). At low densities of collagen I, differences in integrin avidity may not impact cell spreading, as there are already more integrins relative to ligand. However, at higher concentrations of collagen

I, the lower integrin to ligand ratio may reveal differences in avidity, as integrin clustering can positively impact cell spreading, leading to a delay in spreading in cells with reduced clustering, such as may occur in Kindlin-1-deficient cells (Cavalcanti-Adam et al., 2007). While Kindlin-1 has not been shown to impact $\beta 1$ integrin avidity, Kindlin-1 can induce clustering of $\alpha II\beta 3$ integrins (Kukkurainen et al., 2021). Kindlin-1 effects on $\alpha 2\beta 1$ integrin avidity could be measured using an ECM surface reported in Maheshwari et al. (2000), where multiple ECM ligands are tethered to poly-ethylene glycol hydrogels treated with polyethylene oxide which prevents cell adhesion, to ensure cells only adhered to the ligand of interest. The binding of $\alpha 2\beta 1$ integrin to the ligand can then be measured using flow cytometry (Wang et al., 2021).

4.4 Loss of Kindlin-1 Enhances SCC-13 Migration in Culture

From scrape-wound assays, I found that loss of Kindlin-1 increased SCC directional migration (Fig. 3.8). This is consistent with a study conducted by Margadant et al. (2009), which found increased migration in keratinocytes with the loss of $\alpha 3$ integrins, likely due to reduced adhesion at the rear of the cell, allowing it to migrate more persistently. Similarly, in keratinocytes isolated from Kindler Syndrome patients there was an abnormal distribution of focal adhesions, in that majority of the focal adhesions were localized to the leading edge, despite there being the same overall number of focal adhesions in normal and mutant cells (Has et al., 2009). This suggests that with the loss of Kindlin-1 there are fewer adhesion sites at the rear of the cell to anchor it to the ECM, resulting in increased migration. Experiments designed to evaluate the distribution of

focal adhesions in SCC-13 cells containing and lacking Kindlin-1 could address this possibility.

Adhesion strength is another metric important for cell migration. Yeoman et al. (2021), found that lower adhesion strength in some tumor cells induces faster migration relative to higher adhesion strength. This may help explain the increased migration of Kin-1^{KO1} and Kin-1^{KO2} cells, where the loss of Kindlin-1 may reduce integrin activation leading to reduced affinity of integrins for their ECM ligand, reducing the strength of adhesion. This can be tested using a parallel plate flow chamber, which allows separation of cells based on adhesion strength, followed by a directional migration assay (Yeoman et al., 2021).

An important factor related to migration addressed by Yeoman et al. (2021) that was not evaluated in the present study was the effect of substrate stiffness on cell migration. In my experiments, migration was assessed with cells plated directly onto plastic culture dishes, which has a stiffness on the order of megapascals; much higher than that experienced *in vivo* (Skardal et al., 2013). However, the cells were plated 24 h prior to the scrape-wound assay, allowing time for the cells to deposit their own ECM, affecting substrate stiffness (Deville et al., 2019). Substrate stiffness can impact epidermal cell migration, as epidermal cells exposed to high substrate stiffness, such as during wound healing, exhibit faster migration than cells on lower stiffnesses (Wang et al., 2012). The response to substrate stiffness is regulated in part by integrins and the signaling cascades they activate (Chen et al., 2014). The effect of Kindlin-1 on cell migration on different substrate stiffnesses can be tested by plating SCC-13 cells containing and

lacking Kindlin-1 on culture dishes coated with substrates of different stiffnesses, followed by a scrape-wound assay.

4.5 Reverse Phase Protein Array Analysis Reveal Differences in Protein Abundances Important for Carcinogenesis with the Loss of Kindlin-1 in SCC-13 Cells

There were several signaling cascade pathways that were altered in Kindlin-1-deficient SCC-13 cells (Table 3.6), which will be discussed below.

4.5.1 Regulation of the Cell Cycle and Mitosis

Reactome software detected 10 proteins, whose levels were altered in the Kindlin-1-deficient SCC-13 cells, that are involved in regulating the cell cycle (Table 3.6) such as Aurora A (AURKA) and CDC25C, that are involved in regulating cell cycle checkpoints (Liu et al., 2020). During the cell cycle, centrosomes undergo duplication, followed by maturation where proteins are recruited to the centrosomes; recruited proteins are collectively termed pericentriolar material. Mature centrosomes then separate, as they move to opposite ends of the cell, where they organize and extend mitotic spindles composed of tubulin proteins, that attach to and subsequently separate sister chromatids (Nigg et al., 2011). Kindlin-1 can localize to centrosomes in mitotic keratinocytes, where it binds to Aurora A during centrosome maturation, important for proper spindle orientation (Patel et al., 2013). Loss of Kindlin-1 results in abnormal spindle formation, such as monopolar spindles where the centrosomes fail to segregate to opposite ends of the cell, leading to cell death (Patel et al., 2013).

In vivo, *FERMT1* inactivation in the epidermis leads to a significant increase in cell numbers that exhibit mitotic spindles perpendicular to the basement membrane, which is associated with increased frequency of asymmetric divisions of basal cells, whereby only 1 cell remains in the basal layer (Patel et al., 2016). This can lead to a decrease in proliferation as increased asymmetric divisions can cause stem cell depletion (Patel et al., 2016). Furthermore, Kindlin-1 can regulate microtubule stability, as the loss of Kindlin-1 is associated with reduced abundance of acetylated tubulin, a marker of stable microtubules, leading to lagging chromatids during anaphase (Patel et al., 2016). This phenotype occurs as result of dysregulated HDAC6, a key regulator of microtubule stability, which could be reversed with the inhibition of HDAC6. Kindlin-1 can interact directly with HDAC6, which may contribute to its role in regulating microtubule stability (Patel et al., 2016).

4.5.2 Cell Responses to Stress

Six of the 12 proteins involved in cell responses to stress, identified by the Reactome database, have decreased abundance in SCC-13 cells lacking Kindlin-1 (CDKN1A, WIPI1, HSBP1, EIF2AK3, MAPK14, and SOD2), indicating Kindlin-1 role in regulating cell stress responses. Notably, there is a decrease in SOD2 abundance in Kin-1^{KO1} and Kin-1^{KO2} cells relative to Parental SCC-13 cells, and SOD2 is associated with protection against oxidative stress (Robbins et al., 2011). Decreased SOD2 can cause decreased cell viability, and increased risk of ROS induced mutagenesis (Robbins et al., 2011). Perhaps the decrease in SOD2 abundance in Kin-1^{KO1} and Kin-1^{KO2} cells may result in increased oxidative stress, which may induce increased susceptibility to mutagenesis, potentially

resulting in increased cell death or, alternatively, increased tumor aggressiveness, as high mutation rates can positively impact a tumor's ability to populate a distant tissue (Gara et al., 2018). In mouse SCC cells, loss of Kindlin-1 increased reactive oxygen species (ROS) production and reduced levels of the ROS scavenger, glutathione (Emmert et al., 2017). As a result, those SCC cells lacking Kindlin-1 were more prone to oxidative stress following exposure to H₂O₂ or UV treatment (Emmert et al., 2017).

There was also decreased abundance of WIPI1 and EIF2AK3, which are involved in inducing autophagy (Bostanciklioglu, 2015; Tsuyuki et al., 2014). Additionally, while not detected by Reactome as part of the stress response pathway, there was also decreased abundance in ULK1, and MAP1LC3A/B that regulate autophagy (Kim et al., 2011; Zhang et al., 2015). This decrease in abundance of autophagy proteins as a result of loss of Kindlin-1, reveals a potential novel role for Kindlin-1 in regulating autophagy in SCC cells. Autophagy plays complex roles in cancer, and it may serve as a tumor suppressor, removing damaged cellular components that may increase susceptibility of cancer development and progression. Furthermore, autophagy can reduce cellular ROS, thus protecting cellular DNA from mutagenic insults which may lead to tumor formation and progression (Yun et al., 2018).

Other proteins with increased abundance with the loss of Kindlin-1 are largely associated with DNA damage responses following cell stress (ATM, ATR, RPA2) (Yang et al., 2003). It is possible that these proteins have increased abundance as a result of increased cell stress with the loss of Kindlin-1, prompting the need for increased DNA

repair to maintain genome stability required for cancer cell survival (Ghelli Luserna Di Rorà et al., 2020).

The RPPA results regarding cell response to stress reveal both a possible protective and deleterious effect of loss of Kindlin-1 in SCC-13 cells. While loss of Kindlin-1 decreased the abundance of some cell response proteins, such as SOD2, pointing to possible deleterious effects, it also increased the abundance of other proteins, such as ATM and ATR, that may positively regulate cell stress. Future work would need to focus on evaluating the effect of cell stress on the behaviour of SCC-13 cells containing and lacking Kindlin-1 to better parse out the role of Kindlin-1 in cell stress response.

4.5.3 DNA Repair

The Reactome database identified 17 proteins of a total of 19 proteins involved in DNA repair (Table 3.6) had increased abundance in both Kin-1^{KO1} and Kin-1^{KO2} cell lines compared to the Parental cell line, suggesting an increase in DNA repair potential with the loss of Kindlin-1. ATM and ATR are among the proteins with increased abundance, responsible for activating DNA repair pathways and inducing cell cycle arrest following DNA damage (Yang et al., 2003). This increase in DNA damage responses may play a role in tumorigenesis and cancer progression, as cancer cells must maintain a tolerable level of DNA damage so as to continue to function and proliferate (Ghelli Luserna Di Rorà et al., 2020). Loss of Kindlin-1 in SCC cells and keratinocytes is known to increase DNA damage, likely requiring an increase in DNA repair to maintain survival. Emmert et al. (2017) found an increase in DNA damage with the loss of Kindlin-1 in mouse SCC cells and keratinocytes. In response to oxidative stress, the SCC cells lacking Kindlin-1 had less

activation of ERK signaling, compared to cells containing Kindlin-1, which contributed to the increased DNA damage with the lack of Kindlin-1 (Emmert et al., 2017).

Considering that Kindlin-1 can localize to the nucleus in keratinocytes (Lai-Cheong et al., 2008), taken together with my study that inactivation of *FERMT1* leads to increases in DNA repair protein abundances in SCC-13 cells, it is important for future work to elucidate if Kindlin-1 localizes to the nucleus in SCC cells, and whether it participates in regulation of genomic DNA repair.

4.5.4 Cytokine Signaling in the Immune System

Most of the proteins identified by Reactome are involved in cytokine signaling pathway had decreased abundance in Kindlin-1 deficient SCC-13 cells such as MUC1, SYK, and GAB2 (Table 3.6). This may reflect a decrease in signaling to the immune system as a result of loss of Kindlin-1 in SCC-13 cells. Decreased immune signaling may benefit cancer cells and aid in cancer progression, as it allows the cancer cells to evade immune response, preventing cell death (Harjunpää et al., 2019). This may give insight into why loss of Kindlin-1 in humans can lead to increased incidence of aggressive SCC (Guerrero-aspizua et al., 2019), as it may allow the cells to evade immune detection, a necessary step in cancer progression (Hanahan et al., 2000).

Heinemann et al. (2011) found that loss of Kindlin-1 in keratinocytes leads to an increase in expression of cytokines and growth factors, which were found to be further upregulated in response to cell stress. This is contrary to what was found in the RPPA data where most of the proteins associated with cytokine signaling were downregulated in Kindlin-1 deficient SCC-13 cells. However, Heinemann et al. (2011) evaluated the

expression of inflammatory cytokines, which were not represented in the RPPA analysis. It is important for future studies to evaluate Kindlin-1 role in regulating the immune system, as it may give insight into possible treatments for tumors lacking Kindlin-1.

4.5.5 Receptor Tyrosine Kinase Signaling

Kindlin-1 contains a PH domain, which allows it to interact with lipids within the plasma membrane, suggesting that it may interact with transmembrane receptors. One such receptor is EGFR, which directly binds Kindlin-1 in keratinocytes. In these cells, Kindlin-1 prevents the internalization of EGFR through clathrin-mediated endocytosis (Michael et al., 2019). It is noteworthy that the RPPA data suggest a complex role for Kindlin-1 in EGFR pathway regulation. Specifically, the loss of Kindlin-1 in SCC-13 cells revealed an increase in abundance of EGFR, which may reflect the cells attempt to overcome increased EGFR internalization with the loss of Kindlin-1. Future studies could evaluate this potential effect by preventing EGFR internalization through the use of inhibitors of endocytosis and evaluating resulting EGFR abundance. Furthermore, RPPA analysis revealed an increased abundance of PTPN12, that is known to inhibit EGFR signaling through dephosphorylation (Sun et al., 2011), which may also contribute to the increased expression of EGFR to overcome this inhibition. However, there was a decrease in abundance of PTPN11, which is also known to de-phosphorylate EGFR (Prahallad et al., 2015).

4.5.6 Proteins Involved in Negative Regulation of the PI3K/AKT Network

Loss of Kindlin-1 in epidermal SCC-13 cells caused decreased abundance of proteins associated with the PI3K/AKT signaling pathway, such as PI3K, AKT, GRB2, and RICTOR

(Table 3.6), which are known to induce proliferation and survival (Hemmings et al., 2016). There was also decreased abundance of ERBB2 and ERBB3 in Kin-1^{KO1} and Kin-1^{KO2} cell, which are known to bind to and activate PI3K (Ruiz-Saenz et al., 2018). One of the main functions of the PI3K-AKT pathway is to maintain proliferation, survival, and migration (Janus et al., 2017). My studies found no differences in proliferation in SCC-13 cells with the loss of Kindlin-1 (Fig. 3.2 and 3.3). The lack of differences in cell number over 96 h between cells containing and lacking Kindlin-1 (Fig. 3.2) also points to no differences in survival between these cell lines. Contrary to the function of PI3K-AKT signaling in inducing migration, Kin-1^{KO1} and Kin-1^{KO2} cells, which exhibited decreased abundance of the PI3K-AKT proteins, had increased migration (Fig. 3.8). This indicates that negative regulation of PI3K-AKT signaling likely did not impact Kindlin-1-deficient migration, and migration was increased through a different mechanism. Considering there was only a modest decrease in PI3K-AKT protein abundances (Table 3.5), it is likely that the negative regulation of PI3K-AKT signaling did not impact migration, however, more work determining the role of PI3K-AKT signaling in SCC-13 migration would need to be conducted.

4.5.7 Signaling by RhoGTPases

Reactome analysis detected 12 proteins with altered abundance as a result of loss of Kindlin-1 that are involved in RhoGTPase signaling, such as PAK1 and PAK4 (Table 3.6). To my knowledge, this is the first study to show that Kindlin-1 alters the abundance of proteins associated with Rho-GTPase signaling. In keratinocytes, Kindlin-1 is known to regulate the activation of RhoGTPases, where loss of Kindlin-1 resulted in decreased

activation of Rac1, RhoA, and CDC42 (Has et al., 2009). However, the study by Has et al. (2009) assessed activation of these proteins, not their abundances, which may help explain the discrepancy in the effect of Kindlin-1 deficiency on migration between keratinocytes and SCC-13 cells. There was a decrease in migration with the loss of Kindlin-1 in keratinocytes, which differed from my results in SCC-13 cells, where loss of Kindlin-1 enhanced SCC-13 migration (Fig. 3.8). This suggests differences in the effect of Kindlin-1 on RhoGTPases between keratinocytes and epidermal squamous carcinoma cells. Studies evaluating the activation status of RhoGTPases, such as Rac1, RhoA, and CDC42, would need to be performed in SCC-13 cells containing and lacking Kindlin-1 to better characterize its effect on this signaling cascade.

4.6 Future Directions

In this thesis I demonstrated that Kindlin-1 is dispensable for cell proliferation and is involved in spreading, migration, and protein regulation in SCC-13 cells. With each of my assays I have already described future experiments that could better illustrate Kindlin-1 role in a given cellular process, for example cell spreading on ECM substrates of different stiffnesses, or the use of signaling inhibitors to examine pathway activation. In addition to my suggested experiments above, there are many other approaches that can be utilized to elucidate Kindlin-1 function.

While my study found that Kindlin-1 is dispensable for proliferation of SCC-13 cells in culture, I did not evaluate the function of phosphorylated Kindlin-1 in SCC-13 cells, which is involved in maturation of centrosomes and microtubule stability during mitosis in keratinocytes (Patel et al., 2016). It would be important to investigate the function of

phosphorylated Kindlin-1, and its possible effects on regulating mitosis and the cell cycle. Understanding the conditions under which Kindlin-1 may regulate the cell cycle in SCC cells is vital for future treatment of SCC lacking Kindlin-1, as loss of Kindlin-1 can lead to aggressive SCC (Guerrero-aspizua et al., 2019).

To gain a better understanding of Kindlin-1 role in tumor progression, spheroid assays could be utilized to assess the stem-like properties of the SCC-13 cells containing and lacking Kindlin-1 by assessing markers for stemness in spheroids, such as OCT4 and SOX2. While there were no differences in spheroid number formed, there were differences in spheroid perimeter, possibly pointing to differences in cell composition of the spheroids in cells that did not express Kindlin-1. Furthermore, spheroid assays should be used to study Kindlin-1 role in invasion of SCC-13 cells, as the spheroids provide a 3-D system which more closely mimics the microenvironment experienced by tumors.

Adhesion and spreading on the ECM has important implications for tumor progression. Adhesion to the ECM through β 1 integrins is associated with a higher number of stem cells in the cell population, and can trigger outside-in signaling, such as the activation of the ERK pathway, important for proliferation and survival (Janes et al., 2006). It would be important for future research to focus on better understanding the role of Kindlin-1 in focal adhesion dynamics, and resulting adhesion in SCC-13 cells, to better elucidate Kindlin-1 role in adhesion and spreading. This can be accomplished by assessing focal adhesion size, density and localization by labelling focal adhesion proteins such as vinculin, FAK, and paxillin in cells containing and lacking Kindlin-1, as well as adhesion

assays where cells are plated, rinsed at specific intervals to remove non-adhered cells, and counted.

Although RPPA analysis allows for analysis of a large number of proteins, future work could focus on independently validating the results of proteins identified as being significantly different using immunoblot analysis to confirm altered protein abundances with the loss of Kindlin-1. Furthermore, effort should be focused on understanding how Kindlin-1 plays a role in the pathways identified to be overrepresented in the RPPA analysis and identifying any direct interactions of Kindlin-1 with these proteins to better understand where Kindlin-1 functions in these pathways.

Kindlin-1 was found to affect the protein abundance of VEGFR (Table 3.5), suggesting possible differences in tumor vascularization as a result of loss of Kindlin-1. It is important for future studies to work toward understanding Kindlin-1 function in SCC *in vivo*, such as through the use of mouse models, to better understand how the loss of Kindlin-1 affects tumor dynamics such as angiogenesis and metastasis. Additionally, mouse models are important for the study of immune system function to gain an understanding of Kindlin-1 regulation of immune function in tumors. This would provide better insight into the possible treatment options for Kindlin-1 deficient SCC and would provide a framework for future drug development.

4.7 Concluding Remarks

To my knowledge, this study is the first to evaluate Kindlin-1 function in human epidermal SCC cells. I have elucidated important, novel functions of Kindlin-1 in regulating spreading on collagen I, and found Kindlin-1 to be essential for normal

directional migration in human SCC. Moreover, I have revealed novel functions of Kindlin-1 in modulating the abundance of proteins involved in regulation of the cell cycle, stress responses, DNA repair, immune system responses, receptor tyrosine kinase signaling, the PI3K/AKT network, and RhoGTPase signaling in human SCC. Additional work is necessary to further elucidate Kindlin-1 roles in these pathways and how they contribute to the development and progression of SCC.

References

- Abbas, M., & Kalia, S. (2016). Trends in non-melanoma skin cancer (basal cell carcinoma and squamous cell carcinoma) in Canada: A descriptive analysis of available data. *Journal of Cutaneous Medicine and Surgery*, *20*(2), 166–175.
<https://doi.org/10.1177/1203475415610106>
- Adhikary, G., Grun, D., Kerr, C., Balasubramanian, S., Rorke, E. A., Vemuri, M., & Eckert, R. L. (2013). Identification of a population of epidermal squamous cell carcinoma cells with enhanced potential for tumor formation. *PLoS ONE*, *8*(12), 1–14.
<https://doi.org/10.1371/journal.pone.0084324>
- Ainger, S. A., & Sturm, R. A. (2015). Src and SCC: getting to the FAKs. *Experimental Dermatology*, *24*(7), 487–488. <https://doi.org/10.1111/exd.12725>
- Al-Hajj, M., & Clarke, M. F. (2004). Self-renewal and solid tumor stem cells. *Oncogene*, *23*(43 REV. ISS. 6), 7274–7282. <https://doi.org/10.1038/sj.onc.1207947>
- Arda, O., Göksügür, N., & Tüzün, Y. (2014). Basic histological structure and functions of facial skin. *Clinics in Dermatology*, *32*(1), 3–13.
<https://doi.org/10.1016/j.clindermatol.2013.05.021>
- Arden, K. C. (2004). FoxO: Linking new signaling pathways. *Molecular Cell*, *14*(4), 416–418. [https://doi.org/10.1016/S1097-2765\(04\)00213-8](https://doi.org/10.1016/S1097-2765(04)00213-8)
- Azorin, P., Bonin, F., Moukachar, A., Ponceau, A., Vacher, S., Bièche, I., & Driouch, K. (2018). Distinct expression profiles and functions of Kindlins in breast cancer. *Journal of Experimental and Clinical Cancer Research*, *37*(1), 1–15.
<https://doi.org/10.1186/s13046-018-0955-4>

- Back, J. H., Zhu, Y., Calabro, A., Queenan, C., Kim, A. S., Arbesman, J., & Kim, A. L. (2012). Resveratrol-mediated downregulation of rictor attenuates autophagic process and suppresses UV-induced skin carcinogenesis. *Photochem Photobiol*, *88*(5), 1165–1172. <https://doi.org/10.1111/j.1751-1097.2012.01097.x>. Resveratrol-Mediated
- Baker, S. E., DiPasquale, A. P., Stock, E. L., Quaranta, V., Fitchmun, M., & Jones, J. C. R. (1996). Morphogenetic effects of soluble laminin-5 on cultured epithelial cells and tissue explants. *Experimental Cell Research*, *228*(2), 262–270. <https://doi.org/10.1006/excr.1996.0325>
- Bakker, J., Spits, M., Neefjes, J., & Berlin, I. (2017). The EGFR odyssey - from activation to destruction in space and time. *Journal of Cell Science*, *130*(24), 4087–4096. <https://doi.org/10.1242/jcs.209197>
- Bandyopadhyay, A., Rothschild, G., Kim, S., Calderwood, D. A., & Raghavan, S. (2012). Functional differences between kindlin-1 and kindlin-2 in keratinocytes. *Journal of Cell Science*, *125*(9), 2172–2184. <https://doi.org/10.1242/jcs.096214>
- Baroni, A., Buommino, E., De Gregorio, V., Ruocco, E., Ruocco, V., & Wolf, R. (2012). Structure and function of the epidermis related to barrier properties. *Clinics in Dermatology*, *30*(3), 257–262. <https://doi.org/10.1016/j.clindermatol.2011.08.007>
- Becker, J. C., Stang, A., DeCaprio, J. A., Cerroni, L., Lebbé, C., Veness, M., & Nghiem, P. (2018). Merkel cell carcinoma. *Nat Rev Dis Primers*, (3). <https://doi.org/10.1038/nrdp.2017.77>.Merkel
- Behrens, D. T., Villone, D., Koch, M., Brunner, G., Sorokin, L., Robenek, H., & Hansen, U. (2012). The epidermal basement membrane is a composite of separate laminin- or

collagen IV-containing networks connected by aggregated perlecan, but not by nidogens. *Journal of Biological Chemistry*, 287(22), 18700–18709.

<https://doi.org/10.1074/jbc.M111.336073>

Blandin, A. F., Renner, G., Lehmann, M., Lelong-Rebel, I., Martin, S., & Dontenwill, M.

(2015). β 1 integrins as therapeutic targets to disrupt hallmarks of cancer. *Frontiers in Pharmacology*, 6(NOV), 1–10. <https://doi.org/10.3389/fphar.2015.00279>

Bonastre, E., Brambilla, E., & Sanchez-Cespedes, M. (2016). Cell adhesion and polarity in squamous cell carcinoma of the lung. *Journal of Pathology*, 238(5), 606–616.

<https://doi.org/10.1002/path.4686>

Boraschi-Diaz, I., Wang, J., Mort, J. S., & Komarova, S. V. (2017). Collagen type I as a ligand for receptor-mediated signaling. *Frontiers in Physics*, 5(MAY), 1–11.

<https://doi.org/10.3389/fphy.2017.00012>

Bostanciklioglu, M. (2015). The role of autophagy in stress and cancer. *Single Cell Biology*, 04(02), 4–9. <https://doi.org/10.4172/2168-9431.1000111>

Bott, R. (2014). *Lipid and Skin Health. Igarss 2014*.

Brückner, K., Pasquale, E. B., & Klein, R. (1997). Tyrosine phosphorylation of transmembrane ligands for Eph receptors. *Science*, 275(5306), 1640–1643.

<https://doi.org/10.1126/science.275.5306.1640>

Canadian Cancer Statistics 2014: Special topic: Skin cancers. (2014). *Canadian Cancer Society*. Retrieved from <http://www.cancer.ca/~media/cancer.ca/CW/cancer-information/cancer-101/Canadian-cancer-statistics/Canadian-Cancer-Statistics-2014-EN.pdf>

- Cang, Y., Zhang, J., Nicholas, S. A., Kim, A. L., Zhou, P., & Goff, S. P. (2007). DDB1 is essential for genomic stability in developing epidermis. *Proceedings of the National Academy of Sciences of the United States of America*, *104*(8), 2733–2737.
<https://doi.org/10.1073/pnas.0611311104>
- Cañueto, J., Cardeñoso, E., García, J. L., Santos-Briz, Castellanos-Martín, A., Fernández-López, E., & Román-Curto, C. (2017). Epidermal growth factor receptor expression is associated with poor outcome in cutaneous squamous cell carcinoma. *British Journal of Dermatology*, *176*(5), 1279–1287. <https://doi.org/10.1111/bjd.14936>
- Carter, W. G., Kaur, P., Gil, S. G., Gahr, P. J., & Wayner, E. A. (1990). Distinct functions for integrins $\alpha 3\beta 1$ in focal adhesions and $\alpha 6\beta 4$ /bullous pemphigoid antigen in a new stable anchoring contact (SAC) of keratinocytes: Relation to hemidesmosomes. *Journal of Cell Biology*, *111*(6 II), 3141–3154.
<https://doi.org/10.1083/jcb.111.6.3141>
- Cavalcanti-Adam, E. A., Volberg, T., Micoulet, A., Kessler, H., Geiger, B., & Spatz, J. P. (2007). Cell spreading and focal adhesion dynamics are regulated by spacing of integrin ligands. *Biophysical Journal*, *92*(8), 2964–2974.
<https://doi.org/10.1529/biophysj.106.089730>
- Chen, C. C., Juan, C. W., Chen, K. Y., Chang, Y. C., Lee, J. C., & Chang, M. C. (2017). Upregulation of RPA2 promotes NF- κ B activation in breast cancer by relieving the antagonistic function of menin on NF- κ B-regulated transcription. *Carcinogenesis*, *38*(2), 196–206. <https://doi.org/10.1093/carcin/bgw123>
- Chen, H., Padia, R., Li, T., Li, Y., Li, B., Jin, L., & Huang, S. (2012). Signaling of MK2 sustains

robust AP1 activity for triple negative breast cancer tumorigenesis through direct phosphorylation of JAB1. *Npj Breast Cancer*, 7(91), 1–13.

<https://doi.org/10.1038/s41523-021-00300-1>

Chen, L., Bi, S., Hou, J., Zhao, Z., Wang, C., & Xie, S. (2019). Targeting p21-activated kinase 1 inhibits growth and metastasis via Raf1/MEK1/ERK signaling in esophageal squamous cell carcinoma cells. *Cell Communication and Signaling*, 17(1), 1–17.

<https://doi.org/10.1186/s12964-019-0343-5>

Chen, S. Y., Lin, J. S., & Yang, B. C. (2014). Modulation of tumor cell stiffness and migration by type IV collagen through direct activation of integrin signaling pathway. *Archives of Biochemistry and Biophysics*, 555–556, 1–8.

<https://doi.org/10.1016/j.abb.2014.05.004>

Chong, C., Tan, L., Lim, L., & Manser, E. (2001). The mechanism of PAK activation. Autophosphorylation events in both regulatory and kinase domains control activity. *Journal of Biological Chemistry*, 276(20), 17347–17353.

<https://doi.org/10.1074/jbc.M009316200>

Chow, H. Y., Jubb, A. M., Koch, J. N., Jaffer, Z. M., Stepanova, D., Campbell, D. A., & Chernoff, J. (2012). p21-activated kinase 1 is required for efficient tumor formation and progression in a Ras-mediated skin cancer model. *Cancer Research*, 72(22), 5966–5975. <https://doi.org/10.1158/0008-5472.CAN-12-2246>.p21-activated

Cichoń, M. A., Szentpetery, Z., Caley, M. P., Papadakis, E. S., MacKenzie, I. C., Brennan, C. H., & O'Toole, E. A. (2014). The receptor tyrosine kinase Axl regulates cell-cell adhesion and stemness in cutaneous squamous cell carcinoma. *Oncogene*, 33(32),

4185–4192. <https://doi.org/10.1038/onc.2013.388>

Clifford, J. L., Menter, D. G., Yang, X., Walch, E., Zou, C., Clayman, G. L., & Lippman, S. M.

(2000). Expression of protein mediators of type I interferon signaling in human squamous cell carcinoma of the skin. *Cancer Epidemiology Biomarkers and Prevention*, 9(9), 993–997.

Dagnino, L., Ho, E., & Chang, W. Y. (2010). Expression and analysis of exogenous proteins in epidermal cells. In *Methods in Molecular Biology* (Vol. 585, pp. 93–105).

<https://doi.org/10.1007/978-1-60761-380-0>

Dahlhoff, M., Gaborit, N., Bultmann, S., Leonhardt, H., Yarden, Y., & Schneider, M. R.

(2017). CRISPR-assisted receptor deletion reveals distinct roles for ERBB2 and ERBB3 in skin keratinocytes. *FEBS Journal*, 284(19), 3339–3349.

<https://doi.org/10.1111/febs.14196>

Dahlhoff, M., Schäfer, M., Muzumdar, S., Rose, C., & Schneider, M. R. (2015). ERBB3 is required for tumor promotion in a mouse model of skin carcinogenesis. *Molecular Oncology*, 9(9), 1825–1833. <https://doi.org/10.1016/j.molonc.2015.06.007>

Dajee, M., Tarutani, M., Deng, H., Cai, T., & Khavari, P. A. (2002). Epidermal Ras blockade demonstrates spatially localized Ras promotion of proliferation and inhibition of differentiation. *Oncogene*, 21(10), 1527–1538.

<https://doi.org/10.1038/sj.onc.1205287>

Davis, A. J., Tsinkevich, M., Rodencal, J., Abbas, H. A., Su, X. H., Gi, Y. J., & Flores, E. R.

(2020). TAp63-regulated miRNAs suppress cutaneous squamous cell carcinoma through inhibition of a network of cell-cycle genes. *Cancer Research*, 80(12), 2484–

2497. <https://doi.org/10.1158/0008-5472.CAN-19-1892>

Davis, L. E., Shalin, S. C., & Tackett, A. J. (2019). Current state of melanoma diagnosis and treatment. *Cancer Biology and Therapy*, *20*(11), 1366–1379.

<https://doi.org/10.1080/15384047.2019.1640032>

Deville, S. S., & Cordes, N. (2019). The extracellular, cellular, and nuclear stiffness, a trinity in the cancer resistome—A review. *Frontiers in Oncology*, *9*(December), 1–14. <https://doi.org/10.3389/fonc.2019.01376>

Didona, D., Paolino, G., Bottoni, U., & Cantisani, C. (2018). Non melanoma skin cancer pathogenesis overview. *Biomedicines*, *6*(1), 1–15.

<https://doi.org/10.3390/biomedicines6010006>

Dontu, G., & Wicha, M. S. (2005). Survival of mammary stem cells in suspension culture: Implications for stem cell biology and neoplasia. *Journal of Mammary Gland Biology and Neoplasia*, *10*(1), 75–86. <https://doi.org/10.1007/s10911-005-2542-5>

Emmert, H., Culley, J., & Brunton, V. G. (2019). Inhibition of cyclin-dependent kinase activity exacerbates H₂O₂-induced DNA damage in Kindler syndrome keratinocytes. *Experimental Dermatology*, *28*(9), 1074–1078. <https://doi.org/10.1111/exd.14000>

Emmert, H., Patel, H., & Brunton, V. G. (2017). Kindlin-1 protects cells from oxidative damage through activation of ERK signalling. *Free Radical Biology and Medicine*, *108*(May), 896–903. <https://doi.org/10.1016/j.freeradbiomed.2017.05.013>

Ertych, N., Stolz, A., Stenzinger, A., Weichert, W., Kaulfuß, S., Burfeind, P., & Bastians, H. (2014). Increased microtubule assembly rates mediate chromosomal instability in colorectal cancer cells. *Nat Cell Biol*, *18*(8), 779–791.

<https://doi.org/10.1038/ncb2994>.Increased

Fan, X. Y., Tian, C., Wang, H., Xu, Y., Ren, K., Zhang, B. Y., & Dong, X. P. (2015). Activation of the AMPK-ULK1 pathway plays an important role in autophagy during prion infection. *Scientific Reports*, *5*, 1–12. <https://doi.org/10.1038/srep14728>

Fleckman, P., Dale, B. A., & Holbrook, K. A. (1985). Profilaggrin, a high-molecular-weight precursor of filaggrin in human epidermis and cultured keratinocytes. *Journal of Investigative Dermatology*, *85*(6), 507–512. <https://doi.org/10.1111/1523-1747.ep12277306>

Fogarty, S., Ross, F. A., Ciruelos, D. V., Gray, A., Gowans, G. J., & Hardie, D. G. (2016). AMPK causes cell cycle arrest in LKB1-deficient cells via activation of CAMKK2. *Molecular Cancer Research*, *14*(8), 683–695. <https://doi.org/10.1158/1541-7786.MCR-15-0479>

Fuchs, E. (2008). Scratching the surface of skin development Embryonic origins of skin epithelium, *445*(7130), 834–842. Retrieved from <https://www.ncbi.nlm.nih.gov/pmc/articles/PMC2405926/pdf/nihms-44886.pdf>

Gao, Y., Moten, A., & Lin, H. K. (2014). Akt: A new activation mechanism. *Cell Research*, *24*(7), 785–786. <https://doi.org/10.1038/cr.2014.57>

Gara, S. K., Lack, J., Zhang, L., Harris, E., Cam, M., & Kebebew, E. (2018). Metastatic adrenocortical carcinoma displays higher mutation rate and tumor heterogeneity than primary tumors. *Nature Communications*, *9*(1), 1–11. <https://doi.org/10.1038/s41467-018-06366-z>

Gaudet, C., Marganski, W. A., Kim, S., Brown, C. T., Gunderia, V., Dembo, M., & Wong, J.

- Y. (2003). Influence of type I collagen surface density on fibroblast spreading, motility, and contractility. *Biophysical Journal*, *85*(5), 3329–3335.
[https://doi.org/10.1016/S0006-3495\(03\)74752-3](https://doi.org/10.1016/S0006-3495(03)74752-3)
- Geum, D., Son, G. H., & Kim, K. (2002). Phosphorylation-dependent cellular localization and thermoprotective role of heat shock protein 25 in hippocampal progenitor cells. *Journal of Biological Chemistry*, *277*(22), 19913–19921.
<https://doi.org/10.1074/jbc.M104396200>
- Ghelli Luserna Di Rorà, A., Cerchione, C., Martinelli, G., & Simonetti, G. (2020). A WEE1 family business: Regulation of mitosis, cancer progression, and therapeutic target. *Journal of Hematology and Oncology*, *13*(1), 1–17. <https://doi.org/10.1186/s13045-020-00959-2>
- Giubellino, A., Burke, T. J. R., & Bottaro, D. P. (2008). Grb2 signaling in cell motility and cancer. *Expert Opin Ther Targets*, *12*(8), 1021–1033.
<https://doi.org/10.1517/14728222.12.8.1021.Grb2>
- Gordon, R. (2013). Skin cancer: An overview of epidemiology and risk factors. *Seminars in Oncology Nursing*, *29*(3), 160–169. <https://doi.org/10.1016/j.soncn.2013.06.002>
- Gray, S. E., Kay, E. W., Leader, M., & Mabruk, M. J. E. M. F. (2006). Enhanced detection of microsatellite instability and mismatch repair gene expression in cutaneous squamous cell carcinomas. *Molecular Diagnosis and Therapy*, *10*(5), 327–334.
<https://doi.org/10.1007/BF03256208>
- Grose, R., Hutter, C., Bloch, W., Thorey, I., Watt, F. M., Fässler, R., & Werner, S. (2002). A crucial role of β 1 integrins for keratinocyte migration in vitro and during cutaneous

wound repair. *Development*, 129(9), 2303–2315.

Guerrero-aspizua, S., Conti, C. J., Escamez, M. J., Castiglia, D., Zambruno, G., Youssefian, L., & Rio, M. Del. (2019). Assessment of the risk and characterization of non-melanoma skin cancer in Kindler syndrome : study of a series of 91 patients, 6, 1–15.

Hall, B. G., Acar, H., Nandipati, A., & Barlow, M. (2014). Growth rates made easy. *Molecular Biology and Evolution*, 31(1), 232–238.

<https://doi.org/10.1093/molbev/mst187>

Hanahan, D., & Weinberg, R. A. (2000). The hallmarks of cancer. *Cell*, 100(40), 251-57–70.

Hanahan, D., & Weinberg, R. A. (2011). Hallmarks of cancer: The next generation. *Cell*, 144(5), 646–674. <https://doi.org/10.1016/j.cell.2011.02.013>

Harburger, D. S., Bouaouina, M., & Calderwood, D. A. (2009). Kindlin-1 and -2 directly bind the c-terminal region of β integrin cytoplasmic tails and exert integrin-specific activation effects, 284(17), 11485–11497. <https://doi.org/10.1074/jbc.M809233200>

Harjunpää, H., Asens, M. L., Guenther, C., & Fagerholm, S. C. (2019). Cell adhesion molecules and their roles and regulation in the immune and tumor microenvironment. *Frontiers in Immunology*, 10(MAY). <https://doi.org/10.3389/fimmu.2019.01078>

Has, C., Herz, C., Zimina, E., Qu, H. Y., He, Y., Zhang, Z. G., & Bruckner-Tuderman, L. (2009). Kindlin-1 is required for RhoGTPase-mediated lamellipodia formation in keratinocytes. *American Journal of Pathology*, 175(4), 1442–1452.

<https://doi.org/10.2353/ajpath.2009.090203>

He, Y., Esser, P., Heinemann, A., Bruckner-Tuderman, L., & Has, C. (2011). Kindlin-1 and -2 have overlapping functions in epithelial cells: Implications for phenotype modification. *American Journal of Pathology*, *178*(3), 975–982.

<https://doi.org/10.1016/j.ajpath.2010.11.053>

Hegde, G. V., de la Cruz, C., Giltane, J. M., Crocker, L., Gabriele Schaefer, A. V., Dunlap, D., & Jackson, E. L. (2019). NRG1 is a critical regulator of differentiation in TP63-driven squamous cell carcinoma. *ELife*, *8*, 1–31.

<https://doi.org/10.7554/eLife.46551>

Heinemann, A., He, Y., Zimina, E., Boerries, M., Busch, H., Chmel, N., & Has, C. (2011). Induction of phenotype modifying cytokines by FERMT1 mutations. *Human Mutation*, *32*(4), 397–406. <https://doi.org/10.1002/humu.21449>

Hemmings, B. A., & Restuccia, D. F. (2016). PI3K-PKB / Akt Pathway, 1–4.

Hernandez, A. L., Young, C. D., Wang, J. H., & Wang, X. (2019). Lessons learned from SMAD4 loss in squamous cell carcinomas, *58*(9), 1648–1655.

<https://doi.org/10.1002/mc.23049.Lessons>

Herz, C., Aumailley, M., Schulte, C., Schlötzer-Schrehardt, U., Bruckner-Tuderman, L., & Has, C. (2006). Kindlin-1 is a phosphoprotein involved in regulation of polarity, proliferation, and motility of epidermal keratinocytes. *Journal of Biological Chemistry*, *281*(47), 36082–36090. <https://doi.org/10.1074/jbc.M606259200>

Hidalgo-Carcedo, C., Hooper, S., Chaudhry, S. I., Williamson, P., Harrington, K., Leitinger, B., & Sahai, E. (2011). Collective cell migration requires suppression of actomyosin

- at cell-cell contacts mediated by DDR1 and the cell polarity regulators Par3 and Par6. *Nature Cell Biology*, *13*(1), 49–58. <https://doi.org/10.1038/ncb2133>
- Hong, K. O., Oh, K. Y., Yoon, H. J., Swarup, N., Jung, M., Shin, J. A., & Hong, S. D. (2021). SOX7 blocks vasculogenic mimicry in oral squamous cell carcinoma. *Journal of Oral Pathology and Medicine*, (March), 1–10. <https://doi.org/10.1111/jop.13176>
- Horton, E. R., Humphries, J. D., James, J., Jones, M. C., Askari, J. A., & Humphries, M. J. (2016). The integrin adhesome network at a glance. *Journal of Cell Science*, *129*(22), 4159–4163. <https://doi.org/10.1242/jcs.192054>
- Hu, G., Liang, L., Liu, Y., Liu, J., Tan, X., Xu, M., & Xia, Y. (2019). TWEAK/Fn14 interaction confers aggressive properties to cutaneous squamous cell carcinoma. *Journal of Investigative Dermatology*, *139*(4), 796–806. <https://doi.org/10.1016/j.jid.2018.09.035>
- Hutchin, M. E., Kariapper, M. S. T., Grachtchouk, M., Wang, A., Wei, L., Cummings, D., & Dlugosz, A. A. (2005). Sustained Hedgehog signaling is required for basal cell carcinoma proliferation and survival: Conditional skin tumorigenesis recapitulates the hair growth cycle. *Genes and Development*, *19*(2), 214–223. <https://doi.org/10.1101/gad.1258705>
- Ishizawar, R. C., Miyake, T., & Parsons, S. J. (2007). c-Src modulates ErbB2 and ErbB3 heterocomplex formation and function. *Oncogene*, *26*(24), 3503–3510. <https://doi.org/10.1038/sj.onc.1210138>
- Ismail, F., Ikram, M., Purdie, K., Harwood, C., Leigh, I., & Storey, A. (2011). Cutaneous squamous cell carcinoma (scc) and the DNA damage response: Patm expression

- patterns in Pre-Malignant and malignant keratinocyte skin lesions. *PLoS ONE*, 6(7), 1–14. <https://doi.org/10.1371/journal.pone.0021271>
- Itoh, Y., & Nagase, H. (2002). Matrix metalloproteinases in cancer. *Essays in Biochemistry*, 38, 21–36. <https://doi.org/10.1042/bse0380021>
- Janes, S. M., & Watt, F. M. (2006). New roles for integrins in squamous-cell carcinoma. *Nature Reviews Cancer*, 6(3), 175–183. <https://doi.org/10.1038/nrc1817>
- Janus, J. M., O’Shaughnessy, R. F. L., Harwood, C. A., & Maffucci, T. (2017). Phosphoinositide 3-kinase-dependent signalling pathways in cutaneous squamous cell carcinomas. *Cancers*, 9(7). <https://doi.org/10.3390/cancers9070086>
- Jeong, H., Lim, K. M., Kim, K. H., Cho, Y., Lee, B., Knowles, B. C., & Nam, K. T. (2019). Loss of Rab25 promotes the development of skin squamous cell carcinoma through the dysregulation of integrin trafficking. *Journal of Pathology*, 249(2), 227–240. <https://doi.org/10.1002/path.5311>
- Johnson, K. E., & Wilgus, T. A. (2012). Multiple roles for vegf in non-melanoma skin cancer: angiogenesis and beyond. *Journal of Skin Cancer*, 2012, 1–6. <https://doi.org/10.1155/2012/483439>
- Jones, P. H., & Watt, F. M. (1993). Separation of human epidermal stem cells from transit amplifying cells on the basis of differences in integrin function and expression. *Cell*, 73(4), 713–724. [https://doi.org/10.1016/0092-8674\(93\)90251-K](https://doi.org/10.1016/0092-8674(93)90251-K)
- Kalinin, A. E., Kajava, A. V., & Steinert, P. M. (2002). Epithelial barrier function: Assembly and structural features of the cornified cell envelope. *BioEssays*, 24(9), 789–800. <https://doi.org/10.1002/bies.10144>

- Kallini, J. R., Hamed, N., & Khachemoune, A. (2015). Squamous cell carcinoma of the skin: Epidemiology, classification, management, and novel trends. *International Journal of Dermatology*, *54*(2), 130–140. <https://doi.org/10.1111/ijd.12553>
- Kariya, Y., Sato, H., Katou, N., Kariya, Y., & Miyazaki, K. (2012). Polymerized laminin-332 matrix supports rapid and tight adhesion of keratinocytes, suppressing cell migration. *PLoS ONE*, *7*(5). <https://doi.org/10.1371/journal.pone.0035546>
- Katayama, K., Fujita, N., & Tsuruo, T. (2005). Akt/Protein kinase B-dependent phosphorylation and inactivation of WEE1HU promote cell cycle progression at G2/M transition. *Molecular and Cellular Biology*, *25*(13), 5725–5737. <https://doi.org/10.1128/mcb.25.13.5725-5737.2005>
- Kawahira, K. (1999). Immunohistochemical staining of proliferating cell nuclear antigen (PCNA) in malignant and nonmalignant skin diseases. *Archives of Dermatological Research*, *291*(7–8), 413–418. <https://doi.org/10.1007/s004030050431>
- Kim, J., Kundu, M., Viollet, B., & Guan, K.-L. (2011). AMPK and mTOR regulate autophagy through direct phosphorylation of Ulk1. *Nat Cell Biol*, *13*(2), 132–141. <https://doi.org/10.1038/ncb2152>.AMPK
- Kim, J. Y., Cho, B., & Moon, C. (2020). Timely inhibitory circuit formation controlled by Abl1 regulates innate olfactory behaviors in mouse. *Cell Reports*, *30*(1), 187-201.e4. <https://doi.org/10.1016/j.celrep.2019.12.004>
- Kindler, T. (1954). Congenital Poikiloderma with traumatic bulla formation and progressive cutaneous atrophy. *British Journal of Dermatology*.
- Kloeker, S., Major, M. B., Calderwood, D. A., Ginsberg, M. H., Jones, D. A., Beckerle, M.

- C., & Biophys, R. B. (2004). The Kindler Syndrome protein is regulated by transforming growth factor- β and involved in integrin-mediated adhesion, *279*(8), 6824–6833. <https://doi.org/10.1074/jbc.M307978200>
- Kong, J., Du, J., Wang, Y., Yang, M., Gao, J., Wei, X., & Zhang, H. (2016). Focal adhesion molecule Kindlin-1 mediates activation of TGF- β signaling by interacting with TGF- β RI, SARA and Smad3 in colorectal cancer cells. *Oncotarget*, *7*(46), 76224–76237. <https://doi.org/10.18632/oncotarget.12779>
- Koster, M. I., & Roop, D. R. (2004). The role of p63 in development and differentiation of the epidermis. *Journal of Dermatological Science*, *34*(1), 3–9. <https://doi.org/10.1016/j.jdermsci.2003.10.003>
- Kukkurainen, S., Azizi, L., Zhang, P., Jacquier, M. C., Baikoghli, M., von Essen, M., & Wehrle-Haller, B. (2021). The F1 loop of the talin head domain acts as a gatekeeper in integrin activation and clustering. *Journal of Cell Science*, *133*(19), 1–15. <https://doi.org/10.1242/jcs.239202>
- Lai-Cheong, J. E., Ussar, S., Arita, K., Hart, I. R., & McGrath, J. A. (2008). Colocalization of kindlin-1, kindlin-2, and migfilin at keratinocyte focal adhesion and relevance to the pathophysiology of Kindler syndrome. *Journal of Investigative Dermatology*, *128*(9), 2156–2165. <https://doi.org/10.1038/jid.2008.58>
- Lai-Cheong, Joey E., Parsons, M., Tanaka, A., Ussar, S., South, A. P., Gomathy, S., & McGrath, J. A. (2009). Loss-of-function FERMT1 mutations in Kindler syndrome implicate a role for fermitin family homolog-1 in integrin activation. *American Journal of Pathology*, *175*(4), 1431–1441.

<https://doi.org/10.2353/ajpath.2009.081154>

Li, L., Li, F., Xia, Y., Yang, X., Lv, Q., Fang, F., & Jiang, M. (2020). UVB induces cutaneous squamous cell carcinoma progression by de novo ID4 methylation via methylation regulating enzymes. *EBioMedicine*, *57*.

<https://doi.org/10.1016/j.ebiom.2020.102835>

Liu, J., Guo, Y., Huang, Y., Xue, H., Bai, S., Zhu, J., & Fang, W. (2018). Effects of insulin-like growth factor binding protein 3 on apoptosis of cutaneous squamous cell carcinoma cells. *OncoTargets and Therapy*, *11*, 6569–6577.

<https://doi.org/10.2147/OTT.S167187>

Liu, K., Zheng, M., Lu, R., Du, J., Zhao, Q., Li, Z., & Zhang, S. (2020). The role of CDC25C in cell cycle regulation and clinical cancer therapy: A systematic review. *Cancer Cell International*, *20*(1), 1–16. <https://doi.org/10.1186/s12935-020-01304-w>

Liu, L., Rezvani, H. R., Back, J. H., Hosseini, M., Tang, X., Zhu, Y., & Bickers, D. R. (2014). Inhibition of p38 MAPK signaling augments skin tumorigenesis via NOX2 driven ROS generation. *PLoS ONE*, *9*(5), 1–9. <https://doi.org/10.1371/journal.pone.0097245>

Long, M., Cai, L., Li, W., Zhang, L., Guo, S., Zhang, R., & Zheng, H. (2018). DPP-4 inhibitors improve diabetic wound healing via direct and indirect promotion of epithelial-mesenchymal transition and reduction of scarring. *Diabetes*, *67*(3), 518–531.

<https://doi.org/10.2337/db17-0934>

Lu, D., Sun, L., Li, Z., & Mu, Z. (2021). lncRNA EZR-AS1 knockdown represses proliferation, migration and invasion of cSCC via the PI3K/AKT signaling pathway.

Molecular Medicine Reports, *23*(1), 1–11. <https://doi.org/10.3892/mmr.2020.11714>

- Lu, W., Gong, D., Bar-Sagi, D., & Cole, P. A. (2001). Site-specific incorporation of a phosphotyrosine mimetic reveals a role for tyrosine phosphorylation of SHP-2 in cell signaling. *Molecular Cell*, *8*(4), 759–769. [https://doi.org/10.1016/S1097-2765\(01\)00369-0](https://doi.org/10.1016/S1097-2765(01)00369-0)
- Madison, K. C. (2003). Barrier function of the skin: “La Raison d’Être” of the epidermis. *Journal of Investigative Dermatology*, *121*(2), 231–241. <https://doi.org/10.1046/j.1523-1747.2003.12359.x>
- Mahawithitwong, P., Ohuchida, K., Ikenaga, N., Fujita, H., Zhao, M., Kozono, S., & Tanaka, M. (2013). Kindlin-1 expression is involved in migration and invasion of pancreatic cancer. *International Journal of Oncology*, *42*(4), 1360–1366. <https://doi.org/10.3892/ijo.2013.1838>
- Maheshwari, G., Brown, G., Lauffenburger, D. A., Wells, A., & Griffith, L. G. (2000). Cell adhesion and motility depend on nanoscale RGD clustering. *Journal of Cell Science*, *113*(10), 1677–1686. <https://doi.org/10.1242/jcs.113.10.1677>
- Margadant, C., Kreft, M., Zambruno, G., & Sonnenberg, A. (2013). Kindlin-1 regulates integrin dynamics and adhesion turnover. *PLoS ONE*, *8*(6), 1–10. <https://doi.org/10.1371/journal.pone.0065341>
- Margadant, C., Monsuur, H. N., Norman, J. C., & Sonnenberg, A. (2011). Mechanisms of integrin activation and trafficking. *Current Opinion in Cell Biology*, *23*(5), 607–614. <https://doi.org/10.1016/j.ceb.2011.08.005>
- Margadant, C., Raymond, K., Kreft, M., Sachs, N., Janssen, H., & Sonnenberg, A. (2009). Integrin $\alpha 3 \beta 1$ inhibits directional migration and wound re-epithelialization in the

- skin. *Journal of Cell Science*, 122(2), 278–288. <https://doi.org/10.1242/jcs.029108>
- Marur, S., & Forastiere, A. A. (2008). Head and neck cancer: Changing epidemiology, diagnosis, and treatment. *Mayo Clinic Proceedings*, 83(4), 489–501. <https://doi.org/10.4065/83.4.489>
- Marzuka, A. G., & Book, S. E. (2015). Basal cell carcinoma: Pathogenesis, epidemiology, clinical features, diagnosis, histopathology, and management. *Yale Journal of Biology and Medicine*, 88(2), 167–179.
- McGrath, J. L. (2007). Cell spreading: the power to simplify. *Current Biology*, 17(10), 357–358. <https://doi.org/10.1016/j.cub.2007.03.057>
- Michael, M., Begum, R., Chan, G. K., Whitewood, A. J., Matthews, D. R., Goult, B. T., & Parsons, M. (2019). Kindlin-1 regulates epidermal growth factor receptor signaling. *Journal of Investigative Dermatology*, 139(2), 369–379. <https://doi.org/10.1016/j.jid.2018.08.020>
- Millon-Frémillon, A., Bouvard, D., Grichine, A., Manet-Dupé, S., Block, M. R., & Albiges-Rizo, C. (2008). Cell adaptive response to extracellular matrix density is controlled by ICAP-1-dependent β 1-integrin affinity. *Journal of Cell Biology*, 180(2), 427–441. <https://doi.org/10.1083/jcb.200707142>
- Missero, C., & Antonini, D. (2014). Crosstalk among p53 family members in cutaneous carcinoma. *Experimental Dermatology*, 23(3), 143–146. <https://doi.org/10.1111/exd.12320>
- Morse, E. M., Brahme, N. N., & Calderwood, D. A. (2014). Integrin cytoplasmic tail interactions. *Biochemistry*, 53(5), 810–820. <https://doi.org/10.1021/bi401596q>

- Moy, R. L. (2000). Clinical presentation of actinic keratoses and squamous cell carcinoma. *Journal of the American Academy of Dermatology*, 42(1 SUPPL. 1), S8–S10. <https://doi.org/10.1067/mjd.2000.103343>
- Mozaffari, N. L., Pagliarulo, F., & Sartori, A. A. (2021). Human CtIP: A ‘double agent’ in DNA repair and tumorigenesis. *Seminars in Cell and Developmental Biology*, 113(July 2020), 47–56. <https://doi.org/10.1016/j.semcdb.2020.09.001>
- Nagarajan, P., Parikh, N., Garrett-Sinha, L. A., & Sinha, S. (2009). Ets1 induces dysplastic changes when expressed in terminally-differentiating squamous epidermal cells. *PLoS ONE*, 4(1). <https://doi.org/10.1371/journal.pone.0004179>
- Neu, J., Dziunycz, P. J., Dzung, A., Lefort, K., Falke, M., Denzler, R., & Hofbauer, G. F. L. (2017). MiR-181a decelerates proliferation in cutaneous squamous cell carcinoma by targeting the proto-oncogene KRAS. *PLoS ONE*, 12(9), 1–16. <https://doi.org/10.1371/journal.pone.0185028>
- Nguyen, T. T., Gobinet, C., Feru, J., Pasco, S. B., Manfait, M., & Piot, O. (2012). Characterization of type I and IV collagens by Raman microspectroscopy: Identification of spectral markers of the dermo-epidermal junction. *Spectroscopy (New York)*, 27(5–6), 421–427. <https://doi.org/10.1155/2012/686183>
- Nigg, E. A., & Stearns, T. (2011). The centrosome cycle: Centriole biogenesis, duplication and inherent asymmetries. *Nature Cell Biology*, 13(10), 1154–1160. <https://doi.org/10.1038/ncb2345>
- Parikh, R. A., Appleman, L. J., Bauman, J. E., Sankunny, M., Lewis, D. W., Vlad, A., & Gollin, S. M. (2014). Upregulation of the ATR-CHEK1 pathway in oral squamous cell

carcinomas. *Genes Chromosomes Cancer*, 53(1), 25–37.

<https://doi.org/10.1002/gcc.22115>.Upregulation

Patel, H., Stavrou, I., Shrestha, R. L., Draviam, V., Frame, M. C., & Brunton, V. G. (2016).

Kindlin1 regulates microtubule function to ensure normal mitosis. *Journal of Molecular Cell Biology*, 8(4), 338–348. <https://doi.org/10.1093/jmcb/mjw009>

Patel, H., Zich, J., Serrels, B., Rickman, C., Hardwick, K. G., Frame, M. C., & Brunton, V. G.

(2013). Kindlin-1 regulates mitotic spindle formation by interacting with integrins and Plk-1. *Nature Communications*, 4(May). <https://doi.org/10.1038/ncomms3056>

Pollock, N. I., & Grandis, J. R. (2015). HER2 as a therapeutic target in head and neck

squamous cell carcinoma. *Clinical Cancer Research*, 21(3), 526–533.

<https://doi.org/10.1158/1078-0432.CCR-14-1432>

Prahallad, A., Heynen, G. J. J. E., Germano, G., Willems, S. M., Evers, B., Vecchione, L., &

Bernards, R. (2015). PTPN11 is a central node in intrinsic and acquired resistance to targeted cancer drugs. *Cell Reports*, 12(12), 1978–1985.

<https://doi.org/10.1016/j.celrep.2015.08.037>

Pullen, N., & Thomas, G. (1997). The modular phosphorylation and activation of

p70(s6k). *FEBS Letters*, 410(1), 78–82. [https://doi.org/10.1016/S0014-5793\(97\)00323-2](https://doi.org/10.1016/S0014-5793(97)00323-2)

Qu, H., Tu, Y., Guan, J. L., Xiao, G., & Wu, C. (2014). Kindlin-2 tyrosine phosphorylation

and interaction with Src serve as a regulatable switch in the integrin outside-in signaling circuit. *Journal of Biological Chemistry*, 289(45), 31001–31013.

<https://doi.org/10.1074/jbc.M114.580811>

- Que, S. K. T., Zwald, F. O., & Schmults, C. D. (2018). Cutaneous squamous cell carcinoma: Incidence, risk factors, diagnosis, and staging. *Journal of the American Academy of Dermatology*, *78*(2), 237–247. <https://doi.org/10.1016/j.jaad.2017.08.059>
- Ran, F. A., Hsu, P. D., Wright, J., Agarwala, V., Scott, D. A., & Zhang, F. (2013). Genome-scale CRISPR Knock-Out. *Zhang Lab*, *8*(11), 2281–2308. <https://doi.org/10.1038/nprot.2013.143>
- Rao, V. H., Vogel, K., Yanagida, J. K., Marwaha, N., Kandel, A., Trempus, C., & Hansen, L. A. (2015). Erbb2 up-regulation of ADAM12 expression accelerates skin cancer progression. *Molecular Carcinogenesis*, *54*(10), 1026–1036. <https://doi.org/10.1002/mc.22171>
- Rector, J., Kapil, S., Treude, K. J., Kumm, P., Glanzer, J. G., Byrne, B. M., & Oakley, G. G. (2017). S4S8-RPA phosphorylation as an indicator of cancer progression in oral squamous cell carcinomas. *Oncotarget*, *8*(6), 9243–9250. Retrieved from www.impactjournals.com/oncotarget/
- Reszka, A. A., Hayashi, Y., & Horwitz, A. F. (1992). Identification of amino acid sequences in the integrin β 1 cytoplasmic domain implicated in cytoskeletal association. *Journal of Cell Biology*, *117*(6), 1321–1330. <https://doi.org/10.1083/jcb.117.6.1321>
- Rheinwald, J. G., & Beckett, M. A. (1981). Tumorigenic Keratinocyte lines requiring anchorage and fibroblast support cultured from human squamous cell carcinomas. *Cancer Research*, *41*(5), 1657–1663.
- Rittié, L. (2016). Cellular mechanisms of skin repair in humans and other mammals. *Journal of Cell Communication and Signaling*, *10*(2), 103–120.

<https://doi.org/10.1007/s12079-016-0330-1>

- Robbins, D., & Zhao, Y. (2011). The role of manganese superoxide dismutase in skin cancer. *Enzyme Research*, 2011(1). <https://doi.org/10.4061/2011/409295>
- Rognoni, E., Ruppert, R., & Fässler, R. (2016). The kindlin family: Functions, signaling properties and implications for human disease. *Journal of Cell Science*, 129(1), 17–27. <https://doi.org/10.1242/jcs.161190>
- Rognoni, E., Widmaier, M., Jakobson, M., Ruppert, R., Katsougkri, D., Böttcher, R. T., & Rifkin, D. B. (2014). Kindlin-1 controls Wnt and TGF- β availability to regulate cutaneous epithelial stem cell proliferation, 20(4), 350–359. <https://doi.org/10.1038/nm.3490>. Kindlin-1
- Ruiz-Saenz, A., Dreyer, C., Campbell, M. R., Steri, V., Gulizia, N., & Moasser, M. M. (2018). HER2 amplification in tumors activates PI3K/Akt signaling independent of HER3. *Cancer Research*, 78(13), 3645–3658. <https://doi.org/10.1158/0008-5472.CAN-18-0430>
- Sadler, E., Klausegger, A., Muss, W., Deinsberger, U., Pohla-Gubo, G., Laimer, M., & Hintner, H. (2006). Novel KIND1 gene mutation in Kindler Syndrome with severe gastrointestinal tract involvement. *Archives of Dermatology*, 142(12), 1619–1624. <https://doi.org/10.1001/archderm.142.12.1619>
- Sadzak, I., Schiff, M., Gattermeier, I., Glinitzer, R., Sauer, I., Saalmüller, A., & Kovarik, P. (2008). Recruitment of Stat1 to chromatin is required for interferon-induced serine phosphorylation of Stat1 transactivation domain. *Proceedings of the National Academy of Sciences of the United States of America*, 105(26), 8944–8949.

<https://doi.org/10.1073/pnas.0801794105>

Saleva, M., Has, C., He, Y., Snejina, V., Maria, B., & Miteva, L. (2018). Natural history of

Kindler syndrome and propensity for skin cancer – case report and literature

review, *53*, 338–341. <https://doi.org/10.1111/ddg.13435>

Sarvi, S., Patel, H., Li, J., Dodd, G. L., Creedon, H., Muir, M., & Brunton, V. G. (2018).

Kindlin-1 promotes pulmonary breast cancer metastasis. *Cancer Research*, *78*(6),

1484–1496. <https://doi.org/10.1158/0008-5472.CAN-17-1518>

Senoo, M., Pinto, F., Crum, C. P., & McKeon, F. (2007). p63 is essential for the

proliferative potential of stem cells in stratified epithelia. *Cell*, *129*(3), 523–536.

<https://doi.org/10.1016/j.cell.2007.02.045>

Shaheen, S., Ahmed, M., Lorenzi, F., & Nateri, A. S. (2016). Spheroid-Formation

(Colonosphere) Assay for in vitro assessment and expansion of stem cells in colon cancer. *Stem Cell Reviews and Reports*, *12*(4), 492–499.

<https://doi.org/10.1007/s12015-016-9664-6>

Shih, C. M., Huang, C. Y., Huang, C. Y., Wang, K. H., Wei, P. L., Chang, Y. J., & Lee, A. W.

(2018). A dipeptidyl peptidase-4 inhibitor promotes wound healing in

normoglycemic mice by modulating keratinocyte activity. *Experimental*

Dermatology, *27*(10), 1134–1141. <https://doi.org/10.1111/exd.13751>

Shu, Z., Li, Z., Huang, H., Chen, Y., Fan, J., Yu, L., & Chen, G. (2020). Cell-cycle-dependent

phosphorylation of RRM1 ensures efficient DNA replication and regulates cancer

vulnerability to ATR inhibition. *Oncogene*, *39*(35), 5721–5733.

<https://doi.org/10.1038/s41388-020-01403-y>

- Siegel, D. H., Ashton, G. H. S., Penagos, H. G., Lee, J. V, Feiler, H. S., Wilhelmsen, K. C., & Epstein, E. H. (2003). Loss of Kindlin-1 , a human homolog of the caenorhabditis elegans actin – extracellular-matrix linker protein unc-112, causes Kindler Syndrome, 174–187.
- Siegel, J. A., Korgavkar, K., & Weinstock, M. A. (2017). Current perspective on actinic keratosis: a review. *British Journal of Dermatology*, 177(2), 350–358.
<https://doi.org/10.1111/bjd.14852>
- Sin, S., Bonin, F., Petit, V., Meseure, D., Lallemand, F., Biche, I., & Driouch, K. (2011). Role of the focal adhesion protein kindlin-1 in breast cancer growth and lung metastasis. *Journal of the National Cancer Institute*, 103(17), 1323–1337.
<https://doi.org/10.1093/jnci/djr290>
- Singh, B., Schoeb, T. R., Bajpai, P., Slominski, A., & Singh, K. K. (2018). Reversing wrinkled skin and hair loss in mice by restoring mitochondrial function. *Cell Death and Disease*, 9(7). <https://doi.org/10.1038/s41419-018-0765-9>
- Skardal, A., Mack, D., Atala, A., & Sokern, S. (2013). Substrate elasticity controls cell proliferation, surface marker expression and motile phenotype in amniotic fluid-derived stem cells. *Journal of the Mechanical Behavior of Biomedical Materials*, 17, 307–316. <https://doi.org/10.1016/j.jmbbm.2012.10.001>
- So, S., Davis, A. J., & Chen, D. J. (2009). Autophosphorylation at serine 1981 stabilizes ATM at DNA damage sites. *Journal of Cell Biology*, 187(7), 977–990.
<https://doi.org/10.1083/jcb.200906064>
- South, A. P., Purdie, K. J., Watt, S. A., Haldenby, S., Den Breems, N. Y., Dimon, M., &

- Leigh, I. M. (2014). NOTCH1 mutations occur early during cutaneous squamous cell carcinogenesis. *Journal of Investigative Dermatology*, *134*(10), 2630–2638.
<https://doi.org/10.1038/jid.2014.154>
- Squier, C. A., & Kremer, M. J. (2001). Biology of oral mucosa and esophagus. *Journal of the National Cancer Institute. Monographs*, *52242*(29), 7–15.
<https://doi.org/10.1093/oxfordjournals.jncimonographs.a003443>
- Steffen, J. D., Coyle, D. L., Damodaran, K., Beroza, P., & Jacobso, M. K. (2012). Discovery and structure-activity relationships of modified salicylanilides as cell permeable inhibitors of poly(ADP-ribose) glycohydrolase (PARG). *Bone*, *23*(1), 1–7.
<https://doi.org/10.1021/jm200325s>.Discovery
- Streulli, C. H., & Akhtar, N. (2009). Signal co-operation between integrins and other receptor systems. *Biochemical Journal*, *418*(3), 491–506.
<https://doi.org/10.1042/BJ20081948>
- Su, Z., Tian, H., Song, H. Q., Zhang, R., Deng, A. M., & Liu, H. W. (2013). PTPN12 inhibits oral squamous epithelial carcinoma cell proliferation and invasion and can be used as a prognostic marker. *Medical Oncology*, *30*(3). <https://doi.org/10.1007/s12032-013-0618-4>
- Sun, T., Aceto, N., Meerbrey, K. L., Kessler, J. D., Zhou, C., Migliaccio, I., & Kent, C. (2011). Activation of multiple proto-oncogenic tyrosine kinases in breast cancer via loss of the PTPN12 phosphatase, *144*(5), 703–718.
<https://doi.org/10.1016/j.cell.2011.02.003>.Sun
- Takada, Y., Ye, X., & Simon, S. (2007). The integrins. *Genome Biology*, *8*(5).

<https://doi.org/10.1186/gb-2007-8-5-215>

- Takahashi, T., Yamaguchi, S., Chida, K., & Shibuya, M. (2001). A single autophosphorylation site on KDR/Flk-1 is essential for VEGF-A-dependent activation of PLC- γ and DNA synthesis in vascular endothelial cells. *EMBO Journal*, *20*(11), 2768–2778. <https://doi.org/10.1093/emboj/20.11.2768>
- Tanese, K. (2019). Diagnosis and management of basal cell carcinoma. *Current Treatment Options in Oncology*, *20*(2). <https://doi.org/10.1007/s11864-019-0610-0>
- Tho, L. M., Libertini, S., Rampling, R., Sansom, O., & Gillespie, D. A. (2012). Chk1 is essential for chemical carcinogen-induced mouse skin tumorigenesis. *Oncogene*, *31*(11), 1366–1375. <https://doi.org/10.1038/onc.2011.326>
- Tian, Y., Wang, Y., Xu, S., Guan, C., Zhang, Q., & Li, W. (2020). The expression and therapeutic potential of checkpoint kinase 2 in laryngeal squamous cell carcinoma. *Drug Design, Development and Therapy*, *14*, 2613–2622. <https://doi.org/10.2147/DDDT.S245267>
- Trimmer, C., Bonuccelli, G., Katiyar, S., Sotgia, F., Pestell, R. G., Lisanti, M. P., & Capozza, F. (2013). Cav1 suppresses tumor growth and metastasis in a murine model of cutaneous SCC through modulation of MAPK/AP-1 activation. *American Journal of Pathology*, *182*(3), 992–1004. <https://doi.org/10.1016/j.ajpath.2012.11.008>
- Tsuyuki, S., Takabayashi, M., Kawazu, M., Kudo, K., Watanabe, A., Nagata, Y., & Yoshida, K. (2014). Detection of WIPI1 mRNA as an indicator of autophagosome formation. *Autophagy*, *10*(3), 497–513. <https://doi.org/10.4161/auto.27419>
- Ussar, S., Moser, M., Widmaier, M., Rognoni, E., & Harrer, C. (2008). Loss of Kindlin-1

causes skin atrophy and lethal neonatal intestinal epithelial dysfunction, *4*(12), 4–15. <https://doi.org/10.1371/journal.pgen.1000289>

Ussar, S., Wang, H. V., Linder, S., Fässler, R., & Moser, M. (2006). The Kindlins: Subcellular localization and expression during murine development. *Experimental Cell Research*, *312*(16), 3142–3151. <https://doi.org/10.1016/j.yexcr.2006.06.030>

Vanderdys, V., Allak, A., Guessous, F., Benamar, M., Read, P. W., Jameson, M. J., & Abbas, T. (2018). The neddylation inhibitor pevonedistat (MLN4924) suppresses and radiosensitizes head and neck squamous carcinoma cells and tumors. *Molecular Cancer Therapeutics*, *17*(2), 368–380. <https://doi.org/10.1158/1535-7163.MCT-17-0083>

Vijayakumar, S., Liu, G., Wen, H. C., Abu, Y., Chong, R., Natri, H., & Aaronson, S. A. (2017). Extracellular LDLR repeats modulate Wnt signaling activity by promoting LRP6 receptor endocytosis mediated by the Itch E3 ubiquitin ligase. *Genes and Cancer*, *8*(7–8), 613–627. <https://doi.org/10.18632/genesandcancer.146>

Wang, F., Zhang, H., & Cheng, Z. (2021). EPHA2 promotes the invasion and migration of human tongue squamous cell carcinoma Cal-27 cells by enhancing AKT/mTOR signaling pathway. *BioMed Research International*, 2021. <https://doi.org/10.1155/2021/4219690>

Wang, P., Zhan, J., Song, J., Wang, Y., Fang, W., Liu, Z., & Zhang, H. (2017). Differential expression of Kindlin-1 and Kindlin-2 correlates with esophageal cancer progression and epidemiology. *Science China Life Sciences*, *60*(11), 1214–1222. <https://doi.org/10.1007/s11427-016-9044-5>

- Wang, S., Wang, X. L., Wu, Z. Z., Yang, Q. C., Xiong, H. G., Xiao, Y., & Sun, Z. J. (2021). Overexpression of RRM2 is related to poor prognosis in oral squamous cell carcinoma. *Oral Diseases*, *27*(2), 204–214. <https://doi.org/10.1111/odi.13540>
- Wang, Yan, Sun, H., Wang, Z., Liu, M., Qi, Z., Meng, J., & Yang, G. (2014). Aurora-A: A potential DNA repair modulator. *Tumor Biology*, *35*(4), 2831–2836. <https://doi.org/10.1007/s13277-013-1393-8>
- Wang, Yu, Wang, G., Luo, X., Qiu, J., & Tang, C. (2012). Substrate stiffness regulates the proliferation, migration, and differentiation of epidermal cells. *Burns*, *38*(3), 414–420. <https://doi.org/10.1016/j.burns.2011.09.002>
- Wang, Z., & Zhu, J. (2021). Measurement of Integrin activation and conformational changes on the cell surface by soluble ligand and antibody binding assays. In *The integrin interactome: Methods and protocols* (Vol. 2217, pp. 3–15).
- Watt, F. M. (1988). Epidermal stem cells in culture. *Journal of Cell Science*, *94*(SSUPL. 10), 85–94. https://doi.org/10.1242/jcs.1988.supplement_10.7
- Watt, F. M. (2002). The stem cell compartment in human interfollicular epidermis. *Journal of Dermatological Science*, *28*(3), 173–180. [https://doi.org/10.1016/S0923-1811\(02\)00003-8](https://doi.org/10.1016/S0923-1811(02)00003-8)
- Watt, F. M., Frye, M., & Benitah, S. A. (2008). Myc in mammalian epidermis, *8*(3), 234–242. <https://doi.org/10.1038/nrc2328.Myc>
- Watt, F. M. (2002). Role of integrins in regulating epidermal adhesion, growth and differentiation, *21*(15), 1–8. Retrieved from papers3://publication/uuid/CF8BF94B-B29C-4D3D-BB79-9FAA5FDF53AF

Watt, F.M, Hogan, B. L. M., Watt, F. M., & Hogan, B. L. M. (2016). Out of eden : stem cells and their niches, *287(5457)*, 1427–1430.

Weinstein, E. J., Bourner, M., Head, R., Zakeri, H., Bauer, C., & Mazarella, R. (2003).

URP1: A member of a novel family of PH and FERM domain-containing membrane-associated proteins is significantly over-expressed in lung and colon carcinomas.

Biochimica et Biophysica Acta - Molecular Basis of Disease, *1637(3)*, 207–216.

[https://doi.org/10.1016/S0925-4439\(03\)00035-8](https://doi.org/10.1016/S0925-4439(03)00035-8)

Wick, M., Bürger, C., Brüsselbach, S., Lucibello, F. C., & Müller, R. (1994). Identification of serum-inducible genes: Different patterns of gene regulation during G0→S and G1→S progression. *Journal of Cell Science*, *107(1)*, 227–239.

Wilcox, R. A. (2018). Cutaneous B-cell lymphomas: 2019 update on diagnosis, risk stratification, and management. *American Journal of Hematology*, *93(11)*, 1427–1430. <https://doi.org/10.1002/ajh.25224>

Winograd-Katz, S. E., Fässler, R., Geiger, B., & Legate, K. R. (2014). The integrin adhesome: From genes and proteins to human disease. *Nature Reviews Molecular Cell Biology*, *15(4)*, 273–288. <https://doi.org/10.1038/nrm3769>

Won, S. Y., Park, J. J., Shin, E. Y., & Kim, E. G. (2019). PAK4 signaling in health and disease: defining the PAK4–CREB axis. *Experimental and Molecular Medicine*, *51(2)*. <https://doi.org/10.1038/s12276-018-0204-0>

Xue, M., & Jackson, C. J. (2015). Extracellular matrix reorganization during wound healing and its impact on abnormal scarring. *Advances in Wound Care*, *4(3)*, 119–136. <https://doi.org/10.1089/wound.2013.0485>

- Yang, Jing, Nie, J., Ma, X., Wei, Y., Peng, Y., & Wei, X. (2019). Targeting PI3K in cancer: Mechanisms and advances in clinical trials. *Molecular Cancer*, *18*(1), 1–28.
<https://doi.org/10.1186/s12943-019-0954-x>
- Yang, Jun, Yu, Y., Hamrick, H. E., & Duerksen-Hughes, P. J. (2003). ATM, ATR and DNA-PK: Initiators of the cellular genotoxic stress responses. *Carcinogenesis*, *24*(10), 1571–1580. <https://doi.org/10.1093/carcin/bgg137>
- Yates, L. A., Lumb, C. N., Brahme, N. N., Zalyte, R., Bird, L. E., De Colibus, L., & Gilbert, R. J. C. (2012). Structural and functional characterization of the kindlin-1 pleckstrin homology domain. *Journal of Biological Chemistry*, *287*(52), 43246–43261.
<https://doi.org/10.1074/jbc.M112.422089>
- Yeoman, B., Shatkin, G., Beri, P., Banisadr, A., Katira, P., & Engler, A. J. (2021). Adhesion strength and contractility enable metastatic cells to become adurotactic. *Cell Reports*, *34*(10), 108816. <https://doi.org/10.1016/j.celrep.2021.108816>
- Yildirim, T. T., Kaya, F. A., Taşkesen, M., DüNDAR, S., Bozoğlan, A., Tekin, G. G., & Akdeniz, S. (2017). Aggressive periodontitis associated with kindler syndrome in a large kindler syndrome pedigree. *Turkish Journal of Pediatrics*, *59*(1), 56–61.
<https://doi.org/10.24953/turkjped.2017.01.009>
- Yoshida, K., Yokouchi, M., Nagao, K., Ishii, K., Amagai, M., & Kubo, A. (2013). Functional tight junction barrier localizes in the second layer of the stratum granulosum of human epidermis. *Journal of Dermatological Science*, *71*(2), 89–99.
<https://doi.org/10.1016/j.jdermsci.2013.04.021>
- Yu, Z., Pestell, T. G., Lisanti, M. P., & Pestell, R. G. (2012). Cancer Stem Cells.

International Journal of Biochemistry and Cell Biology, 44(12), 2144–2151.

<https://doi.org/10.1016/j.biocel.2012.08.022>.Cancer

Yun, C. W., & Lee, S. H. (2018). The roles of autophagy in cancer. *International Journal of Molecular Sciences*, 19(11), 1–18. <https://doi.org/10.3390/ijms19113466>

Zaidel-Bar, R., Itzkovitz, S., Ma'ayan, A., Iyengar, R., & Geiger, B. (2007). Functional atlas of the integrin adhesome Ronen. *Nat Cell Biol*, 9(8), 858–867.

<https://doi.org/10.1038/ncb0807-858>.Functional

Zhan, J., Zhu, X., Guo, Y., Wang, Y., Wang, Y., Qiang, G., & Zhang, H. (2012). Opposite Role of Kindlin-1 and Kindlin-2 in Lung Cancers. *PLoS ONE*, 7(11), 1–12.

<https://doi.org/10.1371/journal.pone.0050313>

Zhang, L., Zhang, J., Chen, L., & Wang, J. (2015). Autophagy in human skin squamous cell carcinoma: Inhibition by 3-MA enhances the effect of 5-FU-induced chemotherapy sensitivity. *Oncology Reports*, 34(6), 3147–3155.

<https://doi.org/10.3892/or.2015.4302>

Zhang, M., Biswas, S., Qin, X., Gong, W., Deng, W., & Yu, H. (2016). Does Notch play a tumor suppressor role across diverse squamous cell carcinomas? *Cancer Medicine*, 5(8), 2048–2060. <https://doi.org/10.1002/cam4.731>

Zoppoli, G., Solier, S., Reinhold, W. C., Liu, H., Connelly, J. W., Monks, A., & Pommier, Y. (2012). CHEK2 genomic and proteomic analyses reveal genetic inactivation or endogenous activation across the 60 cell lines of the US National Cancer Institute. *Oncogene*, 31(4), 403–418. <https://doi.org/10.1038/onc.2011.283>

Curriculum Vitae

Name: Naomi Mishan

Post-secondary

Education and Degrees:

The University of Western Ontario
London, Ontario, Canada
2015-2019 B.Sc. Honors Specialization in Biology

The University of Western Ontario
London, Ontario, Canada
2019-present M.Sc.

Honours and Awards:

Dean's Honours List, 2016-2019
Global Opportunities Award, 2017
Harrypersad-Tewari Scholarship, 2017
Jack Miller Field Course Travel Award, 2018
Queen Elizabeth II Graduate Scholarship in Science and
Technology (OGS), 2019
Children's Health Research Institute (CHRI) Travel Fund,
2020
Cancer Biology Poster Award, 2020

Related Work

Experience:

Undergraduate Research Assistant
The University of Western Ontario
2017-2019

Teaching Assistant, Biology 1001/1002
The University of Western Ontario
2019-2021

Poster Presentations:

Mishan, N., Damjanovski, S., and Dagnino, L., (2020).
Kindlin-1 is required for normal migration and spreading in
squamous cell carcinoma. Physiology and Pharmacology
Research Day, Online.

Mishan, N., Damjanovski, S., and Dagnino, L., (2020).
Kindlin-1 involvement in bidirectional signaling through
integrins. Child Health Research Day, Online.

Mishan, N., Damjanovski, S., and Dagnino, L., (2020).
Kindlin-1 involvement in bidirectional signaling through
integrins. Cell and Developmental Biology, Virtual
Conference.